

Aus der
Klinik und Poliklinik für Psychiatrie und Psychotherapie
Klinikum der Ludwig-Maximilians-Universität München



**Development of barcoded GPCR assays to assess the effects of
neuroleptics for brain disorders in living cells**

Dissertation
zum Erwerb des Doktorgrades der Medizin
an der Medizinischen Fakultät
der Ludwig-Maximilians-Universität München

vorgelegt von
Yuxin Wu

aus
Shandong

Jahr
2024

Mit Genehmigung der Medizinischen Fakultät der
Ludwig-Maximilians-Universität München

Erstes Gutachten: Priv. Doz. Dr. Michael Wehr

Zweites Gutachten: Prof. Dr. Volker Scheuss

Drittes Gutachten: Prof. Dr. Felix Hausch

weitere Gutachten:

Promovierter Mitbetreuer: Prof. Dr. Moritz Roßner

Dekan: Prof. Dr. med. Thomas Gudermann

Tag der mündlichen Prüfung: 12.08.2024

Affidavit



Affidavit

Wu, Yuxin

Surname, first name

Street

Zip code, town, country

I hereby declare, that the submitted thesis entitled:

Development of barcoded GPCR assays to assess the effects of neuroleptics on brain disorders in living cells

is my own work. I have only used the sources indicated and have not made unauthorised use of services of a third party. Where the work of others has been quoted or reproduced, the source is always given.

I further declare that the dissertation presented here has not been submitted in the same or similar form to any other institution for the purpose of obtaining an academic degree.

Munich 12.08.2024

place, date

Yuxin Wu

Signature doctoral candidate

Table of content

Affidavit	1
Table of content.....	2
List of publications.....	4
List of abbreviations	5
Abstract (English).....	6
Zusammenfassung (Deutsch)	7
1. Aims of the thesis	9
2. Introduction	10
2.1 GPCRs are major drug targets.....	10
2.1.1 GPCR are classified into subgroups according to their sequence similarity.....	11
2.1.2 Transducers and signalling bias.....	15
2.1.3 GPCR are significant in the development of schizophrenia.....	20
2.1.4 Current drugs for GPCR families	21
2.2 Techniques for monitoring GPCR signalling activities	22
2.2.1 Singleplex assays.....	23
2.2.2 Multiplex assays	24
3. Own contribution to the original research papers	30
3.1 Contribution to paper I	30
3.2 Contribution to paper II.....	31
3.3 Contribution to paper III.....	32
4. Results	33
4.1 Summary of published results.....	33
4.2 High robustness and sensitivity of the established stable cell lines with luciferase assays.....	34
4.3 Results on the barcoded GPCR profiling platform	36
4.3.1 The barcoded pathway assays exhibit high robustness and reproducibility.....	36
4.3.2 Crosstalk at the pool barcode level may cause a problem.....	36
5. Paper I	39

6. Paper II	55
7. Paper III	56
8. Discussion and perspective	78
8.1 Considerations in developing barcoded GPCR assays.....	78
8.2 Advantage and limits of the barcoded GPCR assay	79
8.3 Further improvements of the barcoded GPCR assays	80
8.4 The perspectives of barcoded GPCR assays in drug discovery for brain disorders	80
References	82
Acknowledgements.....	89

List of publications

This thesis is based on the following publications, referred to in the text by their Roman numerals.

First author publications for the cumulative dissertation:

- I. **Wu Y**[#], von Hauff IV[#], Jensen N, Rossner MJ, Wehr MC. Improved Split TEV GPCR β -arrestin-2 Recruitment Assays via Systematic Analysis of Signal Peptide and β -arrestin Binding Motif Variants. *Biosensors*. 2023;13(1).
<https://doi.org/10.3390/bios13010048>. (Paper I)
- II. Ma X[#], Mandausch FJ[#], **Wu Y**[#], Sahoo VK, Ma W, Leoni G, Hostiuc M, Wintgens JP, Qiu J, Kannaiyan N, Rossner MJ, Wehr MC. Comprehensive split TEV based protein-protein interaction screening reveals TAOK2 as a key modulator of Hippo signalling to limit growth. *Cellular Signalling*. 2023:110917.
<https://doi.org/10.1016/j.cellsig.2023.110917>. (Paper II)

Co-author publication for the cumulative dissertation:

- III. Popović L, Wintgens JP, **Wu Y**, Brankatschk B, Menninger S, Degenhart C, Jensen N, Wichert SP, Klebl B, Rossner MJ, Wehr MC. Profiling of ERBB receptors and downstream pathways reveals selectivity and hidden properties of ERBB4 antagonists. *iScience*. 2024:108839.
<https://doi.org/10.1016/j.isci.2024.108839>. (Paper III)

Other co-author publication:

- IV. **Wu Y**, Jensen N, Rossner MJ, Wehr MC. Exploiting Cell-Based Assays to Accelerate Drug Development for G Protein-Coupled Receptors. *International Journal of Molecular Sciences*. 2024;25(10):5474.
<https://doi.org/10.3390/ijms25105474>.
- V. Zhao X, Zhao D, **Wu Y**, Gao W, Cui H, Wang Y, Nakaji P, Bao Y. Meningioma in the elderly: Characteristics, prognostic factors, and surgical strategy. *J Clin Neurosci*. 2018;56:143-9.
<https://doi.org/10.1016/j.jocn.2018.06.011>.

[#] These authors contributed equally to the work.

List of abbreviations

2HA	Double HA tag
5-HT	5-Hydroxytryptamine, a.k.a. serotonin
ARBB2	β -arrestin-2
AVPR2	Renal-type arginine vasopressin receptor
BDNF	Brain derived neurotrophic factor
cAMP	cyclic adenosine monophosphate
CRE	Cyclic AMP response element
CREB	cAMP response element-binding protein
CTEV	C-terminal moiety of the TEV protease
DA	Dopamine hydrochloride
DRD1	Dopamine receptor D1
DRD2	Dopamine receptor D2
EGFId	EGF-like domain
EGR1p	Early growth response protein 1 promoter
ERBB4	Erb-b2 receptor tyrosine kinase 4
ERK	Extracellular signal-regulated kinase
FSK	Forskolin
GCGR	Glucagon receptor
GLP1R	Glucagon-like peptide 1 receptor
GPCR	G protein-coupled receptors
GRKs	G protein-coupled receptor kinases
GV	GAL4-VP16
HTR2A	5-hydroxytryptamine (serotonin) receptor 2A
HTS	High-throughput screening
Lira	Liraglutide
MAPK	Mitogen-activated protein kinase
NTEV	N-terminal moiety of the TEV protease
NTRK2	Neurotrophic receptor tyrosine kinase 2
PMA	Phorbol 12-myristate 13-acetate
RTKs	Receptor tyrosine kinases
SP	signal peptide
TCS	TEV-protease cleavage site
TEV	Tobacco etch virus protease
UAS	Upstream activating sequence
V2R	V2 vasopressin receptor
VA	[Arg ⁸]-vasopressin acetate salt

Abstract (English)

Background: G protein-coupled receptors (GPCRs) represent the largest protein family in the human genome and are targeted by 35% of FDA-approved drugs. Their signalling pathways are complex and attractive for drug discovery. GPCR activation can be measured using the split TEV protein-protein interaction technique at the membrane. In addition, pathway reporter gene assays can be used at the transcriptional level via cis-regulatory elements, as these can be activated independently of the transducer pathways of GPCR activation.

Methods: First, I identified whether the combinations of the signal peptide (SP) and the β -arrestin binding motif (i.e., C-terminal tail of the vasopressin 2 receptor (AVPR2); V2R tail) for six GPCRs and cell backgrounds of four cell types affect the β -arrestin recruitments with the split TEV GPCR assay in a transfection-based way. Then I developed a living cell-based platform for the multiplex profiling GPCR signalling activities at the transcriptional level, called the barcoded GPCR pathway assay. GPCRs were stably integrated into HEK293 cells to avoid the variability associated with transient transfection. To monitor the multiplex profiling of G protein-coupled receptor (GPCR) signalling activities, a lentivirus-based sensor library was used encoding various genetically encoded pathway sensors, based on cis-regulatory elements.

Results: The split TEV GPCR assays revealed that the combinations of SP and V2R tail have different effects depending on the GPCR, whereas HEK293 cells provided the best performance in most situations. Then I selected HEK293 cells for the barcoded GPCR pathway assay. The robustness of the barcoded GPCR pathway assay was confirmed by testing various plate formats, MOIs (multiplicity of infection) of the lentiviral sensor library, and ligand stimulation. Furthermore, the reproducibility of the barcoded GPCR pathway assay was demonstrated through seven independent repetitions performed on different days. However, the combination of stable cells and the lentiviral sensor library produced two issues. Firstly, there was crosstalk between different stable cells due to barcode sequencing leakage. Secondly, the next-generation sequencing procedure can result in so-called read eating effects. This occurred because the barcodes from the index sensors, which were introduced when the stable cells were established, have much higher mRNA levels than the barcodes from the lentiviral sensor library. As a result, sequencing resources are intensively used for these frequently occurring barcodes, leaving only a limited and insufficient amount of sequencing resources for low occurring barcodes.

Outlook: Although the above two issues need to be addressed, the success of the project is underlined by the robustness and reproducibility of the barcoded GPCR pathway assay, providing a solid foundation for its further development.

Zusammenfassung (Deutsch)

Hintergrund: G-Protein gekoppelte Rezeptoren (GPCRs) sind die größte Proteinfamilie im menschlichen Genom und das Target von 35% der von der FDA zugelassenen Medikamente. Die Signalwege, die von GPCRs aktiviert werden, sind komplex und zugleich attraktiv für die pharmazeutische Forschung. Die Aktivierung von GPCRs kann einerseits mit der Split-TEV-Protein-Protein-Interaktionstechnik direkt an der Zellmembran gemessen werden. Darüber hinaus können Signalweg-Assays, die auf einem transkriptionellem Readout beruhen und cis-regulierende Elemente nutzen, verwendet werden, da diese Reporter-gen-Assays unabhängig von den aktivierten Signalwegen GPCR-Aktivitäten abbilden können.

Methoden: Zunächst untersuchte ich, ob die Kombinationen des Signalpeptids (SP) und des β -Arrestin-Bindungsmotivs (d.h. C-terminaler Tail des Vasopressin-2-Rezeptors (AVPR2); V2R-Tail) für sechs GPCRs und in vier verschiedenen Zelltypen die β -Arrestin-Rekrutierung mit dem Split-TEV-GPCR-Assay auf transfektionsbasierte Weise beeinflussen. Anschließend entwickelte ich eine auf lebenden Zellen basierende Plattform für die multiparametrische Profilierung von GPCR-Signalaktivitäten auf transkriptioneller Ebene, den sogenannten *Barcoded GPCR Pathway Assay*. Die GPCRs wurden einzeln in HEK293-Zellen integriert, um die mit der transienten Transfektion verbundene Variabilität zu vermeiden. Um die Profilierung der Signalaktivitäten von G-Protein gekoppelten Rezeptoren (GPCRs) zu messen, wurde eine Lentivirus-basierte Sensorbibliothek mit verschiedenen genetischen Signalwegensensoren infiziert.

Ergebnis: Die Split-TEV-GPCR-Assays zeigten, dass die Kombinationen von SP und V2R-Schwanz je nach GPCR unterschiedliche Effekte hatten, wobei HEK293-Zellen in den meisten Situationen die beste Assay-Performance zeigten. Daher wählte ich HEK293-Zellen für den Test mit dem multiparametrischen GPCR-Signalweg-Assay aus. Die Robustheit des dieses Assays wurde durch das Testen verschiedener Plattenformate, MOIs (*Multiplicity of Infection*) der lentiviralen Sensorbibliothek und der Stimulation mit verschiedenen Liganden bestätigt. Darüber hinaus wurde die Reproduzierbarkeit des multiparametrischen GPCR-Signalweg-Assays durch sieben unabhängige Wiederholungen an verschiedenen Tagen nachgewiesen. Die Kombination von stabilen Zellen und der lentiviralen Sensorbibliothek war jedoch mit zwei Problemen verbunden. Zum einen kam es aufgrund von Crosstalk in der Barcode-Sequenzierung zu Überlappungen zwischen verschiedenen stabilen Zellen. Zweitens kann die NGS-Sequenzierungstechnik zu sogenannten Read-Eating-Effekten führen. Diese treten auf, wenn die Barcodes der Index-Sensoren, die bei der Etablierung der stabilen Zellen eingeführt wurden, wesentlich höhere mRNA-Werte aufweisen als die Barcodes der lentiviralen Sensorbibliothek. Dies hat zur Folge, dass die Sequenzierressourcen für diese häufig

vorkommenden Barcodes intensiv genutzt werden und nur eine begrenzte und unzureichende Menge an Sequenzierressourcen für die selten vorkommenden Barcodes übrig bleibt.

Ausblick: Obwohl die beiden oben genannten Probleme noch gelöst werden müssen, wird der Erfolg des Projekts durch die Robustheit der Sequenzierbibliothek gewährleistet.

1. Aims of the thesis

G protein-coupled receptors (GPCRs) represent the largest family of proteins in the human genome. They serve as the targets of 35% of FDA-approved drugs and act as the receptors for two-thirds of all human hormones^[1-3]. The discovery that individual GPCRs can activate multiple signalling pathways has created the potential for developing drugs that selectively target therapeutically relevant pathways. Techniques to monitor their signalling pathways are important for drug discovery and the exploration of new therapeutics, for example, GPCR activation has been shown to be measured at the membrane using the split TEV protein-protein interaction technique in many different cell lines such as HEK293 cell.

In this thesis, I first aim to provide an optimized split TEV-based readout for GPCRs to maximize sensitivity and reproducibility of assays in living cells. Secondly, the objective is to develop a robust multiplexed cell-based platform to simultaneously profile the complex signalling pathways following GPCR activation. This is termed barcoded GPCR pathway assays. The bioassay platform, which is embedded in HEK293 cells, is a reporter gene assay in which stable cell lines are generated individually. These integrate a specific GPCR with a barcode reporter that is uniquely assigned, in conjunction with a cis-regulatory element that is responsive and serves as the sensor. Additionally, a variety of sensors with distinct barcodes are introduced into these stable cells, allowing for the monitoring of multiple pathways. Barcodes are short nucleic acids (either DNA or RNA) with exponential sequence differences that can be distinguished and quantified by next-generation sequencing (NGS). Using this barcoded assay platform, I aim to monitor the selective activation of five GPCRs and two receptor tyrosine kinase as unrelated controls in a proof-of-principle assay.

2. Introduction

G protein-coupled receptors (GPCRs) represent the largest family of integral membrane proteins in the human genome and are targeted by 35% of FDA-approved drugs^[2-3]. Their signalling pathways are complex and attractive for drug discovery. GPCRs are among the six major drug targets, together with ion channels, nuclear hormone receptors, catalytic receptors, enzymes, and transporters.

In this project, I developed a living cell-based platform to monitor the multiplex profiling of GPCR signalling activities at the transcriptional level, called the barcoded GPCR pathway assay.

2.1 GPCRs are major drug targets

GPCRs represent the largest family of proteins, comprising 826 out of 20283 (4%) human genes^[4-6]. They are also the largest family of cell surface receptors in other eukaryotes, such as fungi^[7]. In humans, the majority of GPCRs are olfactory receptors, and the approximately remaining 350 non-olfactory GPCRs are considered druggable, of which 165 have been validated as drug targets^[6]. The term “7TM receptor” is often interchangeably used with “GPCR”, because the GPCRs have seven hydrophobic transmembrane domains (TM1-TM7) and share a conventional structure. A GPCR is composed of a single polypeptide chain with an extracellular N-terminus, an intracellular C-terminus, three extracellular loops (ECL1-ECL3), and three intracellular loops (ICL1-ICL3). When viewed from the extracellular side, the 7 TM regions are arranged in an anti-clockwise direction^[8]. However, it is important to note that not all integral membrane proteins with 7TM domains are GPCRs^[9].

GPCRs play a crucial role in pathway signalling and diverse cellular responses, which includes sensory perception (e.g., rhodopsin), neurotransmitter (e.g., aminergic neurotransmitter) and hormone (e.g., calcitonin) signalling, immune responses (e.g., chemokines), cardiovascular regulation (e.g., corticotropin), gastrointestinal function (e.g., releasing digestive enzymes), and metabolism (e.g., carbohydrate metabolism). Essentially, GPCRs can help eukaryotes sense their environment and coordinate appropriate responses. GPCRs are the primary targets for drugs in pharmacology, making them the focus of intensive investment by pharmaceutical companies^[2].

2.1.1 GPCR are classified into subgroups according to their sequence similarity

The first attempt to classify GPCRs was made by Attwood and Findlay in 1993^[5], when they study the seven hydrophobic domains of GPCRs to create the sequence-based fingerprints. In 1994, Kolakowski classified the GPCRs into six families, from A to F subclassed, based on the homology of amino acid sequences. In 2003, Fredriksson and his colleagues discovered over 800 human GPCRs. They then analyzed them with phylogenetic analyses to develop the GRAFS classification system with five families, where the letters in GRAFS stand for Glutamate, Rhodopsin, Adhesion, Frizzled/Taste2, and Secretin respectively^[10]. In 2011, the GRAFS system was extended to include another member of the T family^[11]. The unclassified GPCRs are also grouped into the 'other' subclass, referred to as the O subclass (**Table 1**).

It is noteworthy that the A-F classification system applies to both vertebrates and invertebrates, whereas the GRAFS classification system applies only to vertebrates and that the GPCR classification systems are still evolving along with new emerging knowledge.

In this thesis, I will mainly use the GRAFS classification system, because it focuses on vertebrates.

Table 1 A-F classification system and the GRAFS classification system

A-F Class	GRAFS	#Human GPCRs ^[12]	Note
A	Rhodopsin	719	Have the most drug targets, especially the aminergic GPCRs
B1	Secretin	15	Accept peptides as ligands and play a key role as receptors for peptide hormones.
B2	Adhesion	33	Important in many pathologies, but not yet targeted by drugs ^[13]
C	Glutamate	22	<ul style="list-style-type: none"> •Incl. three Taste 1 receptors for sweet and umami tastes •Either heterodimers or homodimers are essential for its biological function.
D	N.A.	N.A.	Fungal mating pheromone receptors
E	N.A.	N.A.	Cyclic AMP receptors
F	Frizzled	11	FDA-approved drugs only available at SMO
T	Taste 2	25	Sense bitter and not used for drugs
O	Other	5	7TM receptors not belonging to any of the above classes

Note: The original 6-member A-F classification is extended by two more subclasses, such as T in 2011 (Taste 2) and O (Other) subclasses^[11], where O (other) indicates either that the GPCRs are classified as unique receptors that do not belong to any family, or that these receptors are considered to have 7TM domains but have not yet been confirmed as GPCRs by functional studies. Notably, vertebrates have no classes D and E. The tastes of bitter, sweet and umami are sensed by specialized GPCRs, while the tastes of sour and salty foods are sensed by the activity of ion channels.

2.1.1.1 Glutamate family/class C

The glutamate family of GPCRs completely overlaps with the class C, consisting of 22 human GPCRs, such as eight metabotropic glutamate (mGlu) receptors (GRM), two gamma-aminobutyric acid (GABA) type B receptors (GABA_{B1} and GABA_{B2}), one calcium sensing receptor (CASR), three taste receptors type 1 (TAS1R1-3) for sweet and umami tastes, GPRC6A (G Protein-Coupled Receptor Class C Group 6 Member A), and seven orphan receptors^[5]. The defining characteristic of glutamate family GPCRs is their constitutive homo- or heterodimerization, facilitated by their extensive N-terminal extracellular domain (ECD)^[14]. In other words, either heterodimers or homodimers are essential for its biological function^[15]. Glutamate family GPCRs bind small molecules with their N-terminal region as ligands, such as the acidic amino acids (L-glutamate for GRMs and GABA for GABA_B receptors), basic amino acids (the L- α -amino acids arginine, lysine and ornithine for GPRC6A), Ca²⁺ for CASR, and the small molecular sweeteners for TAS1R1-3^[5]. Notably, the binding specificity mediated by the N-terminus is not high, which hinders the development of specific drugs.

2.1.1.2 Rhodopsin receptor family/class A

The rhodopsin receptor family completely overlaps with the class A. There are 719 human receptors in this family, forming four subgroups - α , β , γ and δ - with 13 subbranches based on phylogenetic analysis^[12, 16]. Rhodopsin receptor family of GPCRs is the largest GPCR family with high heterogeneity in both sequence and ligand preference, but they generally have short N-termini where the ligand-binding domain is located^[16]. Rhodopsin was the first GPCR to be discovered in the 1876^[17], although the concept of a GPCR was not introduced until the late 1970s and 1980s thanks to the pioneering work on adrenergic receptors (which are also rhodopsin-like receptors) by Robert J. Lefkowitz and Brian Kobilka, who won the 2012 Nobel Prize in Chemistry for their research on GPCRs^[18]. Bovine rhodopsin was also the first GPCR whose crystal structure (Protein Data Bank accession number: 1F88) was solved in 2000, whereas the first structure of GPCR-G-protein complex (Protein Data Bank accession number: 3SN6; beta2 adrenergic receptor-Gs protein complex) was solved in 2011^[6, 19].

With respect to the high heterogeneity in ligand preference, the rhodopsin receptor family can be classified into 11 subtypes based on differences in ligand type, such as arylcarboxylic acid, aminergic, lipid, melatonin, nucleotide, olfactory, orphan, peptide, protein, sensory (opsin receptors) and steroid rhodopsin GPCRs^[20].

The vasopressin receptor 2 (AVPR2), dopamine receptor D1 (DRD1), dopamine receptor D2 (DRD2), and 5-hydroxytryptamine receptor 2A (HTR2A) were included in the Paper I. AVPR2

is a peptide rhodopsin GPCR that uses vasopressin as its endogenous ligand, and its C-terminal intracellular domain (V2R tail, amino acids 343-371) contains 11 serine and threonine residues that can be phosphorylated by GPCR kinases (GRKs) and provide a docking site for β -arrestin-2^[21]. DRD1, DRD2 and HTR2A are aminergic rhodopsin GPCRs, and both DRD1 and DRD2 use dopamine as their endogenous ligand, while HTR2A uses the amine of 5-hydroxytryptamine (5-HT) as its endogenous ligand.

2.1.1.3 Adhesion receptor family/class B2

The second largest family, with 33 members^[13], has been also named the LNB7TM family, where LN stands for long N-termini which undergo autoproteolytic cleavage from the first hydrophobic transmembrane domain (TM1) at a conserved "GPCR proteolysis site" (GPS) which is located in a much larger (~320 residues) "GPCR autoproteolysis-inducing" (GAIN) domain, and B stands for sequence homology between the 7TMs of adhesion GPCRs and secretin GPCR. The nomenclature of adhesion GPCRs implies their potential dual roles in cellular adhesion and signalling.

The GRAFS system, based on the phylogenetic analysis, is the first time to define adhesion GPCRs as a separate family^[13]. Furthermore, based on the detailed phylogenetic relationships of the TM regions, these 33 members can be classified into eight subclasses I-VIII. Unlike the secretin receptor family, whose ligands are peptides, the ligands of the adhesion GPCRs are extracellular matrix molecules such as glycosaminoglycans^[13].

2.1.1.4 Frizzled Receptor family/class F

Frizzled Receptor family completely overlaps with the class F. The human genome contains eleven members of the frizzled receptor family, including ten frizzled receptors (FZD1-10) and the smoothed receptor (SMO)^[22]. The first frizzled receptor was reported in *Drosophila melanogaster* in 1989^[5], where the mutant frizzled gene changed the polarity of the trichomes in the wing, causing them to swirl rather than point distally. This type of receptor was later named frizzled to indicate its important role in maintaining the orientation property of trichomes^[23]. The ten FZDs are localized exclusively at the plasma membrane, have 19 Wnt glycoproteins as the ligands, and control three distinct signalling pathways for cell growth. These include the planar cell polarity (PCP) pathway, the Wnt/calcium pathway, and the canonical Wnt/beta-catenin pathway. SMO works in a ligand-independent way in the Hedgehog pathway in humans, which was also first identified in *Drosophila*^[24]. When dysregulated, SMO plays key roles in the formation of developmental disorders and cancers.

2.1.1.5 Secretin receptor family/class B1

The secretin receptor family has 15 GPCRs, classified into five subtypes based on the peptide hormones they bind, such as calcitonin receptors, parathyroid hormone receptors, vasoactive intestinal peptide and pituitary adenylate cyclase-activating peptide (VIP and PACAP) receptors, glucagon receptor family, and corticotropin-releasing factor receptors, all of which contain a hormone-binding domain at the N-terminus and are activated by peptidomimetic hormones^[5, 25]. The family name is derived from the rat secretin receptor (SCTR), which was the first secretin GPCR to be discovered^[26]. The GPCRs belonging to the secretin receptor family hold significant promise as drug development targets, because they all use peptide hormones as their endogenous ligands and play a key role in maintaining systemic homeostatic functions in humans.

Examples are glucagon-like peptide 1 receptor (GLP1R), with glucagon, glucagon-like peptide 1-(7-37), and glucagon-like peptide 1-(7-36) amide as its endogenous ligands, which has the most drugs in the secretin family (six FDA-approved drugs and 23 ligands in clinical trials)^[27].

Due to the significance of the glucagon receptor (GCGR) and GLP1R as therapeutic targets in type II diabetes and obesity, and the involvement of the GLP1R in neurological disorders such as Alzheimer's disease (AD), Parkinson's disease (PD) and amyotrophic lateral sclerosis (ALS), the GCGR and GLP1R were included in the Paper I as well.

2.1.1.6 Taste 2 receptor family

The taste type 2 receptors (TAS2) were recently considered as a separate sixth subclass in 2011^[11], which is evolved from class A but has the close phylogenetic relationship with FZD receptors. There are 25 TAS2 receptors in the human genome, mostly clustered on chromosomes 7q31 and 12p13^[5]. TAS2s sense bitter tastes rather than sweet and umami tastes (Taste type 1 receptors within the glutamate GPCR family). Interestingly, FZDs have the closer phylogenetic relationship to bitter taste receptors, supporting the idea that cell growth regulation may have something in common with bitter taste perception.

In particular, in the paper I, published in Biosensors, the six GPCRs from two GPCR families, such as the rhodopsin receptor family/class A (AVPR2, DRD1, DRD2, and HTR2A) and the secretin receptor family/class B1 (such as GCGR and GLP1R), were selected as a proof of concept to show that the effects of the signal peptide (SP) and the C-terminal tail of the vasopressin 2 receptor (AVPR2; V2R tail) on the split TEV GPCRs assays are GPCR type-dependent.

2.1.2 Transducers and signalling bias

As membrane receptors, GPCRs have three main transducers to mediate signalling pathways following agonist activation, such as heterotrimeric G proteins, GPCR kinases (GRKs), and arrestins. The Nomenclature and Standards Committee of the International Union of Basic and Clinical Pharmacology (NC-IUPHAR) has defined transducers as proteins that bind directly to activated GPCRs to coordinate downstream signalling, trafficking, or internalisation. Downstream regulated pathways are often named after these transducers^[28]. In other words, a transducer protein defines a GPCR signalling pathway. In contrast to direct binding to GPCRs, effectors are defined as signalling proteins that lie downstream in a transducer pathway^[28].

GPCR signalling bias refers to the difference in signalling intensity that occurs at any hierarchical level within all the pathways following a given GPCR activation, such as the transducer, the effector, the second messenger, and the transcription factors. The multiple alternative transducers and their various downstream pathway components for a given GPCR contribute to signalling bias, which is divided into ligand bias and system bias^[28].

Different agonists can lead to different conformational changes in a given GPCR, recruiting transducers with biases, known as ligand bias. Essentially, conformational selection contributes to ligand bias. Ligand bias can be explained in mechanistic terms, where a ligand binding and a transducer binding from opposite sides of the cell membrane may prefer the same conformation of the receptor structure and thus allosterically select each other^[28]. In other words, the three conjugate factors, different ligands, subsequent different GPCR conformations and transducer-receptor conformational binding preferences, contribute simultaneously to ligand bias. As a result of ligand bias, signalling bias can occur at any signalling component, such as transducers, effectors, second messengers, etc.^[28], although ligand bias is initiated at ligand binding.

In contrast, the different concentrations of particular transducers, subsequent effectors, second messengers and so on, in different cell types lead to signalling selectivity following unique GPCRs, which is referred to as system bias.

2.1.2.1 Heterotrimeric G proteins

Heterotrimeric G proteins consist of three subunits, i.e., the α , β , and γ subunits. In the inactivated state, heterotrimeric G proteins are anchored to the membrane by the α and γ subunits and pre-bound to GPCRs due to the selectivity between α subunits and GPCRs^[28]. The α subunit binds to GDP in the inactivated state. Upon activation, GPCRs change stereoscopically and act as guanyl nucleotide exchange factors^[29] for $G\alpha$ proteins to replace GDP with GTP,

which results in the disassociation of the $\beta\gamma$ complex to mediate signalling such as the activation of MAPK pathways, while activated $G\alpha$ regulates cAMP and calcium mediated signalling. Notably, both GTP-bound $G\alpha$ and free $G\beta\gamma$ can act as transducers to initiate signalling through interactions with downstream effector proteins^[30] (**Figure 1**).

In humans, there are 16 subtypes of the α subunit (**Table 2**), and they are grouped into four families based on protein sequence homology and their associated downstream pathways: Gs (2 subtypes), Gi/o (8 subtypes), Gq/11 (4 subtypes), and G12/13 (2 subtypes)^[31]. The Gs family mediates the activation of adenylyl cyclase, whereas the Gi/o family inhibits it. The Gq/11 family mainly mediates the activation of phospholipase C. The G12/13 family is involved in the Rho/Rho kinase signalling pathway. These four main α subunit-mediated pathways are summarized in **Figure 1**.

The 16 α subunit subtypes also contribute to the signalling bias^[32]. In particular, it is worth distinguishing the GPCR- α subunit *coupling selectivity* from the α subunit *contributing signalling bias*. GPCR- α subunit coupling is often referred to as G protein coupling, which implies all practical potential couplings between a GPCR and one or more α subunits^[32-33]. G protein coupling selectivity refers to the different potential GPCR- α subunit couplings for each GPCR. To define the selectivity determinants of GPCR-G protein binding, Flock et al. provided a selectivity barcode, a pattern of amino acids, on each of the 16 human G proteins^[32].

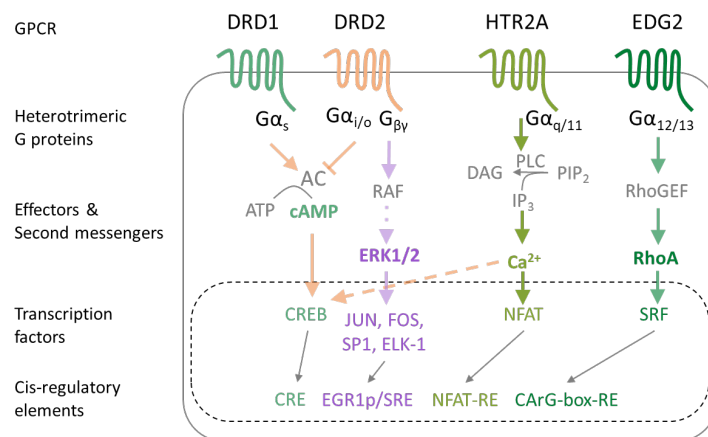


Figure 1. Diagram of heterotrimeric G protein-mediated signalling pathways. Four GPCRs, such as DRD1, DRD2, HTR2A and EDG2, individually coupled to one of the four α subunit families are selected to indicate G protein coupling selectivity and to show the α subunit-mediated pathways as well as the involvement of the $\beta\gamma$ complex in the MAPK pathway. The GPCR activation can alter gene transcription via the Cis-regulatory elements, such as the cAMP response element (CRE), the early growth response protein 1 promoter (EGR1p), the serum response element (SRE), the nuclear factor of activated T-cells response element (NFAT-RE), and CarG-box-RE ([CC(A+T-rich)₆GG] box response element)^[34]. Notably, only one coupling for the four GPCRs is shown for readability, but a GPCR can potentially couple to more than one α -subunit. For example, DRD1 may couple with Gs, Gi/o and Gq/11, DRD2 may couple with Gi/o and Gq/11, HTR2A may couple with Gi/o and Gq/11 and EDG2 may couple with Gi/o and G12/13^[32].

However, signalling biases contributed by α subunits emphasize the functional coupling selectivity between a GPCR and one or more α -subunits in specific contexts, such as different ligand treatments or different cell types^[28].

In human and mouse^[30], there are 5 types of β subunits and twelve different γ units, known as β 1-5, γ 1-5 and γ 7-13. These β and γ subunit subtypes can pair with each other to generate all the 60 theoretically possible unique $\beta\gamma$ dimeric complexes^[35], but with pairing preferences between them^[36].

Similar to the G α protein subunit anchoring to the plasma membrane, these 60 $\beta\gamma$ dimeric complexes are initially anchored to the plasma membrane by the γ subunit and, after GPCR activation, translocate to different organelles depending on the type of $\beta\gamma$ complex, such as the Golgi apparatus, early endosome, endoplasmic reticulum, and mitochondria^[35]. Like the GPCR- α subunit coupling selectivity, specific $\beta\gamma$ dimeric complexes may work with specific GPCRs^[30]. Moreover, $\beta\gamma$ dimeric complex-mediated signalling by GPCRs may be as prevalent as that mediated by G α subunits^[30], which has not yet received the same attention.

In contrast, the diversity of $\beta\gamma$ dimeric complexes contributes to the unique spatial and temporal signalling biases of a given GPCR^[35], which may contribute to $\beta\gamma$ dimeric complex-based ligand biases. In general, the current focus on ligand biases is predominantly on α -subunits and β -arrestins^[28, 37]. Therefore, G protein mediated bias mainly refers to α subunit rather than $\beta\gamma$ dimeric complex-based ligand biases.

Table 2. 16 subtypes of α subunit in human genome.

Family	Member	Gene Symbol	Expression specificity				Note
			Tissue	Cell	Brain region	Brain cell	
s	$G\alpha_s$	GNAS	Low	Low	Low	Low (higher expression in inhibitory neurons)	•localized to the nucleoplasm, the plasma membrane and the cytosol •50 transcripts •high expression in the brain
	$G\alpha_{olf}$	GNAL	High (enriched in brain)	High (enriched in inhibitory neurons, excitatory neurons)	Low	High (enriched in inhibitory, excitatory neurons)	•localized to the nucleoplasm and cytosol •8 transcripts
i/o	$G\alpha_{i1}$	GNAI1	High (enriched in brain)	High (enriched in oligodendrocytes, syncytiotrophoblasts, melanocytes)	Low	High (enriched in oligodendrocytes)	•localized to the centrosome, the nucleoplasm and nucleoli •18 transcripts
	$G\alpha_{i2}$	GNAI2	Low	High (enriched in monocytes, adipocytes)	Low	High (enriched in glial cell, such as microglia, oligodendrocytes, and astrocytes)	•localized to the cytosol, the nucleoplasm and plasma membrane •5 transcripts
	$G\alpha_{i3}$	GNAI3	Low	High (enriched in monocytes)	Low	Low	•localized to the centrosome, the nucleoplasm and nucleoli •1 transcript
	$G\alpha_{r1}$	GNAT1	High (enriched in retina)	High (enriched in rod photoreceptor cells)	Low	Low (very low expression in astrocytes)	•cytoplasmic expression in rods in retina. •3 transcripts •Very low expression in brain
	$G\alpha_{r2}$	GNAT2	High (enriched in retina)	High (enriched in cone photoreceptor cells)	Low	Low	•3 transcripts •Very low expression in brain
	$G\alpha_{r3}$	GNAT3	High (enriched in intestine)	High (enriched in early spermatids, late spermatids, excitatory neurons)	Low	High (enriched in excitatory neurons)	•cytoplasmic expression in enteroendocrine cells in duodenum and small intestine. •1 transcript •Very low expression in brain
	$G\alpha_z$	GNAZ	High (enriched in brain)	High (enriched in Horizontal cells, Adipocytes, Cone photoreceptor cells, Rod photoreceptor cells)	Low	Low (lowest expression in microglia)	•localized to the vesicles inside cells •1 transcript • High expression in brain
	$G\alpha_o$	GNAO1	High (enriched in brain, retina)	High (enriched in oligodendrocytes, excitatory neurons, astrocytes, Inhibitory neurons)	Low	Low (highest expression in oligodendrocytes)	•cytoplasmic expression in neuropil, pancreatic islets and peripheral nerves. •10 transcripts
q/11	$G\alpha_q$	GNAQ	Low	High (enriched in astrocytes, oligodendrocytes, excitatory neurons, microglial cells)	Low	Low	•localized to the nuclear speckles, plasma membrane, and cytosol •2 transcripts • High expression in brain
	$G\alpha_{11}$	GNA11	Low	High (enriched in proximal enterocytes, distal enterocytes)	Low	Low	•membranous and cytoplasmic expression •3 transcripts • High expression in brain
	$G\alpha_{14}$	GNA14	Low	High (enriched in astrocytes, oocytes, late spermatids)	Low	High (enriched in astrocytes)	•membranous and cytoplasmic expression •1 transcript
	$G\alpha_{16}$	GNA15	High (enriched in bone marrow)	High (enriched in dendritic cells, Langerhans cells, monocytes)	Low	High (enriched in microglia)	•1 transcript •involved in the innate immune system
12/13	$G\alpha_{12}$	GNA12	Low	High (enriched in dendritic cells, Syncytiotrophoblasts, Langerhans cells)	Low	Low (highest expression in oligodendrocyte precursor cells)	•localized to the cytosol •4 transcripts •involved in the antigen presentation
	$G\alpha_{13}$	GNA13	High (enriched in bone marrow)	High (enriched in Langerhans cells, monocytes, Schwann cells, dendritic cells)	Low	Low (highest expression in astrocytes and microglia)	•localized to the cytosol •2 transcripts •involved in the antigen presentation

Note: The expression specificity is defined based on the single cell transcriptomics data from the Human Protein Atlas^[38], but not based on its knowledge-based annotation for protein expression^[39]. The specificity level is simply categorized into high and low. The expression level is briefly described in the Note section. Tissue specificity indicates the expression specificity across the human tissues. Cell specificity indicates the expression specificity across the human cell types. In contrast, brain regional specificity represents the different expression levels in the different brain regions, and brain cell specificity indicates the expression specificity across all brain cell types. Cell types in the human brain are divided into neuronal cells (including excitatory and inhibitory neurons) and glial cells (such as astrocytes, oligodendrocytes precursor cells, oligodendrocytes, and microglia). Notably, GNA16 is the homologues of GNA15 in mouse.

2.1.2.1 GPCR kinases and arrestins as initial transducers of biased signalling

The human genome contains seven types of GRKs, which are grouped into three subfamilies, such as the GRK1 subfamily (including GRK1 and GRK7), the GRK2 subfamily (including GRK2 and GRK3) and the GRK4 subfamily (including GRK4, GRK5 and GRK6)^[40]. GRKs belong to the AGC kinase superfamily, which uses ATP to add phosphate to serine and threonine residues and was first defined by Hanks and Hunter in 1995 as proteins containing kinase domains most similar to protein kinase A, protein kinase G and protein kinase C^[40-41]. There are four types of arrestins in the human genome, divided into two subfamilies, such as visual subtypes (S-antigen visual arrestin (SAG) and arrestin 3 (ARR3)) and non-visual subtypes (arrestin beta 1 (ARRB1) and arrestin beta 2 (ARRB2))^[29] (**Table 3**).

Table 3. Four types of arrestins in the human genome.

Symbol	Expression specificity				Note
	Tissue	Cell	Brain region	Brain cell	
SAG	High (enriched in retina)	High (enriched in rod photoreceptor cells)	Low	Low	<ul style="list-style-type: none"> •localized to the cytosol in photoreceptors in retina •3 transcript variants •Almost no expression in human brain •highly antigenic inducing experimental autoimmune uveoretinitis
ARR3	High (enriched in retina)	High (enriched in cone photoreceptor cells)	Low	Low	<ul style="list-style-type: none"> •localized to the cytosol and the Golgi apparatus in cones in retina •3 transcript variants •low expression in human brain •a part of the centrosome
ARRB1	Low	Low	Low	Low	<ul style="list-style-type: none"> •localized to cytoplasmic and nuclear in most tissues •4 transcript variants •highest expression in microglia, astrocytes, and inhibitory neurons, following by immune cells such as Kupffer cells and monocytes •very high expression in human brain
ARRB2	High (enriched in bone marrow, lymphoid tissue)	High (enriched in monocytes, Hofbauer cells, macrophages, Kupffer cells)	Low	High (enriched in microglia)	<ul style="list-style-type: none"> •localized to the nucleoplasm, plasma membrane, and the cytosol •9 transcript variants •involved in the innate immune response •half the expression of ARRB1 in human brain

Note: The expression specificity is defined based on the single cell transcriptomics data from the Human Protein Atlas^[38], but not based on its knowledge-based annotation for protein expression^[39]. The specificity level is simply categorized into high and low. The expression level is briefly described in the Note section. Tissue specificity indicates the expression specificity across the human tissues. Cell specificity indicates the expression specificity across the human cell types. In contrast, brain regional specificity represents the different expression levels in the different brain regions, and brain cell specificity indicates the expression specificity across all brain cell types. Cell types in the human brain are divided into neuronal cells (including excitatory and inhibitory neurons) and glial cells (such as astrocytes, oligodendrocytes precursor cells, oligodendrocytes, and microglia).

Upon agonist activation, GPCRs recruit GRKs, which undergo a conformational change that promotes kinase activation and phosphorylate intracellular domains of these GPCRs^[40]. Subsequently, arrestins can bind to these phosphorylated residues. GRKs work in tandem with ARRs to modulate GPCR sensitivity in two ways: desensitization, by blocking GPCR coupling to G proteins, and internalization, by endocytosing GPCRs for either degradation or recycling

back to the plasma membrane (resensitization)^[29]. Arrestins can also act as transducers, allowing GPCRs to signal via G protein-independent pathways^[42], which was not previously anticipated and leads to the concept of biased agonism or signalling bias. Therefore, arrestin-mediated ligand bias compared to G protein mediated ones has received a lot of attention in recent decades^[28]. In particular, in the paper I, published in Biosensors, the ARRB2 was selected as interacting protein recruited to activated GPCRs in split TEV GPCR assays^[21].

2.1.2.2 Non-canonical transducers of GPCR

In addition to the three main transducers mentioned above, the newer transducers called 14-3-3 proteins have recently been reported^[43]. 14-3-3 protein signal transduction is GPCR phosphorylation dependent and occurs later than desensitisation and internalisation, whereas it is β -arrestin independent^[43]. In addition, different agonists can have varying potencies on 14-3-3 and β -arrestin signalling, which contributes to the new resources for ligand bias^[43].

It has been reported that cyclin-dependent kinase 5 (CDK5) has a direct physical interaction with the serotonin receptor 7 (HTR7A) and mediate G-protein-independent signaling, suggesting that it may be a novel GPCR transducer candidate^[44].

2.1.3 GPCR are significant in the development of schizophrenia.

As the largest family of proteins, GPCRs are involved in many complex disorders, including psychiatric disorders, neurodegenerative diseases, brain injury, cancer, metabolic diseases, immunological and infectious diseases^[45-46]. This project focuses on the establishment of robust assays for GPCRs impacting schizophrenia (SCZ) as a proof of concept.

SCZ is a neurodevelopmental mental disorder and featured by recurrent episodes of psychosis, which has three predominant symptoms, such as positive, negative, and cognitive symptoms. Although its incidence rate is only 0.25% to 0.75%^[47], it caused serious disease and social burden because of its long-life psychosis course. However, as SCZ is a genetically complex disorder its exact cause is not fully understood. There are several evidences to try to explain its pathogenesis from the perspectives of organic causes, such as the hyperactive DRD2 receptor in the striatum^[48], the HTR2A hypersensitivity on glutamatergic neurons^[49], the hyperactive neuregulin1/receptor tyrosine-protein kinase ERBB4 (NRG1/ERBB4) signaling pathway on inhibitory parvalbumin (PV) interneurons and the hypoactive dimeric brain-derived neurotrophic factor/neurotrophic receptor tyrosine kinase (BDNF/NTRK2) signaling pathway on the PV interneurons^[50-51]. All the evidence have the same underlying common feature, which is the abnormalities of the neural circuits, especially the dopaminergic neural circuits. Striatal dopamine dysfunction has been regarded as fundamental cause for SCZ. The striatum,

rich in dopamine receptors, is an integrative hub for information processing of the corticobasal ganglia circuitry^[52].

The endogenous receptors for dopamine is called as the dopamine receptors, including DRD1-like (DRD1 and DRD5) and DRD2-like (DRD2, DRD3 and DRD4)^[53-54]. In the central nerve system, DRD1 is predominantly expressed in cerebral cortex, hippocampus, and striatum^[55]. DRD2 is primarily expressed in the pituitary gland, followed by cerebral cortex and striatum^[55]. Endogenous dopamine predominantly activates neurons expressing DRD1, while simultaneously suppressing those expressing DRD2^[56]. The imbalance of DRD1 and DRD2 activation within the striatum (that is, striatum dysfunction in dopaminergic system) can comprehensively explain the pathobiology of schizophrenia well and can be regarded as an integral pathological hypothesis of schizophrenia.

The aforementioned evidences are also indirectly related to striatal dysfunction in the dopaminergic system. For example, the hyperactive HTR2A signaling on glutamatergic neurons, the hyperactive NRG1/ERBB4 on the PV inhibitory interneurons and the hypoactive BDNF/NTRK2 signaling on the PV inhibitory interneurons, can ultimately result in the imbalance activities between DRD1 and DRD2 in the striatum.

ERBB4 and NTRK2 are the receptor tyrosine kinases (RTKs), which have 58 members that are grouped into 20 families and are mainly involved in cell growth^[57]. Considering the roles of DRD1, DRD2, HTR2A, ERBB4, NTRK2 in SCZ, I selected them along with two additional AVPR2 and GLP1R for a proof of concept to test the performance of the cellular barcoded platform for GPCRs as well as RTKs.

2.1.4 Current drugs for GPCR families

GPCRs dominate FDA drug approvals, and ~34% of those act on GPCR targets^[3]. The drug-gable GPCRs and their relevant drugs can be found in the GPCR database ([GPCRdb](#)) with the additional search for newly approved entities at Drugs@FDA ([New Drugs at FDA](#)) and cross-referencing with the Drugbank, PubChem, IUPHAR and ChEMBL databases.

Glutamate family/class C: Eight of the 22 members of the glutamate GPCR family have been used as targets by 16 drugs approved by the FDA^[6]. The TM regions have many allosteric interaction sites and allosteric ligands for the GRMs (metabotropic glutamate (mGlu) receptors), the CASR (calcium-sensing receptor), the GABA_B receptors (gamma-aminobutyric acid (GABA) type B receptors) have also been used^[6]. The ligands that bind to the N-terminus of glutamate GPCRs are likely to be less specific than those that bind to the TM regions, so the development of specific high-affinity allosteric ligands seems more attractive^[14].

Rhodopsin receptor family/class A: Most of the FDA-approved drugs for GPCRs target the rhodopsin GPCRs. Of these, the aminergic GPCRs have the largest number of FDA-approved drugs, and to date, with the exception of HRH4 (histamine receptor H4), all aminergic GPCRs have corresponding drugs^[27].

Adhesion receptor family/class B2: There are no approved or clinically tested therapies targeting any of the 33 adhesion GPCRs^[13].

Frizzled Receptor family: To date, the SMO receptor is the only frizzled-like GPCR for which drugs have been approved by the FDA and are used as anti-neoplastic agents^[6]. There is a need to find ligands for the ten frizzled receptors (FZD1-10), particularly in the field of cancer research^[58].

Secretin receptor family/class B1: Of the 15 members, 14 secretin GPCRs have drugs either in trials or approved, except for the PAC1 receptor (pituitary adenylate cyclase activating polypeptide 1 receptor). GLP1R is the receptor for glucagon-like peptide 1 (GLP-1) and plays a role in regulating insulin secretion in response to GLP-1, which is the hot therapeutic target for type 2 diabetes (T2D) and obesity^[59]. Of the 15 members, GLP1R has received the most attention, with six FDA-approved drugs and at least 23 trials^[27]. GLP-1 is an incretin hormone that is secreted by L-cells in the lower intestine^[60]. GLP-1 is responsible for up to 70% of insulin secretion in response to nutrient intake. It can also mediate the incretin effect, which is the phenomenon of a two- to three-fold higher insulin secretory response to oral glucose administration compared to intravenous glucose administration^[60]. The short half-life of native GLP-1 (1.5 min to 1.5 h, depending on the route of administration) limited its use and much effort was put into the discovery of long-acting GLP-1 analogues such as liraglutide and semaglutide^[61]. Liraglutide, discovered by the company of Novo Nordisk, has a prolonged half-life of 13 hours and can be administered by daily subcutaneous injection to treat type 2 diabetes, obesity and reduce cardiovascular events^[61-62]. Semaglutide, also discovered by Novo Nordisk, has an even longer half-life of 46.1 hours and can be administered orally once a week for the treatment of type 2 diabetes, obesity and non-alcoholic fatty liver disease (NASH)^[61, 63].

Taste 2 receptor family: There are currently no drugs approved or in trials for this family of bitter taste receptors.

2.2 Techniques for monitoring GPCR signalling activities

Due to the important roles of GPCRs in physiology, pathology and pharmacology, techniques for monitoring GPCR activities need to be well developed^[64]. These techniques use different detection methods to monitor GPCR activities at different hierarchical levels of signalling

pathways, such as transducer level, effector level, second messenger level, transcriptional level, etc^[21, 65-66].

Assay categories can be classified in different ways based on the characteristics of the assays, such as throughput, monitoring levels, detection methods, whether the measured object is transcriptionally expressed (i.e. transcript derived) or not, qualitative, or quantitative, and so on. Based on throughput, assays can be divided into singleplex and multiplex assays. Based on whether the measured object is transcript-derived or not, assays can be divided into transcriptional and non-transcriptional assays. Notably, the classification criteria are independent of each other, and a given assay may have different characteristics.

There are several singleplex and multiplex assays that have been used to monitor GPCR related activities, and the principles, the selected subtypes, the corresponding signalling hierarchical levels of the selected subtypes are summarized in **Table 4**.

Table 4. Singleplex and multiplex assays for monitoring GPCR signalling

Assay Type	Principle	Selected Subtype	Corresponding Signalling Hierarchical Level
Singleplex	Luminescence	Split TEV GPCR assay ^[67]	β -arrestin-2 recruitment
		Full TEV GPCR assay ^[68]	β -arrestin-2 recruitment
	FRET	smFRET ^[69]	GPCR dimer
	BRET	EMTA (ebBRET-based) ^[70]	α and effector activation as well as β -arrestin-1 and 2 recruitments
Multiplex	Absorbance	TGF- α shedding assay ^[31]	α recruitment
	NGS	GPCRprofiler ^[71]	β -arrestin-2 recruitment
		Multiplex CRE assay ^[72]	Transcription
	Microarray approach	Cell microarray ^[73]	Second messenger (Ca ²⁺)
		GPCR microarray ^[74]	Ligand binding
	Multiple distinguished fluorescent proteins	Multiplex fluorescent assay ^[75]	Second messenger (Ca ²⁺)
Multiple luminescence with spectral decomposition	Multiplex hexuple luciferase assaying ^[76]	Transcription	

Abbreviations: FRET, fluorescence resonance energy transfer; smFRET, single-molecule fluorescence resonance energy transfer; BRET, bioluminescence resonance energy transfer; EMTA, effector membrane translocation assay; ebBRET, enhanced bystander bioluminescence resonance energy transfer; TGF- α , transforming growth factor- α ; NGS, next generation sequencing; CRE, cAMP response element.

2.2.1 Singleplex assays

Singleplex assays can only generate one data point for a single measurement, whereas multiplex assays can generate more data points. The advantages of singleplex assays include easier design and implementation and a wider choice of detection methods.

For example, the split TEV GPCR β -arrestin-2 recruitment assay is originally a singleplex assay^[21, 67, 71, 77], which is based on β -arrestin-2 recruitment and relies on the functional complementation of TEV protease fragments (**Figure 5**). ARRB2 (β -arrestin-2) is a transducer for GPCRs. The tobacco etch virus (TEV) protease identifies a particular cleavage site and is split

into two fragments: N-terminal TEV (NTEV) and C-terminal TEV (CTEV). NTEV is fused to the C-terminus of GPCRs, whereas CTEV is linked to the C-terminus of ARRB2^[21, 67, 71]. Upon GPCR activation, the recruitment of ARRB2 leads to the proximity of NTEV and CTEV, and subsequently this complementation is functional, and the TEV protease can cut its specific cleavage site to release GV (GAL4-VP16, a synthetic co-transcriptional co-activator) to initiate transcription of the firefly luciferase, which can catalyse its substrates to release the luminescent photons as a quantitative readout (**Figure 5**)^[21, 67]. The luminescent photons from different samples have the same wavelength, so only one sample can be measured at a time. Therefore, the split TEV GPCR β -arrestin-2 recruitment assay is considered a singleplex assay, as are the other singleplex assays.

2.2.2 Multiplex assays

Multiplex assays can simultaneously generate multiple data points from a single measurement. In essence, both the diversity of the measured target and the detection method are the key determinants of whether an assay is multiplex or not. Barcodes, which are short stretches of nucleotides (DNA or RNA), can have exponentially high diversity due to the coexistence of 5 nucleobases, adenine, guanine, thymine (uracil), and cytosine in RNA or DNAs^[78]. NGS (next generation sequencing) can simultaneously detect the diversity of short barcodes. NGS is a technique that uses massively parallel or high-throughput sequencing to identify many DNA and RNA species simultaneously^[79]. The coexistence of artificial barcodes and NGS contributes to the realization of NGS-based multiplex assays.

Based on the monitoring levels, barcoded GPCR assays can be further divided into two types, such as barcoded GPCR receptor assays and barcoded GPCR pathway assays (**Figure 2**). Notably, because the reporter is the barcode that is expressed by transcription within the nuclei, both these barcoded GPCR assays are using a transcription-based readout. In other words, both the two barcode-based assays are reporter gene assays, which use a genetically encoded reporter to quantify altered transcription.

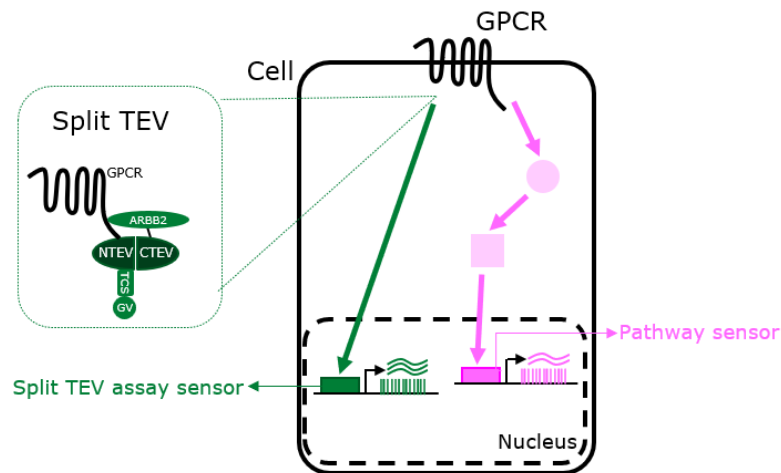


Figure 2. Comparison between the barcoded GPCR receptor assay and the barcoded GPCR pathway assay. Bar-coded GPCR receptor assays monitor the recruitment activity of GPCR transducers based on the split TEV GPCR β -arrestin-2 recruitment assay using a split TEV assay sensor. Barcoded GPCR pathway assays monitor gene transcription downstream of GPCR activation using a pathway sensor. Of note, both assays use genetically encoded barcodes as reporters and are transcription level assays. ARBB2, β -arrestin-2; NTEV, the N-terminal moiety of the TEV protease; CTEV, the C-terminal portion of the TEV protease; TCS, TEV protease cleavage site; GV, the synthetic co-transcriptional co-activator of GAL4-VP16.

2.2.2.1 Barcoded GPCR receptor assays

Barcoded GPCR receptor assays directly monitor the recruitment activity of GPCR transducers without considering their subsequent altered gene transduction. Theoretically, all three major GPCR transducers can be directly monitored with the barcoded GPCR receptor assays using the genetic barcode as an assay reporter, if the appropriate GPCR transducer recruitment assays are available^[71, 80], for example, the split TEV GPCR β -arrestin-2 recruitment assay can be modified to use the barcodes as its reporters (**Figure 2**) Galinski et al in this lab developed the first barcoded GPCR receptor assay in 2018, termed GPCRprofiler, using the split TEV GPCR β -arrestin-2 recruitment assay (**Table 4**)^[80]. The GPCRprofiler is a transient assay by transfecting GPCR and the β -arrestin-2 adapter plasmids into U2OS and PC12 cells. Transient assays can reduce reagent costs and assay time and are a good way to quickly provide proof of concept for a novel technique. However, their limitation is that numerous factors (such as day to day variations of transfection efficiency, cell line status/passage number, performance by different scientists) affect the efficiency of transient transfection, which can lead to low robustness^[81-84]. To eliminate, or at least minimize these constraints of using transient transfections, I stably integrated targets like GPCRs and RTKs into HEK293 cells.

2.2.2.2 Barcoded GPCR pathway assays

It is widely recognised that GPCR activation can modify gene transcription through cis-regulatory elements for transcription factors that are involved in downstream GPCR pathways (**Figure 1**), irrespective of the transducer pathways of GPCR activation^[64, 85]. Furthermore, the need to monitor multiple transcriptional events simultaneously has increased due to the recognition (e.g. HTR2A activation can alter both CRE- and NFAT-RE-regulated gene transcription in Figure 1), which motivated us to develop the multiplex barcoded GPCR pathway assays.

As a reporter gene assay, the barcoded GPCR pathway assay, as its name suggests, focuses on the downstream pathways of GPCR signalling, which are monitored as barcoded transcriptional readouts via the pathway sensors (**Figure 2**). Therefore, reporter gene assays, which can quantitatively measure the binding of transcription factors to their specific genomic response elements (i.e., the responsive cis-regulatory elements), offer the possibility of deciphering the various GPCR activations simultaneously^[86]. Furthermore, because the amplification effects of upstream pathways on gene transcription can amplify the distal magnitude of activity, the advantages of reporter gene assays include a wide linear dynamic range, high sensitivity (i.e., a large signal-to-background ratio) and low data variation, making it possible to detect weak GPCR agonists^[64].

In this project, I established cell lines containing the stably integrated GPCRs and infected barcoded sensors with lentiviral barcodes to monitor the activity of different GPCR signalling pathways, and we also developed the barcoding technique to quantitatively measure pathway signalling (**Figure 3**).

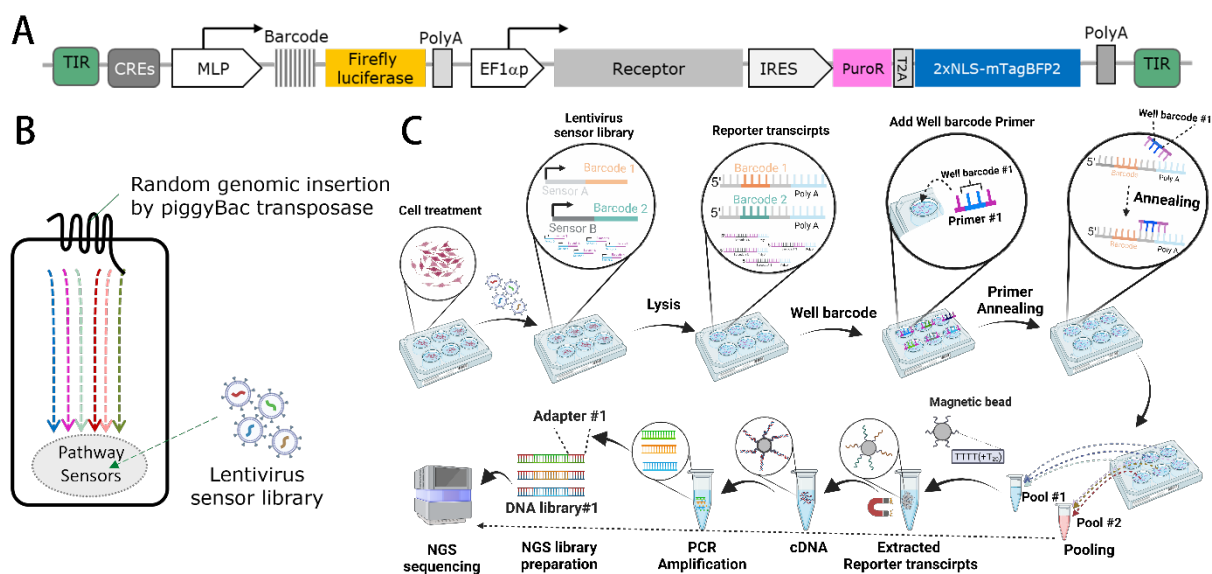


Figure 3. Schematic of the barcoded GPCR pathway assay. (A) The plasmid map for making stable cell lines with an integrated receptor and the barcoded sensor. TIR, terminal inverse repeats for the piggyBac transposon system. CREs, cis-regulatory elements, referred to as index sensors in this project; MLP, major late promoter of

adenovirus; IRES, internal ribosome entry site; T2A, Thosea asigna virus 2A peptide. (B) The goal of establishing a stable platform for barcoded GPCR pathway assays. (C) The workflow for barcode extraction, purification, and quantification. The barcodes are applied at three levels, such as sensor barcodes, well barcodes and pool barcodes.

The stable cell lines for six receptors (AVPR2, GLP1R, HTR2A, DRD1, ERBB4 and NTRK2) were established via co-transfecting two plasmids, containing a specific GPCR or RTK with a specific relevant sensor (called as the index sensor, which monitors the main pathway activity of a given GPCR or RTK) followed by two index reporters (firefly luciferase and barcodes) (**Figure 3**) and the piggyBac transposase individually (**Figure 6**). The firefly luciferase index reporters have been used to rapidly validate the functionality of established stable cell lines (**Figure 6**), while the index barcodes are used for multiplex assays (**Figure 8**).

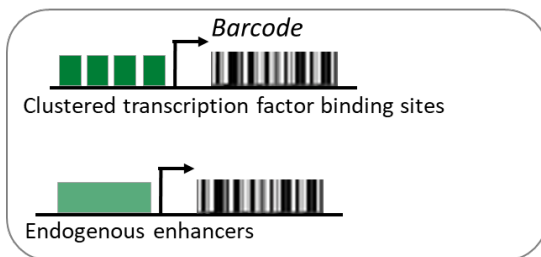
A single receptor per cell is randomly inserted into the cell genome by the piggyBac transposase, producing stable cells with multiple copies. Notably, multi-copy integration of GPCRs was found to be essential for GPCR activation^[72].

2.2.2.3 Cis-regulatory elements

Cis-regulatory elements can activate transcription within a specific spatial and/or temporal expression domain, which can be subdivided into transcription factor binding sites (TFBSs) and other non-coding DNA^[87]. Cis-regulatory elements associated with transcriptional regulation have been identified as playing a particularly central role in gene regulation. Cell type-specific gene expression profiles are mainly determined by these cis-regulatory elements on the chromosome. Reporter-based assays are the most common methods for identifying a given DNA sequence to act as an enhancer^[88] To date, 1,063,878 human sequences have been analysed as candidate cis-regulatory elements based on the Encyclopedia of DNA Elements (ENCODE) data, which indicates that the number of cis-regulatory elements is greater than the number of coding genes^[87].

For a proof of concept in this project, we have chosen 31 sensors that either consist of cis-regulatory elements linked to a minimal promoter or endogenous promoter sequences (**Table 5**). A minimal promoter was used as an internal control (**Table 5**). These sensors are endogenously responsive to various physiological and pathological pathways (**Figure 4**). We have compiled these 31 sensors and the internal control to create a lentivirus-based library, which we then used to infect HEK293 cells. The info of the lentivirus-based library is listed in **Table 5**.

A Two types of Cis-regulatory elements



B

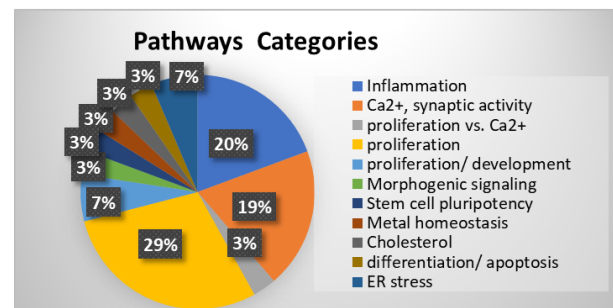


Figure 4. This project explores various pathways associated with two types of cis-regulatory elements. (A) The lentivirus-based library contains two types of cis-regulatory elements, followed by a minimal promoter and a barcode reporter. **(B)** This pie chart shows the corresponding pathways monitored by the 31 selected cis-regulatory elements.

Table 5. Information on the 31 cis-regulatory elements.

Name	Global Category	Category	Pathway	Barcodes
MLP	background control			*4
IL6p	Immune response	Inflammation	Inflammation/ DEG response	*2
IL8p	Immune response	Inflammation	Inflammation/ DEG response	*2
NFKB-RE_v2	Immune response	Inflammation	Inflammation/ DEG response	*2
TNFAp	2nd messenger	Ca2+, synaptic activity	cAMP - PKA	*2
CRE	2nd messenger	Ca2+, synaptic activity	cAMP, Ca2+	*2
UPRE_v2	2nd messenger	Ca2+, synaptic activity	cAMP, Ca2+	*2
SARE	2nd messenger	Ca2+, synaptic activity	Ca2+, cAMP, SRF	*2
NR4A1p	Cell cycle/ fate	proliferation vs. Ca2+	MAPK, SRE vs. Ca2+	*2
EGR1p	Cell cycle/ fate	proliferation	MAPK/ IEG response	*2
FOSBp	Cell cycle/ fate	proliferation	MAPK/ IEG response	*2
TEAD-RE_v4	Cell cycle/ fate	proliferation/ development	Hippo - YAP1/TAZ	*2
hCTGFp	Cell cycle/ fate	proliferation/ development	Hippo - YAP1/TAZ	*2
Wnt-RE	Cell cycle/ fate	Morphogenic signalling	Wnt - beta-catenin	*2
SRE	Cell cycle/ fate	proliferation	MAPK / IEG response	*2
OCT4-RE	Cell cycle/ fate	Stem cell pluripotency	OCT4-SOX2-Nanog	*2
AP1_v1	Cell cycle/ fate	proliferation	MAPK/ IEG response	*2
DUSP5p	Cell cycle/ fate	proliferation	MAPK/ DEG response	*2
EGR2p	Cell cycle/ fate	proliferation	MAPK/ IEG response	*2
FOSp	Cell cycle/ fate	proliferation	MAPK/ IEG response	*2
MRE	Metabolism	Metal homeostasis	metal homeostasis	*2
SREBP-RE_v2	Metabolism	Cholesterol	cholesterol, insulin	*2
E2F-RE_v2	Cell cycle/ fate	differentiation/ apoptosis	G1/S Check Point	*2
EIF2AK2p	Immune response	Inflammation	JAK - STAT	*2
DUSP1p	Cell cycle/ fate	proliferation	MAPK/ DEG response	*2
6xNFAT	2nd messenger	Ca2+, synaptic activity	Ca2+	*2
HSE	Metabolism	ER stress	heat shock	*2
HSPA1Ap	Metabolism	ER stress	heat shock	*2
SRF-RE_v2	Cell cycle/ fate	proliferation	MAPK/ IEG response	*2
MEF2-RE	2nd messenger	Ca2+, synaptic activity	Ca2+	*2
IL2p	Immune response	Inflammation	Inflammation/ DEG response	*1
IL17Ap	Immune response	Inflammation	Inflammation/ DEG response	*1

Note: The adenovirus major late promoter (MLP) is a minimal promoter that drives a constitutively expressed barcode, serving as an internal control for quantification to resolve false positive reads. The Barcodes column displays the number of barcodes applied to each cis-regulatory element.

3. Own contribution to the original research papers

3.1 Contribution to paper I

The paper I, published in *Biosensors*, was on the improvement of split TEV GPCR β -arrestin-2 recruitment assays using the signal peptide (SP) and the C-terminal tail of the vasopressin 2 receptor (AVPR2; V2R tail), where we identified the best combination of the signal peptide and the β -arrestin binding motif for six GPCRs (DRD1, DRD2, HTR2A, AVPR2, GCGR and GLP1R) in four cell types (HEK293, PC12 Tet-off, U2-OS and HeLa).

I optimized the protocol of the luciferase assay itself using the reverse pipetting technique, which reduced the variability of the assay and increased its robustness. As a result, a high robustness was achieved across all luciferase assays, and we can use these data to easily draw solid conclusions.

Either a SP at the 5' end or a V2R tail at the 3' end was added to each GPCR, and four combinations per GPCR were generated, such as native, native with the SP, native with the V2R tail, and native with both the SP and the V2R tail. Therefore, for each GPCR assay, one plasmid was constructed, resulting in 24 plasmids in total. All 24 assays were conducted per cell line tested. To validate their expression stability, I performed Western blotting after transfecting each of these plasmids into the HEK293 cells. To validate their expression locations, I transfected them and performed immunocytochemistry stainings (ICCs) with or without permeabilization with 0.1% Triton X-100 using the antibodies against the extracellularly expressed FLAG and the intracellularly expressed 2xHA tag, and then imaged them using fluorescence microscopy. For the firefly assays, I made transfection mixes with the corresponding reporter plasmid (containing the UAS firefly luciferase cassette) and the transfection efficiency control plasmid (containing the nuclear EYFP) for subsequent convenient transfections. These 24 transfection mixtures were then applied to the four cell types to test cell line-dependent performance.

To show the workload of the luciferase assay in this paper, the number of data points is a good indicator. As there were four cell types, the total number of experimental conditions (i.e. experimental units^[89-90]) was 96 ($24 \times 4 = 96$). To increase the statistical power, I used six replicates and generated 576 ($96 \times 6 = 576$) data points. From these 576 data points, two types of data were calculated, such as fold changes and Z'-factor, which were used to assess the assay window and assay robustness. Furthermore, in terms of data presentation, I summarized these 192 ($96 \times 2 = 192$) individual calculated data points into a table to clearly show the results, and this table is labelled as Table 1 in this paper.

Finally, I performed dose-response assays in HEK293 cells transfected with GCGR and GLP1R constructs to compare the target-based split TEV assays with the cellular cAMP pathway assay. After I finished the data analysis, Michael Wehr, my supervisor, and I contributed to the interpretation of the data.

The manuscript was written in collaboration with Michael Wehr, who guided the study.

3.2 Contribution to paper II

Paper II, published in *Cellular Signalling*, identified TAOK2 (thousand-one-amino-acid kinase 2) as a key modulator of the Hippo signalling pathway, which limits cell growth. TAOK2 was retrieved as a key candidate from a split TEV based protein-protein interaction screen and was shown to modulate the activity of the core kinase cassette kinases STK3/4 and LATS1/2, as well as the anti-apoptotic transcriptional co-activator Yes1 associated transcriptional regulator (YAP1), the key downstream target of the pathway. In Hippo signalling, YAP1 is inactivated by cytoplasmic retention through upstream-mediated phosphorylation. In other words, once phosphorylated, YAP1 moves from the nucleus to the cytoplasm.

To confirm that TAOK2 can contribute to the redistribution of YAP1 from the nucleus to the cytoplasm, I performed ICC in HEK293 cells with stably integrated doxycycline-inducible TAOK2 (HEK293_TAOK2-dox cells) at low density (i.e. 20,000 cells per 24-well). As high cell densities can activate the Hippo pathway leading to YAP1 redistribution to the cytosol, a rather low cell density was aimed for assessing the TAOK2's effect on YAP1 distribution. Therefore, the seeding density was also optimised to avoid activation without adding doxycycline and to remain sufficient after the complex and harsh staining procedures. In order to achieve these two goals simultaneously, I tested several seeding cell numbers per 24-well, such as 10000, 20000, 50000 and 100000 cells per 24-well, and then decided to use 20000 cells as the final density for ICC staining, where the cell confluence was 10% when the fixation with 4% paraformaldehyde for 10 min was initiated. Under these conditions, TAOK2 overexpression resulted in the nuclear YAP1 staining. This ICC staining result is shown in **Figure 2G** of this paper.

Likewise, we assessed the effect of TAOK2 knockdown on Hippo signalling, including YAP1 distribution. To confirm the effect of TAOK2 inactivation on YAP1 localisation, I seeded 10000 HEK293 cells stably carrying a dead Cas9 gene fused to a ZIM3-KRAB domain and the CRISPRi sgRNA #3 for TAOK2 knockdown (HEK293_sgTAOK2i cells) per 24-well plate at high density. Cells were cultured for 24 hours to 50% confluence and then fixed with 4% paraformaldehyde for 10 minutes. In this case, the phenotypic distribution of YAP1 was suppressed. The results are shown in Figure 3E.

After identifying that TAOK2 can limit the growth of HEK293 cells, I confirmed that the growth-limiting effects also exist in human cancer cell lines. To conduct proliferation assays using the Cell Counting Kit-8 (CCK8), I established two stable cell lines by transducing lentivirus containing doxycycline-inducible TAOK2 into A549 (human lung cancer) and U-138 cells (human glioblastoma). Subsequently, I performed CCK8 assays with these two stable cell lines. The results of the proliferation assays are displayed in Figure 6A and D, and Figure S6A and D.

In addition to the above, I prepared all the lysates for Western blotting shown in Figure 2O and P, in Figure 6B, C, E and F, in Figure S6, as well as in Figure S5C and D.

To confirm that TAOK2 can increase p-LATS1 without STK3/4 in HEK293 cells is displayed in Figure 2O and P. Figure S6B, C, E and F display that 8 hours were a suitable time for doxycycline induction in A549 and U-138 cells. Furthermore, Figure 6B, C, E, and F confirmed that TAOK2 can increase p-LATS1 in A549 and U-138 cells. Figure S5C and D show the redundancy between TAOK2 and TAOK1/3. For clarity and comprehension, I have summarised the details of the 24 cell lines used, including their function and culture information, in Table S6.

The manuscript was written in collaboration with Michael Wehr, and my co-authors Xiao Ma and Fiona Mandausch. Michael Wehr guided the study.

3.3 Contribution to paper III

In paper III, published in *iScience*, we developed a transfection-based multilevel barcoded reporter assay to assess activities of ERBB receptors that can be monitored both at the receptor level using the split TEV technique and at the pathway level using pathway sensors. We used this assay to profile known ERBB antagonists. Furthermore, we identified two new ERBB4 selective antagonists representing promising lead compounds.

In this paper, I prepared the various plasmids for transfections to perform the multiplex profiling assays and I performed singleplex dose-response luciferase assays to validate several findings from the multiplex profiling assays. I also contributed to the discussion and writing of the paper. The remaining experimental work was mainly conducted by the first author, Luksa Popovic. The study was directed by Michael Wehr.

4. Results

4.1 Summary of published results

In the first publication, I optimized the split TEV GPCR β -arrestin-2 recruitment assays for six GPCRs implicated in SCZ, Parkinson's disease, diabetes mellitus, obesity, etc. in four different cell backgrounds. The effects of the signal peptide (SP) and the C-terminal tail of the vasopressin 2 receptor (AVPR2; V2R tail) attached to GPCRs were tested in the split TEV GPCR β -arrestin-2 recruitment assay, which we call the improved split TEV GPCR β -arrestin-2 recruitment assay (**Figure 5**).

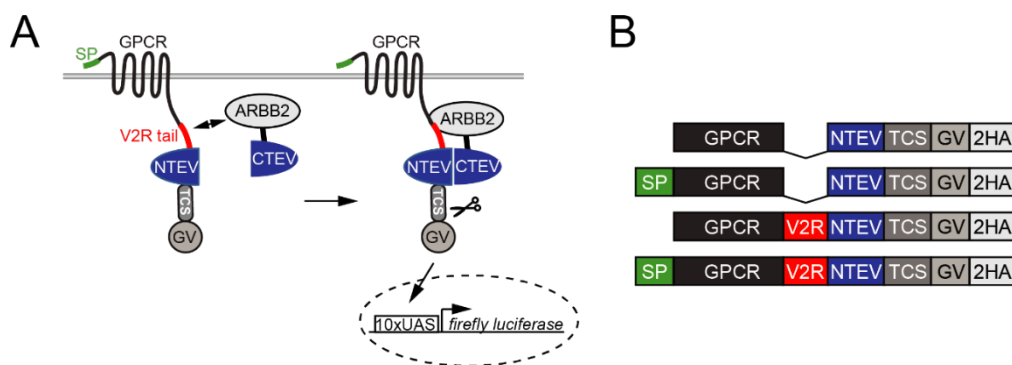


Figure 5. Diagram of the improved split TEV GPCR β -arrestin-2 recruitment assay. (A) To test the performance of the assay, a GPCR could be fused to the signal peptide (SP) and/or the tail of the vasopressin receptor 2 (V2R). (B) This is a graphical representation of the split TEV GPCR fusions. ARRB2 refers to β -arrestin-2, while TCS stands for TEV protease cleavage site. NTEV is the N-terminal moiety of the TEV protease. CTEV is the C-terminal portion of the TEV protease. GV is for the synthetic co-transcriptional co-activator of GAL4-VP16. UAS is for the clustered upstream activated sequences. (Taken from Wu et al., 2022^[21])

It was discovered that the performance of the assay varied significantly for each GPCR variant and was dependent on the cell line used. I also found that HEK293 cells provided the best performance for most of these GPCRs, except for HTR2A. In particular, DRD2 activity can be monitored with high dynamic range and robustness in HEK293, which is particularly important when suitable cis-regulatory elements cannot be used to monitor DRD2-altered gene transcription downstream.

In the second publication, we developed a genetically encoded split TEV technique to quantify protein-protein interactions within the Hippo signalling pathway and identified the central role of TAOK2 in this pathway. The success of the protein-protein interaction screening further demonstrates that split TEV-based methods can provide high sensitivity and fidelity to elucidate functions of proteins in vivo.

In the third published paper, we developed a barcoded assay for ERBB receptor tyrosine kinases, called ERBBprofiler, to monitor both ERBB receptor activities via split TEV and ERBB downstream pathway activities via cis-regulatory elements. All four ERBB receptors such as

EGFR, ERBB2/3 and ERBB4 were included in this assay. HTR2A was used as a control assay for an unrelated target, as it is a GPCR. We used the ERBBprofiler to profile eight established ERBB antagonists, confirming known effects and providing previously unreported properties, such as pyrotinib's preference for ERBB4 over EGFR.

The three published papers provided a solid foundation for the development of the barcoded GPCR pathway assay, where we can either use the split TEV technique to monitor GPCRs without identified relevant cis-regulatory elements such as DRD2 or use multiple cis-regulatory elements within a cell to achieve multiplex profiling of GPCRs.

4.2 High robustness and sensitivity of the established stable cell lines with luciferase assays

Prior to generating the stable cell lines for AVPR2, GLP1R, HTR2A, DRD1, DRD2, ERBB4 and NTRK2, their responsive index sensors were selected. The cAMP response element (CRE) was used as the index sensor for AVPR2, GLP1R, HTR2A and DRD1, and the promoter of the early growth response protein 1 gene (EGR1p) was used as the index sensor for ERBB4 and NTRK2. DRD2 is coupled to Gi/o proteins, and HEK293 has been reported to be able to monitor Gi/o protein activation in a $\beta\gamma$ dimeric complex-dependent manner, so I transiently transfected five individual sensors associated with Gi/o or $\beta\gamma$ dimeric complex-related pathways into HEK293 to determine if DRD2 activity could be monitored^[85]. However, no suitable sensors were identified for DRD2 (**Figure 6A**).

The plasmids containing a specific GPCR or RTK with a specific index sensor plus reporters (**Figure 3**) were co-transfected with the piggyBac transposase plasmid to generate stable cell lines (**Figure 6B**). After stable transfection, single cell clones were picked up to proliferate for the subsequent validations. To validate the GPCR expression characteristics, the intensity of blue fluorescent protein was imaged by fluorescence microscopy and the expression of HA-tag was checked by Western blotting, and their surface expression was validated by ICC (**Figure 6C**). For functional validation of the cell clones, the endpoint luciferase assays were used to check the robustness with Z'-factors and the sensitivity with agonist-induced fold changes (**Figure 6C and 6D**), and the specificity of the cell clones was validated with both agonist and antagonist dose-response curves (**Figure 6C**).

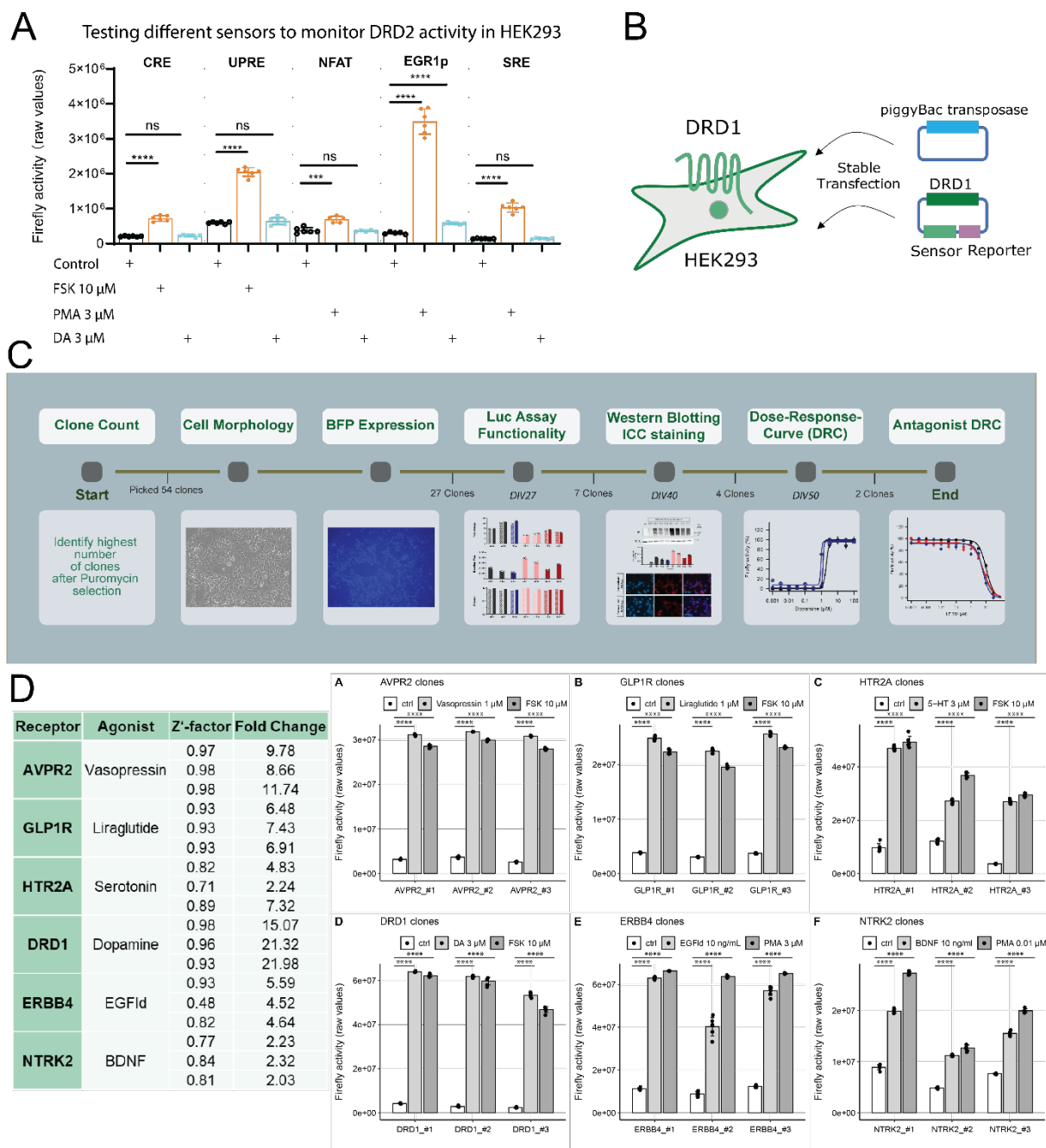


Figure 6. Generation of stable cell lines. (A) Five individual sensors with DRD2 were transiently transfected into HEK293. Forskolin (FSK) and phorbol 12-myristate 13-acetate (PMA) were used to activate the corresponding sensors as a positive control. Notably, only EGR1p gave a response with a 1.9-fold change, which is empirically not enough for generating functional stable cell lines. CRE, cyclic AMP response element; UPRE, unfolded protein response element; NFAT, the nuclear factor of activated T-cells; EGR1p, the promoter of the early growth response protein 1 gene; SRE, the serum response element. (B) Generation of stable cell lines by co-transfection (with DRD1 as example). (C) The workflow for generating and validating stable cell lines with DRD1 as an example. (D) High robustness and sensitivity of the established stable cell lines with luciferase assays. Z'-factor represents the assay's robustness with the range $(-\infty, 1]$, and the values larger than 0.5 indicate robust assays. BDNF, brain-derived neurotrophic factor; Ctrl, control; DA, dopamine; EGFId, epidermal growth factor-like domain. The statistical test used was ordinary one-way ANOVA and Dunnett's multiple comparison test. ns, not significant; ****, p-values are less than 0.0001.

4.3 Results on the barcoded GPCR profiling platform

4.3.1 The barcoded pathway assays exhibit high robustness and reproducibility

To ensure comparability within and between the barcoded pathway assays, it is essential to identify and consistently use positive control ligands throughout platform development^[91]. In this study, I utilized forskolin (FSK; 10 μ M) and phorbol 12-myristate 13-acetate (PMA; 3 μ M) as the positive control ligands. In HEK293 and HeLa cells, FSK stimulates adenylyl cyclase, resulting in an increase in intracellular cAMP levels^[92], and PMA activates protein kinase C, leading to the activation of both the JNK and ERK pathways^[93]. Both FSK and PMA induce gene expression by altering gene transcription.

The performance of the barcode pathway assays was initially tested by introducing only the lentivirus-based sensor library into the HEK293 cells without integrated GPCRs or RTKs (**Figure 7A**). To assess the robustness of the lentivirus-based sensor library, I tested four vessel formats and three MOIs (multiplicity of infection). I observed a repeated response pattern across each vessel format, as shown in **Figure 7B**. To test reproducibility, I repeated the same assay condition (i.e., using 96-well plates with an MOI of 2000 of the sensor library) seven times on different days (**Figure 7C**). The responses of each sensor to FSK or PMA stimulation from the seven batch tests showed a high degree of consistency, as shown by two boxplots (**Figure 7C**).

4.3.2 Crosstalk at the pool barcode level may cause a problem

After confirming the stable performance of the barcode pathway assays, I tested the barcoded GPCR pathway assays. In this assay, both the receptors and the lentivirus-based sensor library were introduced into the HEK293 cells (**Figure 8A**). **Figure 8B** shows the three levels of barcodes, such as sensor level, well level and pool level. Regrettably, there was clear crosstalk at the pool barcode level between pools (**Figure 8C**). The crosstalk was also accompanied by the so-called read-eating effects, a phenomenon in NGS where highly enriched barcodes use most of the allocated sequencing depth, leaving the less frequent barcodes underrepresented in the final readout. Therefore, sequencing data of the barcoded GPCR pathway assay indicates that the index barcodes (introduced by piggyBac transposon system) had much higher expression levels than those of the lentivirus-introduced barcodes (**Figure 8C**).

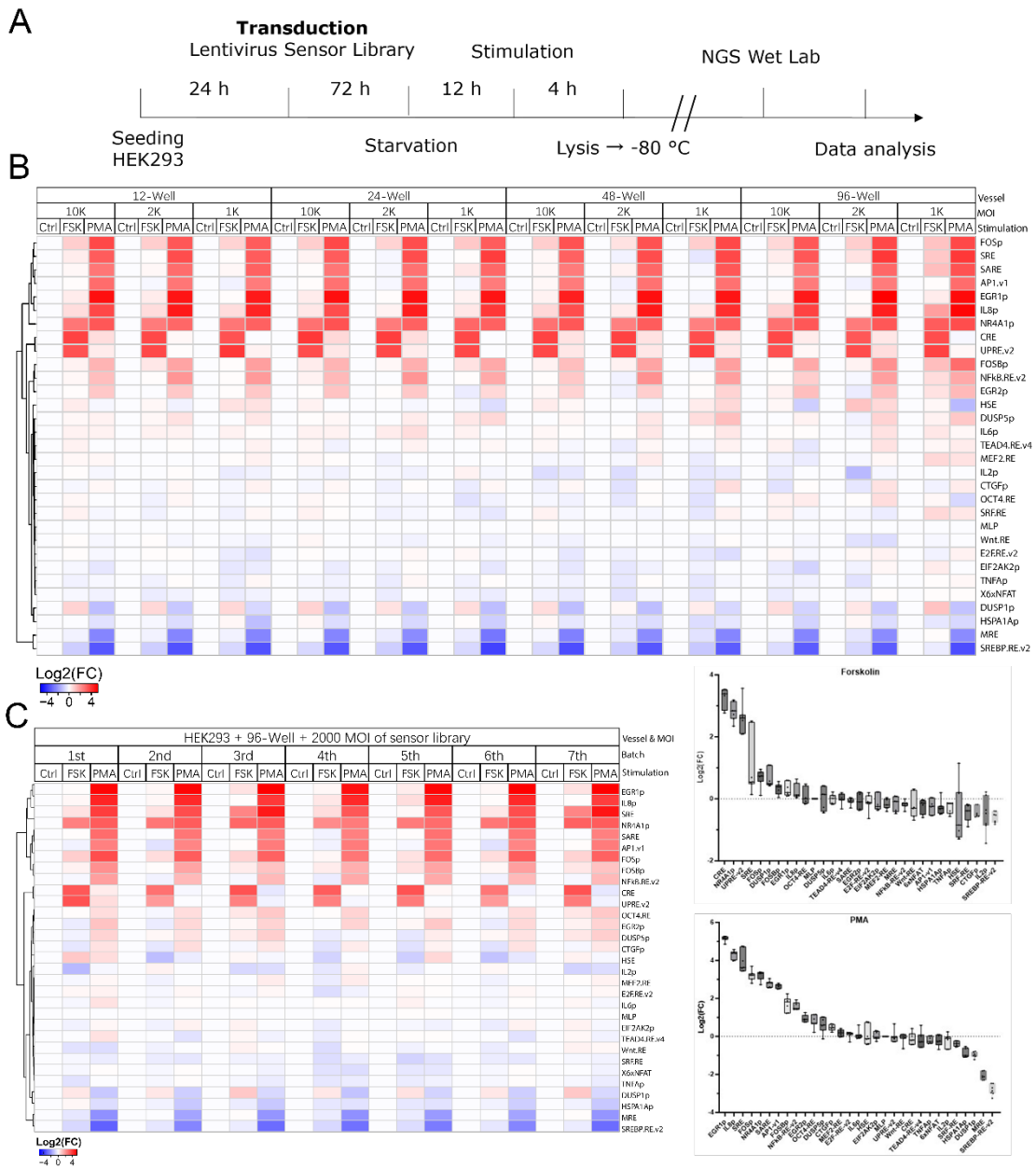


Figure 7. The barcoded pathway assays exhibit high levels of robustness and reproducibility. (A) The time-line for the barcoded pathway assays. (B) The heatmap demonstrates the consistent performance of the assays across different vessel formats and various MOIs with four replicates. (C) Both a heatmap and boxplots illustrate the high reproducibility of the assays, with the same condition repeated seven times with 4 to 8 replicates on different days. The boxplots display 7 individually extracted data points from the heatmap for both FSK and PMA stimulation. The sensors were sorted by decreasing log₂-scaled fold changes, and the inverse induction was also measured. It should be noted that the IL17Ap sensor activity was not detected and, therefore, its readings were excluded. Ctrl, control; FSK, forskolin; PMA, phorbol 12-myristate 13-acetate.

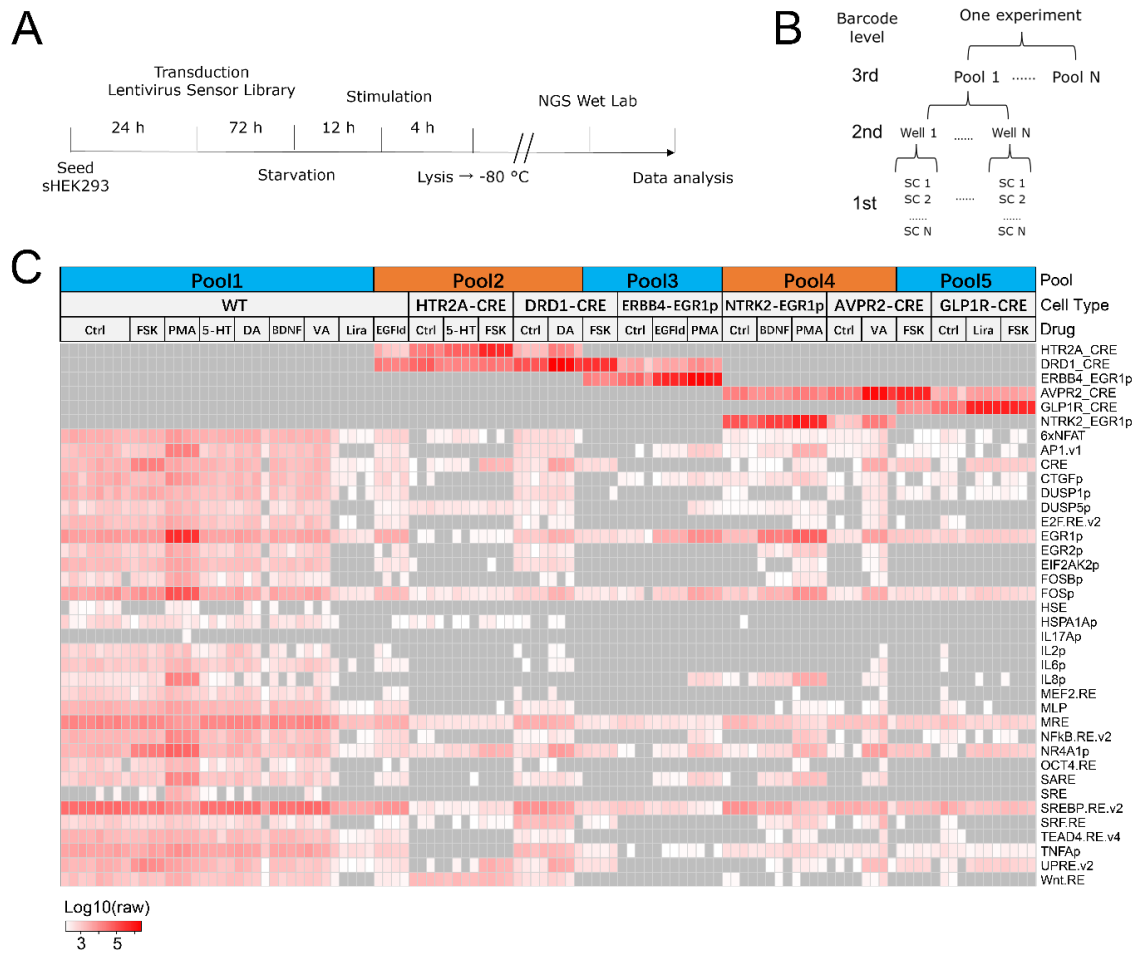


Figure 8. Crosstalk occurs at the pool barcode level. (A) The timeline for the barcoded GPCR pathway assays is presented. The term sHEK293 refers to stable cells that contain either a specific GPCR or RTK. (B) The barcoded GPCR pathway assays employ three levels of barcodes: sensor barcodes, well barcodes, and pool barcodes. The sensor barcode is abbreviated as SC. (C) Crosstalk and read-eating effects. The assay was conducted in a 96-well plate with a 2000 MOI with 4 to 8 replicates. Squares with a grey colour indicate raw reads lower than 100, and their corresponding values are considered missing. The initial barcode level encoded the sensor barcodes within each well of the 96-well plate. The raw reads are represented by the colour in each square of the heatmap. The second barcode level encoded each well on the 96-well plate, i.e., it coded each column of the heatmap. The pools were labelled on the top row of the heatmap using the third barcode level for coding. The index barcode raw reads for each cell type are displayed in the first six rows individually. In general, the index barcode should be specific to each cell type. However, crosstalk occurred between cell types within each pool. BDNF, brain-derived neurotrophic factor; Ctrl, control; DA, dopamine; EGFId, epidermal growth factor-like domain; FSK, forskolin; Lira, liraglutide; PMA, phorbol 12-myristate 13-acetate; VA, vasopressin.

5. Paper I

Improved Split TEV GPCR β -arrestin-2 Recruitment Assays via Systematic Analysis of Signal Peptide and β -arrestin Binding Motif Variants¹

Authors:

Yuxin Wu^{1,#}, Isabelle V. von Hauff^{1,#}, Niels Jensen², Moritz J. Rossner^{2,3}, Michael C. Wehr^{1,3,*}

Affiliations:

¹ Research Group Cell Signalling, Department of Psychiatry, Ludwig Maximilian University of Munich, Nussbaumstr. 7, 80336 Munich, Germany

² Section of Molecular Neurobiology, Department of Psychiatry, Ludwig Maximilian University of Munich, Nussbaumstr. 7, 80336 Munich, Germany

³ Systasy Bioscience GmbH, Balanstr. 6, 81699 Munich, Germany



These authors contributed equally to this work.

* Correspondence: Michael C. Wehr, Michael.Wehr@med.uni-muenchen.de

¹ Wu Y, von Hauff IV, Jensen N, Rossner MJ, Wehr MC. Improved Split TEV GPCR β -arrestin-2 Recruitment Assays via Systematic Analysis of Signal Peptide and β -arrestin Binding Motif Variants. Biosensors. 2023;13(1). <https://doi.org/10.3390/bios13010048>.

Article

Improved Split TEV GPCR β -arrestin-2 Recruitment Assays via Systematic Analysis of Signal Peptide and β -arrestin Binding Motif Variants

Yuxin Wu ^{1,†}, Isabelle V. von Hauff ^{1,†}, Niels Jensen ², Moritz J. Rossner ^{2,3}  and Michael C. Wehr ^{1,3,*} 

¹ Research Group Cell Signalling, Department of Psychiatry and Psychotherapy, University Hospital, Ludwig Maximilian University of Munich, Nussbaumstr. 7, 80336 Munich, Germany

² Section of Molecular Neurobiology, Department of Psychiatry and Psychotherapy, University Hospital, Ludwig Maximilian University of Munich, Nussbaumstr. 7, 80336 Munich, Germany

³ Systasy Bioscience GmbH, Balanstr. 6, 81699 Munich, Germany

* Correspondence: michael.wehr@med.uni-muenchen.de

† These authors contributed equally to this work.

Abstract: G protein-coupled receptors (GPCRs) are major disease-relevant drug targets; robust monitoring of their activities upon drug treatment is key to drug discovery. The split TEV cell-based assay technique monitors the interaction of an activated GPCR with β -arrestin-2 through TEV protein fragment complementation using a luminescent signal as the readout. In this work, split TEV GPCR β -arrestin-2 recruitment assays were optimized to monitor the endogenous ligand-induced activities of six GPCRs (DRD1, DRD2, HTR2A, GCGR, AVPR2, and GLP1R). Each GPCR was tested in four forms; i.e., its wildtype form, a variant with a signal peptide (SP) to facilitate receptor expression, a variant containing the C-terminal tail from the V2 vasopressin receptor (V2R tail) to promote β -arrestin-2 recruitment, and a variant containing both the SP and V2R tail. These 24 GPCR variants were systematically tested for assay performance in four cell lines (HEK-293, PC12 Tet-Off, U-2 OS, and HeLa). We found that the assay performance differed significantly for each GPCR variant and was dependent on the cell line. We found that V2R improved the DRD2 split TEV assays and that HEK-293 cells were the preferred cell line across the GPCRs tested. When taking these considerations into account, the defined selection of assay modifications and conditions may improve the performance of drug development campaigns that apply the split TEV technique as a screening tool.

Keywords: GPCR; drug screening; drug discovery; cell-based assay; split TEV technique



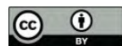
Citation: Wu, Y.; von Hauff, I.V.; Jensen, N.; Rossner, M.J.; Wehr, M.C. Improved Split TEV GPCR β -arrestin-2 Recruitment Assays via Systematic Analysis of Signal Peptide and β -arrestin Binding Motif Variants. *Biosensors* **2023**, *13*, 48. <https://doi.org/10.3390/bios13010048>

Received: 14 November 2022

Revised: 21 December 2022

Accepted: 25 December 2022

Published: 29 December 2022



Copyright: © 2022 by the authors. Licensee MDPI, Basel, Switzerland. This article is an open access article distributed under the terms and conditions of the Creative Commons Attribution (CC BY) license (<https://creativecommons.org/licenses/by/4.0/>).

1. Introduction

G protein-coupled receptors (GPCRs), which constitute the largest class of cell surface receptors, regulate various biological processes in health and disease, including the proliferation and differentiation of cells, neuronal activity, immune response, hormonal modulation, vision, taste, and smell [1,2]. Abnormal GPCR activity and altered downstream cellular signaling is implicated in various human diseases such as cancer and diabetes as well as in neurological and psychiatric disorders, including schizophrenia [3,4]. Because GPCRs have critical roles in the pathophysiology of many complex diseases, they are key drug targets. Consequently, GPCRs are currently targeted by 33% of all marketed drugs, which makes them the largest druggable class of receptors [5].

GPCRs are seven-transmembrane receptors that have three intracellular loops and a C-terminal tail for transducing cellular signals [1]. G proteins and β -arrestins can bind to those intracellular regions of GPCRs, thereby constituting options for biased signaling [6,7]. The previously canonical signaling route is via G proteins that can be categorized into stimulating or inhibitory effectors that initiate specific downstream signaling events such as cAMP-mediated or calcium-dependent pathways [8]. Activation of GPCRs causes the G

protein-dependent phosphorylation of the C-terminal tail by G protein-coupled receptor kinases (GRKs), which provides docking sites for β -arrestins. Arrestin recruitment to the GPCR leads to the desensitization of the primary signaling response by internalizing the GPCR/ β -arrestin complex and initiates cellular signaling responses that include the activation of ERK signaling. Importantly, G protein- vs. β -arrestin-mediated signaling, also known as biased signaling, defines the physiological response of an activated GPCR [8,9]. While, for example, G α s proteins link GPCR activity to increased cAMP signaling, activated β -arrestins initiate mitogen-activated protein kinase (MAPK) signaling cascades. In addition, by deciphering these mechanisms of cellular signaling, there is the opportunity to create better drugs with fewer side effects [10].

In drug discovery, cell-based assays are often applied for GPCR-targeting drugs [11]. For example, the activity of GPCRs can be monitored via genetically encoded reporter gene assays: either indirectly using pathway assays such as CREB responsive element (CRE) assays that depend on cAMP and calcium levels [12] or directly using target-based assays that are based on β -arrestin-2 recruitment and rely on proximity [13,14]. One type of such a GPCR/ β -arrestin-2 recruitment assay is based on the split TEV assay, which is based on the functional complementation of TEV protease fragments [15,16]. When brought into proximity, the TEV protease fragments functionally complement to form an active protease and release a GPCR-anchored transcriptional co-activator that migrates into the nucleus to initiate a reporter gene of choice such as firefly luciferase. Whereas CRE pathway assays use the physiology of the cell and depend on intracellular cAMP levels, target-based assays such as the split TEV assay enable the direct monitoring of GPCR activity. The C-terminal intracellular domain of the vasopressin receptor 2 (V2R tail, amino acids 343–371) contains 11 serine and threonine residues that can be phosphorylated by GRKs and constitutes a docking site for β -arrestin-2. The V2R tail has been shown to promote assay performance for full-length TEV GPCR/ β -arrestin-2 recruitment assays [17]. Therefore, the V2R tail has also been applied to split TEV GPCR assays [15,16]. Furthermore, the fusion of a cleavable signal peptide (SP) derived from influenza virus hemagglutinin to the N-terminal end of a GPCR was reported to enhance surface expression and to be beneficial for assay performance [18].

Here, we describe a systematic approach to develop sensitive and robust target-based split TEV assays for GPCRs in which we measured whether an additional artificial SP and/or the V2R tail fused to a GPCR improved assay performance. We applied this approach to six GPCRs of various subfamilies, including class A receptors (the dopamine receptors DRD1 and DRD2, serotonin receptor 2A (HTR2A), and vasopressin receptor 2 (AVPR2)) and class B receptors (the glucagon receptor (GCGR) and glucagon-like peptide 1 receptor (GLP1R)). In addition, we tested assay performances in various cell lines used for GPCR biology, including HEK-293, U2-OS, HeLa, and PC12 Tet-Off (PC12-TO) cells. We found that it was critical to test whether the addition of the artificial SP and/or the V2R tail helped to establish a sensitive and robust assay in a given cell line because in most cases, the addition of either the SP or V2R tail compromised the assay performance as measured by the fold change and the Z' factor [19]. DRD2 assays benefited from the addition of the V2R tail to improve the assay performance in HEK-293 cells. In contrast, for the other GPCRs tested, the fusion of the SP had a negligible effect on the assay performance. In addition, we found that the cell line of choice was critical for a given split TEV GPCR assay.

2. Materials and Methods

2.1. Plasmids

The GPCR ORFs were amplified via PCR using the Q5 High-Fidelity DNA Polymerase (NEB), and the resulting PCR was BP-recombined into the pDONR/Zeo plasmid using Gateway recombination cloning (Thermo Fisher Scientific, Waltham, MA, USA). Each entry clone plasmid was control-digested using BsrGI, which cut inside the recombination sequences and thus released the insert. Lastly, the GPCR ORF sequences were verified via Sanger sequencing. Gateway LR recombination was used to transfer the ORFs from the

entry vectors into the split TEV destination vectors (either pcDNA3_attR1-ORF-attR2-NTEV-TCS-GV-2xHA_DEST or pcDNA3_attR1-ORF-attR2-V2R-NTEV-TCS-GV-2xHA_DEST). The signal peptide (SP; peptide sequence: MKTIIALSYIFCLVFA↓DYKDDDDASID, cleavage site indicated by the arrow) derived from hemagglutinin [13] was added via 2-step PCR to the GPCR ORFs. Gateway entry clones for DRD2, HTR2A, and AVPR2 without SP, as well as the Gateway expression clone for ARBB2-CTEV (pcDNA3.1_Zeo_ARRB2-1-383-CTEV-2xHA), were described previously [16]. The Gateway entry clone for GLP1R was obtained from Harvard PlasmID (pENTR223-1_GLP1R_Cop, HsCD00082670). The plasmids used in this study are listed in Supplementary Table S1 and are available at Addgene. The oligos used for cloning are listed in Supplementary Table S2.

2.2. Compounds

The dopamine hydrochloride, [Arg8]-vasopressin acetate salt, and glucagon were purchased from Sigma-Aldrich (St. Louis, MO, USA). The serotonin hydrochloride was obtained from Tocris. The liraglutide (NN2211) was purchased from Selleck Chemicals (Houston, TX, USA).

2.3. Cell Culture

The HEK-293 (ATCC, CRL-1573) and HeLa (ATCC, CCL-2) cells were cultured in DMEM (4.5 g/L glucose, Thermo Fisher Scientific) supplemented with 2 mM GlutaMAX (Thermo Fisher Scientific), 10% FCS (Thermo Fisher Scientific), 100 U/mL of penicillin, and 100 µg/mL of streptomycin (Thermo Fisher Scientific). The PC12 Tet-Off cells (Clontech, 631134; PC12-TO) were maintained in DMEM medium (1 g/L glucose, Thermo Fisher Scientific) supplemented with 10% FCS, 5% horse serum (HS), 2 mM GlutaMAX, 100 U/mL penicillin, and 100 µg/mL streptomycin (all Thermo Fisher Scientific). The osteosarcoma U-2 OS cells (ATCC, HTB-96) were cultured in McCoy's 5A (Modified) Medium supplemented with GlutaMAX containing 10% FCS, 100 U/mL penicillin, and 100 µg/mL streptomycin (all Thermo Fisher Scientific). The PC12-TO cells were grown on surfaces coated with poly-L-lysine (PLL, Sigma-Aldrich) for the maintenance and experiments. For coating, the plates were incubated with PLL (0.02 mg/mL final concentration diluted in ddH₂O) for 30 min at 37 °C, washed twice with ddH₂O, and air-dried. The cells were cultured at 37 °C and 5% CO₂.

2.4. Luciferase Assays

For the luciferase assays, the cells were plated on flat-bottom 96-well clear plates (Falcon) at 2×10^4 HEK-293 cells/well, at 4×10^4 HeLa cells/well, at 4×10^4 U-2 OS cells/well, or at 5×10^4 PC12-TO cells/well one day before the experiment. All of the luciferase assays were performed using 6 replicates per condition. For the split TEV assays, the cells were transfected with split TEV plasmids (GPCRs and β -arrestin-2) and the UAS reporter plasmid (pGL4_10xUAS-MLPmin-luc2). For the CRE pathway assays, the cells were transfected with GPCR and a CRE reporter (pGL4_CRE-CMVmin-luc2) plasmids. All of the transfection mixes also contained a plasmid that encoded a nuclear variant of EYFP (1 ng per 96-well plate) for visual control of the transfection efficiency. Thus, we consistently transfected 31 ng for the split TEV assays and 21 ng for the CRE assays per 96-well plate. The transfection was conducted according to the manufacturer's instructions. The plasmids and the transfection reagent (Turbofect (Thermo Fisher Scientific) for the HEK-293 cells at a ratio of 1 µg of DNA to 3 µL of Turbofect; and Lipofectamine 3000 (Thermo Fisher Scientific) for the U2-OS, HeLa, and PC12-TO cells at a ratio of 1 µg of DNA to 2 µL of P3000 and 1 µg of DNA to 1.5 µL of Lipofectamine 3000) were diluted in Opti-MEM (Thermo Fisher Scientific) and incubated for 20 min at room temperature and added to the cells. Next, the medium was removed from the cells, the transfection mix was added, and the assay plates were incubated for 2 h at 37 °C. Double the volume of the culture medium (final volume: 90 µL per well) was then added to dilute the transfection reagents. The next day, the culture medium was replaced with serum-free assay medium (HEK-293: DMEM (4.5 g/L glucose)

supplemented with 2 mM GlutaMAX; HeLa: DMEM (4.5 g/L glucose) supplemented with 2 mM GlutaMAX; U-2 OS: McCoy's 5A medium; and PC12-TO: serum-reduced medium (DMEM (1 g/L glucose) supplemented with 1% dialyzed FBS (Thermo Fisher Scientific), 2 mM GlutaMAX, and 0.1 mM non-essential amino acids (NEAA, Thermo Fisher Scientific)) for 17–18 h. On the second day, the medium was removed, and the cells were treated with compounds diluted in the assay medium at various concentrations for 6 h at 37 °C. For the dose–response analyses, the compounds were diluted on a semi-logarithmic scale using 15 concentrations that ranged from 1 pM to 10 µM. Next, the medium was removed, and the cells were lysed with 30 µL of passive lysis buffer (Promega, Madison, WI, USA). To measure the firefly luciferase activity, the lysates were transferred to white flat-bottom 96-well plates (Falcon, Minato City, Tokyo). The firefly luciferase activity was measured with a Mithras LB 940 Microplate Reader (Berthold Technologies, Bad Wildbad, Germany) using the MicroWin 2000 software. The data were exported to Excel and processed with R-based scripts based on the *ggplot2* package to calculate and plot bar graphs with mean values, the standard deviation (s.d.), and the data points of the 6 replicates. To plot and analyze the dose–response curves, the R-based *drc* package [20] was used with the four-parameter log logistic function for curve fitting. The data were plotted as means with the standard error of the mean (s.e.m.) of the 6 replicates of the firefly readings. The assays were repeated twice.

2.5. Western Blotting and Antibodies

To measure the expression levels of the split TEV GPCR fusion constructs, the plasmids were transfected into HEK-293 cells using Lipofectamine 3000 according to the manufacturer's instructions. After allowing the plasmids to express for 24 h, the cells were washed 1× with PBS and lysed in a Triton-X lysis buffer (1% Triton-X100, 50 mM Tris pH 7.5, 150 mM NaCl, and 1 mM EGTA) containing the Complete protease inhibitor cocktail (Roche, Basel, Switzerland) and the PhosSTOP phosphatase inhibitor (Roche). The lysed cells were kept on ice for 10 min, sonicated 3× for 10 s at 4 °C, and denatured for 10 min at 70 °C. The Mini-PROTEAN Tetra Electrophoresis System (Bio-Rad, Hercules, CA, USA) was used for running and blotting the protein gels. For the chemiluminescence detection of proteins, the Pierce ECL Western Blotting Substrate (Thermo Fisher Scientific) was used followed by imaging with a ChemoStar ECL imager (Intas Science Imaging Instruments, Göttingen, Germany). The HA-tagged proteins were visualized using an HA antibody (clone 3F10, dilution 1:500, No. 11 867 423 001, Roche).

2.6. Immunocytochemistry of Cells

A total of 200,000 HEK293 cells were seeded per 24 wells, and 200 ng of each GPCR plasmid was transfected using Lipofectamine 3000. The cells were allowed to express the plasmids for 24 h and then were washed with PBS and fixed with 4% paraformaldehyde for 10 min at room temperature. Next, after three washes with TBS for 5 min each, the cells were blocked with 3% BSA in TBS for 1 h at room temperature. To stain for surface expression of SP-GPCRs (note that the SP harbored a FLAG tag), the cells were not permeabilized, but rather directly incubated with an anti-FLAG M2 antibody (dilution 1:500, F1804, Sigma-Aldrich). For the intracellular staining (note that the HA tag was intracellular), the cells were permeabilized via two washes with TBS/Triton X-100 (0.1%) (TBS-T) for 5 min each, blocked with 3% BSA in TBS-T for 1 h at room temperature, and incubated with an anti-HA antibody (clone 3F10, dilution 1:500, No. 11 867 423 001, Roche). The primary antibodies were incubated for 3 h at room temperature. Next, the cells were washed 3× with TBS (or TBS-T for intracellular staining) and incubated for 1 h at room temperature with fluorescent conjugate cross-adsorbed secondary antibodies (Alexa 488 and Alexa 647, Thermo Fisher Scientific) at a dilution of 1:500. The cells were mounted in EverBrite™ Hardset Mounting Medium (Biotium, Fremont, CA, USA) that contained Dapi for nuclear staining. The cells were imaged on a ZEISS Axio Observer.Z1 microscope with a C-Apochromat 63×/1.20 W Corr objective.

3. Results

3.1. Construction of a Versatile Split TEV GPCR Assay Expression System Using Gateway Recombination Cloning

We previously established high-throughput applicable split TEV β -arrestin-2 recruitment assays for various GPCRs, including DRD1, DRD2, AVPR2, and HTR2A [15,16]. Given the importance of GCGR and GLP1R as therapeutic targets in type II diabetes [21,22] and obesity [23,24], as well as GLP1R's implication in neurological disorders such as Alzheimer's disease (AD), Parkinson's disease (PD), and amyloid lateral sclerosis (ALS) [21,25,26], we established split TEV assays for those receptors as well. In our split TEV assay, the GPCR was fused to the N-terminal moiety of the TEV protease (NTEV), a TEV protease cleavage site (TCS), and the artificial transcriptional co-activator GAL4-VP16 (GV). The ligand-activated GPCR bound to β -arrestin-2, which, as a truncated version, was fused to the C-terminal moiety of the TEV protease (CTEV). Binding of the GPCR to β -arrestin-2 led to the functional complementation of the TEV protease fragments, thereby resulting in proteolytic activity. The TEV protease-cleaved GV migrated to the nucleus to bind to clustered upstream activated sequences (UAS) and initiated the transcription of a firefly luciferase reporter gene (Figure 1A). The GPCR in such a split TEV assay could be modified (1) with the N-terminally fused cleavable SP to enhance surface expression and (2) with a C-terminally fused V2R tail to enhance β -arrestin-2 binding to promote the assay performance (Figure 1B) [13,17]. The V2R tail may be particularly important for GPCRs with weak or absent endogenous activity-dependent β -arrestin-2-binding, which is also the case for DRD2 [27]. To test this, we selected six GPCRs from classes A and B that had a varying number of serine (Ser) and threonine (Thr) residues in their C-terminal tail. While DRD1, HTR2A, AVPR2, GCGR, and GLP1R all have 11 or more serine/threonine residues in combination with a different total length of the C-terminal tail, DRD2 had a very short C-terminus without Ser/Thr residues (Figure S1). To systematically test whether the V2R tail and SP improved the split TEV assay performance, we used the Gateway recombination system to clone for each GPCR (1) its native form, (2) a variant with an N-terminal SP (SP-GPCR), (3) a variant fused to the V2R tail (GPCR-V2R), and (4) a variant fused to both the SP and V2R (SP-GPCR-V2R) (Figure 1B). To confirm that each of the 24 GPCR constructs (Table S1) was correctly expressed, we transfected all GPCR-NTEV-TCS-GV fusions into HEK-293 cells. The expression of each GPCR construct was validated via Western blotting against an HA tag that was present in all of the GPCR fusions (Figure 1C–E). The surface expression of GPCR split TEV fusions was validated via immunocytochemistry staining. While the localization for both the native and SP-GPCR-V2R variants was examined with an antibody against the C-terminal HA tag (Figure 1F,G), the SP-GPCR-V2R variants were additionally tested against an extracellular FLAG epitope located C-terminally to the SP (Figure 1H).

3.2. Performance of Split TEV GPCR Assays Depended on Modifications and Cell Type

Next, transient split TEV GPCR β -arrestin-2 recruitment assays were conducted for all 24 constructs in HEK-293 cells (Figure 2A–F), U2-OS cells (Figure S2), HeLa cells (Figure S3), and PC12-TO cells (Figure 3A–F). Each GPCR was stimulated with its cognate agonist for 6 h in accordance with previous continuous online luciferase assays for split TEV GPCR assays [16]. GLP1R was stimulated with the peptide mimetic agonist liraglutide [28]. For each assay, the fold-change ratios based on the firefly luciferase values of non-stimulated and stimulated samples were calculated (Table 1). We found that the assays for DRD1, DRD2, AVPR2, and GCGR performed best in the HEK-293 cells (Figure 2, Table 1), while the HTR2A and GLP1R assays performed best in the PC12-TO cells (Figure 3C,F, Table 1). Specifically, the highest fold changes were obtained with the native forms of DRD1, DRD2, AVPR2, and GCGR in the cells and the native forms of HTR2A and GLP1R in the PC12-TO cells. The Z' -factor is an indicator of assay performance that integrates both the baseline and activated means as well as the standard deviations thereof to determine a statistical effect size [19]. Excellent assays; i.e., assays with a large separation window that are compatible with high-throughput applications, have Z' -factor values between 0.5 and

1.0. Split TEV GPCR assays with the highest fold-change values correlated largely with the highest Z' -factors when considering only the optimal cell line for a top-performing assay (i.e., for DRD1, DRD2, AVPR2, and GCGR in HEK-293 cells) (Table 1).

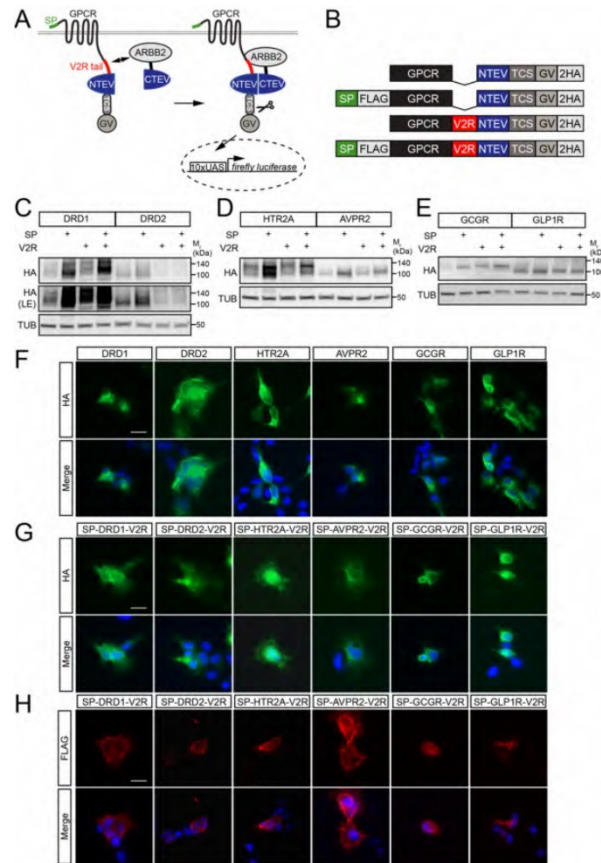


Figure 1. GPCRs for split TEV β-arrestin-2 recruitment assays were modified by the addition of a signal peptide, a V2R tail, or both. (A) Scheme of the GPCR β-arrestin-2 split TEV recruitment assay. A GPCR could be fused to the signal peptide (SP) and/or the tail of vasopressin receptor 2 (V2R) to test assay performance. ARRB2, β-arrestin-2; TCS, TEV protease cleavage site. (B) Graphical representation of the split TEV GPCR fusions. Depicted are the four variants of the GPCRs tested: native GPCR, SP-GPCR fusion, GPCR-V2R fusion, and SP-GPCR-V2R fusion. FLAG, single FLAG tag; NTEV, N-terminal moiety of the TEV protease; TCS, TEV protease cleavage site; GV, synthetic co-transcriptional activator GAL4-VP16; 2HA, double HA tag. (C–E) Split TEV GPCR constructs were properly expressed in HEK-293 cells. Western blots of the split TEV GPCR fusion constructs for DRD1 and DRD2 (C), HTR2A and AVPR2 (D), and GCGR and GLP1R (E). All proteins were detected with an HA antibody. LE, longer exposure. (F–H) Surface expression of selected GPCR split TEV fusions using immunocytochemistry staining. Native GPCR split TEV fusions were stained against the cytosolic HA epitope (F). SP-GPCR-V2R split TEV fusions were stained against the cytosolic HA epitope (G) and an extracellular FLAG epitope that was located C-terminal to SP (H). Note that FLAG staining was performed without permeabilizing cells. The merge was Dapi and antibody staining. Scale bar = 20 μM.

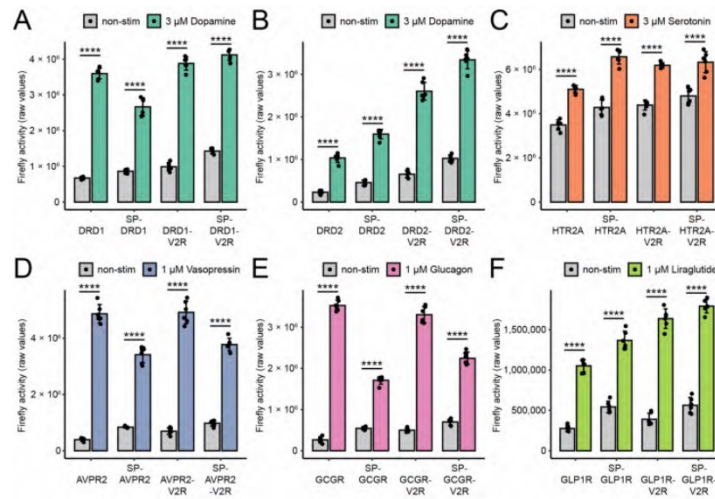


Figure 2. Split TEV GPCR β -arrestin-2 recruitment assays in HEK-293 cells. (A–F) Luciferase endpoint assays for DRD1 (A), DRD2 (B), HTR2A (C), AVPR2 (D), GCGR (E), and GLP1R (F). All assays were conducted in HEK-293 cells in a 96-well format. Cells were stimulated for 6 h with their agonists. Note that the addition of the signal peptide and the V2R tail affected the performance of the split TEV GPCR β -arrestin-2 recruitment assays. Bar graphs display the means; the error bars represent the s.d. with six replicates per conditions. A two-tailed Student’s *t* test was used to determine the *p*-values for treatment versus control. **** $p \leq 0.0001$.

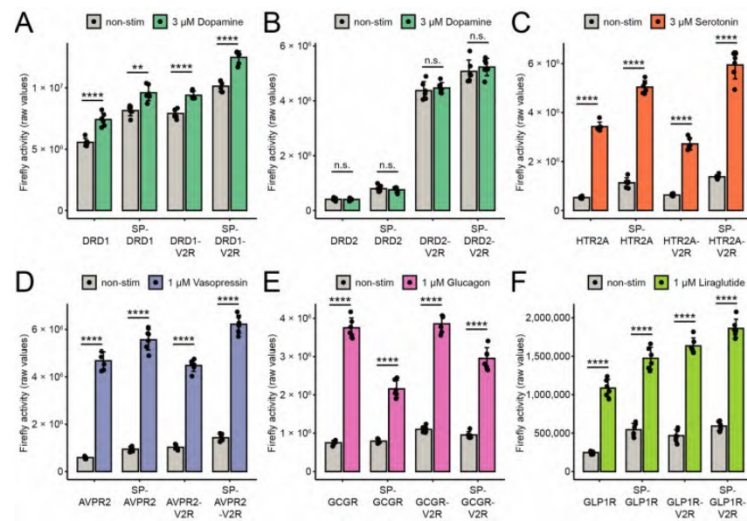


Figure 3. Split TEV GPCR β -arrestin-2 recruitment assays in PC12-TO cells. (A–F) Luciferase endpoint assays for DRD1 (A), DRD2 (B), HTR2A (C), AVPR2 (D), GCGR (E), and GLP1R (F). All assays were conducted in a 96-well format. Assays were stimulated for 6 h with their agonists. Bar graphs display the means; the error bars represent the s.d. with six replicates per conditions. A two-tailed Student’s *t* test was used to determine the *p*-values for treatment versus control. ** $p \leq 0.01$; **** $p \leq 0.0001$, n. s., not significant.

Table 1. Robustness of split TEV GPCR assays. Fold-change and Z'-factor values of all split TEV GPCR β -arrestin-2 assays that were conducted in HEK-293, HeLa, U 2-OS, and PC12-TO cells.

HEK-293	DRD1		DRD2		HTR2A		AVPR2		GCCGR		GLP1R	
	FC	Z'-Factor	FC	Z'-Factor	FC	Z'-Factor	FC	Z'-Factor	FC	Z'-Factor	FC	Z'-Factor
Native	5.34 ¹	0.81	4.52	0.46	1.46	0.25	12.37	0.74	13.32	0.81	3.82	0.56
SP	3.09	0.50	3.51	0.55	1.54	0.12	4.07	0.63	3.15	0.67	2.52	0.32
V2R tail	3.92	0.69	3.99	0.56	1.41	0.42	7.06	0.63	6.63	0.74	4.20	0.53
SP and V2R tail	2.89	0.74	3.26	0.62	1.32	−0.63	3.85	0.65	3.22	0.56	3.19	0.56
HeLa	DRD1		DRD2		HTR2A		AVPR2		GCCGR		GLP1R	
	FC	Z'-factor	FC	Z'-factor	FC	Z'-factor	FC	Z'-factor	FC	Z'-factor	FC	Z'-factor
Native	2.33	0.28	3.46	0.09	1.41	0.17	1.42	−1.93	1.31	−0.39	1.43	− 0.48
SP	1.64	−0.27	2.05	−0.98	(1.03) ₂	(−7.90)	2.54	0.05	1.14	−2.90	1.26	−0.97
V2R tail	2.18	0.24	2.93	0.57	1.15	−2.40	1.52	−1.04	1.56	0.25	(1.06)	(−6.53)
SP and V2R tail	2.27	0.44	2.99	0.46	(0.97)	(−14.80)	2.08	0.44	0.75	−0.46	(1.10)	(−4.71)
U-2 OS	DRD1		DRD2		HTR2A		AVPR2		GCCGR		GLP1R	
	FC	Z'-factor	FC	Z'-factor	FC	Z'-factor	FC	Z'-factor	FC	Z'-factor	FC	Z'-factor
Native	2.06	0.38	1.41	0.30	1.12	− 2.56	1.86	0.36	1.47	−0.29	1.20	−1.99
SP	1.83	0.45	1.79	0.19	(1.07)	(−5.23)	1.61	0.13	1.18	−1.45	1.40	−0.55
V2R tail	1.72	0.32	2.71	0.65	(1.06)	(−7.04)	1.67	0.16	1.46	0.07	1.36	− 0.11
SP and V2R tail	1.84	0.37	2.67	0.69	(1.07)	(−4.35)	1.57	0.31	1.28	−0.40	1.29	−0.52
PC12-TO	DRD1		DRD2		HTR2A		AVPR2		GCCGR		GLP1R	
	FC	Z'-factor	FC	Z'-factor	FC	Z'-factor	FC	Z'-factor	FC	Z'-factor	FC	Z'-factor
Native	1.33	−0.40	(0.98)	(−38.38)	6.45	0.76	7.92	0.68	4.99	0.68	4.38	0.53
SP	1.18	−1.18	(0.95)	(−14.82)	4.45	0.64	5.89	0.65	2.72	0.40	2.71	0.28
V2R tail	1.19	−0.46	(1.02)	(−15.37)	4.29	0.58	4.36	0.69	3.50	0.66	3.49	0.53
SP and V2R tail	1.23	− 0.21	(1.03)	(−13.06)	4.32	0.57	4.35	0.66	3.09	0.45	3.15	0.58

¹ Numbers highlighted in bold indicate the highest fold-change and Z'-factor values for each GPCR in each cell line; i.e., considering the four variants of each GPCR used (native form, SP-GPCR variant, GPCR-V2R variant, and SP-GPCR-V2R variant). Results were calculated from experiments with 6 replicates. ² Numbers in parentheses indicate that the *p*-value was larger than 0.05 as calculated via the two-sided Student's *t* test.

GPCRs fused to the SP and/or the V2R tail mostly retained their biological function with respect to mediating an agonist-induced β -arrestin-2 recruitment, but in some cases resulted in a considerable loss of activation in a cell-type-dependent manner; e.g., for HTR2A and GLP1R in the HeLa cells and for HTR2A in the U-2 OS cells (Table 1). The baseline luciferase readings of the SP-GPCR assays were invariably larger than the ones of the native forms, which also was reflected by the higher expression levels of the SP-GPCRs observed in the Western blot analysis (Figure 1C–E and Figure 2A–F).

For the DRD2 assays, the addition of the V2R tail considerably improved the assay performance in the HeLa and U-2 OS cells as determined by the Z'-factors (Figures S2 and S3, Table 1), while in HEK-293 cells, the additional V2R tail had a less pronounced effect (Figure 2B, Table 1). Nonetheless, the DRD2 assays overall performed best in the HEK-293 cells when taking both the Z'-factor and fold change into account. The addition of the V2R tail, especially when combined with the SP, to the DRD2 substantially increased the absolute luciferase reporter readings in the HEK-293, HeLa, and U-2 OS cell lines, but the overall performance was the best in the DRD2-V2R fusion. In contrast, the DRD2 assays did not perform in the PC12-TO cells at all. Of note, the GLP1R assays that used the native form and the V2R variant also performed robustly in the HEK-293 cells in terms of both the fold change and the Z'-factor. The preferred variant and cell line for each GPCR tested is summarized in Table 2.

3.3. Split TEV Assays for GCCGR and GLP1R Correlated with a cAMP Response Element Pathway Assay

Here, we report for the first time the establishment of split TEV β -arrestin-2 assays for GCCGR and GLP1R. To further characterize the assays for these two GPCRs in terms of sensitivity and robustness, we conducted dose–response assays with their respective ligands: glucagon (Figure 4A) and liraglutide (Figure 4B). HEK-293 cells were used for both assays because the GLP1R assays were robust both in HEK-293 cells (Figure 2F) and PC12-TO cells (Figure 3F). In the GCCGR assay, glucagon had an EC₅₀ of 4 nM, while liraglutide

yielded an EC_{50} of 1 nM in the GLP1R assay. GCGR and GLP1R signaled via $G_{\alpha s}$ proteins and the second messenger cAMP to regulate the cellular signaling [21,29]. Therefore, the activity of these GPCRs could also be indirectly monitored using a cAMP response element (CRE) sensor assay [12]. To compare the target-based split TEV assays with this widely used cellular pathway assay, we performed dose–response assays in HEK-293 cells by transfecting the GCGR and GLP1R constructs with a CRE reporter plasmid that drove a firefly luciferase reporter gene. Both the glucagon (Figure 4C) and liraglutide (Figure 4D) treatments yielded dose-dependent responses: an EC_{50} of 25 nM for glucagon and of 7 nM for liraglutide, which were in the range of previously reported data obtained in HEK-293 cells [30].

Table 2. Preferred GPCR variant and cell line for split TEV assays: effects of signal peptide (SP), V2R tail, and cell line on assay performance. The best variant was identified by the highest fold change and a paralleled Z' -factor ≥ 0.5 across the cell lines tested.

Target	Preferred Variant	Preferred Cell Line
DRD1	Native	HEK-293
DRD2	V2R variant ¹	HEK-293
HTR2A	Native	PC12-TO
AVPR2	Native	HEK-293
GCGR	Native	HEK-293
GLP1R	Native ² , V2R variant ³	PC12-TO ² , HEK-293 ³

¹ The DRD2-V2R variant had the highest fold change for a Z' -factor ≥ 0.5 . ² The fold change for GLP1R was highest in PC12-TO cells with the native version. ³ The use of the V2R variant in HEK-293 cells was preferred due to compatibility with other GPCR assays.

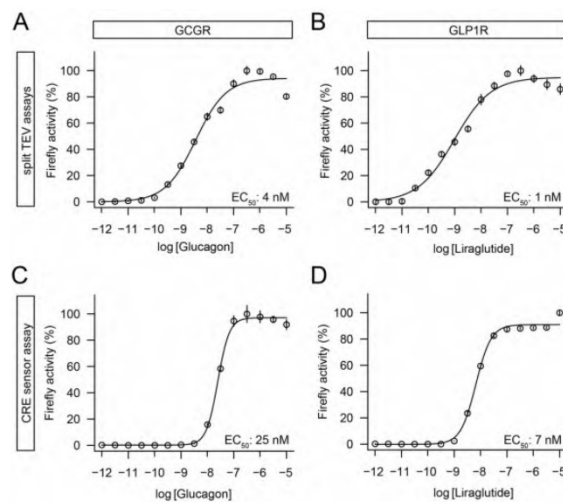


Figure 4. Dose–response curve analysis identified robust agonist assays for GCGR and GLP1R using both target-based split TEV and pathway-based CRE reporters. (A) Dose–response assay for native GCGR using glucagon as stimulus and split TEV as readout. Hill slope = 0.741. (B) Dose–response assay for GLP1R-V2R using liraglutide as stimulus and split TEV as readout. Hill slope = 0.602. (C) Dose–response assay for native GCGR split TEV construct as used in (A) using glucagon as stimulus and a CRE reporter as readout. Hill slope = 1.991. (D) Dose–response assay for GLP1R-V2R split TEV construct as used in (B) using liraglutide as stimulus and a CRE reporter as readout. Hill slope = 1.491. Receptors were stimulated for 6 h. Data represent mean \pm s.e.m. Firefly counts were normalized to the minimum and maximum of ligand response.

4. Discussion

Arrestin-2-mediated transduction of GPCR signaling is nearly always assayed at the level of recruitment because downstream effectors or second messengers do not converge on a single pathway [8,10]. Split TEV GPCR assays are highly sensitive and directly transform GPCR-triggered β -arrestin-2 recruitment into luminescent signals. They are regularly used to measure GPCR activity in compound screens [15,16,31]. To establish split TEV assays with improved characteristics, we designed vectors compatible with Gateway recombination cloning to shuffle GPCRs of interest with and without an SP and V2R tail into expression cassettes to identify the most sensitive and robust assay. We tested six GPCRs that were selected from class A and class B subfamilies that were either stimulated by small molecules (biogenic amines) or peptide ligands to cover a rather broad range of GPCRs. Across the selected GPCRs, the split TEV assays for DRD1, DRD2, AVPR2, and GCGR performed best in HEK-293 cells as evidenced by the fold-change and Z' -factor values, both of which were the highest for many assays in this cell line. However, the HTR2A assays performed best in the PC12-TO cells, which was consistent with our previous report [16]. The GLP1R assays performed well in both the HEK-293 and PC12-TO cells.

The addition of SP (either alone or in combination with V2R) generally did not improve the split TEV assay performance (except marginally for DRD2). The added SP instead led to increased readout activity as observed in the absolute luciferase readings and also as supported by the Western blot analysis. We confirmed surface expression for native and a subset of SP-fused GPCRs linked to the NTEV moiety. Furthermore, GPCRs with a hemagglutinin-derived SP linked to full TEV moieties were previously shown to be efficiently transported to the cell surface [13]. We noted, however, that overexpressed GPCRs accumulated inside the cells. Thus, the SP may also have exacerbated an incorrect transport of overexpressed GPCRs in the cell, thereby precluding an improved assay performance. In some cases; i.e., for AVPR2 and GCGR in the HEK-293 cells, the addition of SP even reduced the fold changes strongly. Notably, GCGR contained an SP as part of its open reading frame [32]. Therefore, the endogenous SP provided the best assay performance, thereby making the addition of the additional SP obsolete [33]. Further, we point out that the activation of peptidergic GPCRs (in this study: AVPR2, GCGR, and GLP1R) could only occur at the cell surface because peptide ligands could not pass through the plasma membrane, supporting the notion of efficient surface expression.

The addition of the V2R tail improved the assay performance for DRD2 in the HEK-293, HeLa, and U-2 OS cells, and the addition of the SP further marginally improved the assay robustness as indicated by the Z' -factor values in the HEK-293 and U-2 OS cells. However, the other GPCR assays that were tested in the split TEV assays were not improved by the V2R tail. This contrasted with GPCR β -arrestin-2 recruitment assays that used a full TEV protease approach and were reported to be improved by the addition of V2R [13,17]. We also found that the DRD2 split TEV assays performed reasonably well in the HEK-293, HeLa, and U-2 OS cells even without a V2R tail, although less efficiently. DRD2 does not have serine and threonine residues in its C-terminal tail, which, when phosphorylated after receptor activation, are a common β -arrestin binding motif. However, β -arrestin-2 can also bind to phosphorylated serine and threonine motifs located within the third intracellular loop, which suggests that the V2R tail might be redundant or sensitive to the local environment [27,34]. In other cases, as for AVPR2, DRD1, and GCGR, the addition of the V2R tail did not improve the assay performance, but instead led to a substantial decrease in both the fold change and Z -factor. As summarized in Table 2, the native form followed by the V2R variant were the preferred variants to use depending on the GPCR.

All of the split TEV assays were based on transient transfection with pcDNA3-based vectors, which are some of the most frequently used vectors in molecular and cellular biology [35]. However, we cannot rule out any differences in assay performance that may occur when using different vector backbones or different promoters (we used the CMV promoter; other options are, e.g., human EF1 α or UbC promoters) for expressing split TEV fusion proteins. Furthermore, pcDNA3 expression plasmids harbor the bovine

growth hormone polyadenylation signal sequence to increase expression in mammalian cells [36]. Therefore, we selected the pcDNA3 plasmid as the backbone, introduced corresponding GPCR cassettes via Gateway cloning, and validated the plasmid expression using Western blotting.

All of the assays presented here were based on transient transfections. We would like to note that rather low amounts of plasmids (c.f. the Section 2) were efficient in producing robust and sensitive assays. We regularly co-transfect a fluorescent marker plasmid (here: the nuclear form of EYFP) to assess efficiency. Therefore, we recommend always using clear plates for culturing the cells even if this requires a later transfer into white 96-well plates to measure the signals of the firefly luciferase. For the transfection reagent, we recommend testing with fluorescent marker plasmids first to find a suitable reagent because the performance can vary significantly from cell type to cell type. In addition, it may be helpful to co-transfect a constitutively active *Renilla* plasmid to assess the potential toxicity of compounds.

For GCGR and GLP1R, the split TEV and pathway assays correlated well, including for the range of EC_{50} values. However, the dose–response assays that used pathway sensors had a steeper Hill slope when compared to the split TEV assays, potentially implicating that the signals, which were initiated at the cell membrane and captured downstream, reached signal saturation via amplification inside the cell and/or were subject to feedback regulation [37,38].

GPCR biology is critical to complex disorders such as schizophrenia and type II diabetes. To provide alternative approaches for the discovery of therapeutic agents that simultaneously modulate DRD1, DRD2, and HTR2A or allosterically target GLP1R and the closely related GCGR, we developed and optimized genetically encoded cell-based split TEV assays for these targets to enable the profiling of compound libraries to identify selective agonists. DRD1, DRD2, and HTR2A have been implicated as drug targets in schizophrenia [39,40]. Schizophrenic patients suffering from positive symptoms such as hallucinations benefit from DRD2 and HTR2A antagonists [41], but potentially also from low-efficacy DRD1 agonists [42]. The anticipated medication paradigms are thus complex, and the development of drugs with a desired range of polypharmacology in disease-relevant targets is very demanding. Although each receptor can be efficiently targeted by many approved drugs (e.g., risperidone, which antagonizes DRD2 and HTR2A [43]; or lisuride, which is a partial agonist for DRD1 [44]), a multitarget drug that combines the features is still elusive.

GCGR and GLP1R are key targets to treat type II diabetes [21,22]. For both GCGR and GLP1R, multiple ligands have been approved by the FDA and EMA [45–47], even as the orally administrable peptide analogon known as semaglutide [48,49]. Nevertheless, the development of small-molecule drugs with an improved polypharmacological profile and an increased half-life is desired, and the search as well as clinical testing are still ongoing [50–52]. Furthermore, the activation of GLP1R was implicated in neuroprotective effects in ALS [25], and GLP-1 mimetics could alleviate ALS relevant phenotypes in both cellular and murine models [53,54]. However, liraglutide was recently reported to have failed to exert beneficial effects in a mouse model of ALS [55], thus still requiring better drugs to be developed.

Robust and sensitive assays using the technology outlined in this study could be applied in a multiplexed approach. In these assays, multiple experimental conditions can be monitored in parallel in a single well, and it is expected that such multiplexed assays will promote the broad screening for more selective drugs with fewer side activities [56,57]. In such multiparametric assays, each assay cell type expresses a different target linked to a unique barcode as the reporter and enables the pooling of single assays [16]. In addition, signaling cascades and pathways such as $G\alpha_s$ -dependent cAMP and $G\alpha_q$ -stimulated calcium responses or β -arrestin-2 mediated ERK1/2 signaling can be simultaneously monitored using barcoded CRE and EGR1 promoter (MAPK) pathway reporters, thus linking target and pathway responses. For example, each of the GPCR split TEV assays could be multi-

plexed with CRE and EGR1 promoter sensor pathway assays in one cell: different barcode reporters could be linked to the 10xUAS sensors used for split TEV assays, CRE sensors could be used to assess the cAMP/calcium signaling, and EGR1-promoter sensors could be used to assess the MAPK signaling. Such an approach may be particularly attractive to researchers in drug development because the monitoring of both GPCR activities and the elicited biased signaling actions are expected to generate better drugs with higher efficacies and reduced adverse effects [10,58].

5. Conclusions

Taken together, we provided a technical resource for optimizing split TEV GPCR β -arrestin-2 recruitment assays. For each unique GPCR, the effects of genetic modifications; i.e., the addition of an SP and/or a V2R tail, and the cell line of choice should be thoroughly tested to determine the best assay performance.

Supplementary Materials: The following supporting information can be downloaded at: <https://www.mdpi.com/article/10.3390/bios13010048/s1>, Figure S1: Split TEV GPCR constructs were properly expressed in HEK-293 cells. (A) GPCRs tested in this study. Note that the GPCRs had different C-terminal tails with varying numbers of phosphorylatable serine and threonine residues that when phosphorylated impacted on β -arrestin-2 binding. (B) Protein sequences of the C-terminus tails of the GPCRs shown in (B). Serine and threonine residues are highlighted in red. Figure S2: Split TEV GPCR β -arrestin-2 recruitment assays in HeLa cells. (A–F) Luciferase end-point assays for DRD1 (A), DRD2 (B), HTR2A (C), AVPR2 (D), GCGR (E), and GLP1R (F). All assays were conducted in a 96-well format. Assays were stimulated for 6 h using cognate agonists. Bar graphs display means; error bars represent s.d. with six replicates per conditions. A two-tailed Student's *t* test was used to determine the *p*-values for treatment versus control. * $p \leq 0.05$; ** $p \leq 0.01$; *** $p \leq 0.001$; **** $p \leq 0.0001$, n. s., not significant. Figure S3: Split TEV GPCR β -arrestin-2 recruitment assays in U-2 OS cells. (A–F) Luciferase end-point assays for DRD1 (A), DRD2 (B), HTR2A (C), AVPR2 (D), GCGR (E), and GLP1R (F). All assays were conducted in a 96-well format. Assays were stimulated for 6 h using cognate agonists. Bar graphs display means; error bars represent the s.d. with six replicates per conditions. A two-tailed Student's *t* test was used to determine the *p*-values for treatment versus control. * $p \leq 0.05$; ** $p \leq 0.01$; *** $p \leq 0.001$; **** $p \leq 0.0001$, n. s., not significant. Table S1: Plasmid information (plasmids are available at Addgene). Table S2: Oligonucleotides used for cloning.

Author Contributions: Y.W. and I.V.v.H. performed the experiments; Y.W., I.V.v.H., N.J. and M.C.W. analyzed the data; M.J.R. provided the reagents and supported the study; Y.W. and M.C.W. wrote the manuscript; M.C.W. devised and orchestrated the study. All authors have read and agreed to the published version of the manuscript.

Funding: This research was funded by the China Scholarship Council (grant number 201906230338) and Faculty of Medicine of the Ludwig-Maximilians-Universität München.

Institutional Review Board Statement: Not applicable.

Informed Consent Statement: Not applicable.

Data Availability Statement: Raw data of split TEV GPCR assays are available at Mendeley Data. DOI: 10.17632/fd45dm2bz5.1.

Acknowledgments: We thank Johanna Zach, Barbara Meisel, and Monika Rübkeil for their excellent technical support.

Conflicts of Interest: The authors declare a competing financial interest: M.C.W. and M.J.R. are shareholders of and are employed by Systasy Bioscience GmbH.

References

1. Dorsam, R.T.; Gutkind, J.S. G-protein-coupled receptors and cancer. *Nat. Rev. Cancer* **2007**, *7*, 79–94. [[CrossRef](#)] [[PubMed](#)]
2. Gurevich, V.V.; Gurevich, E.V. GPCR Signaling Regulation: The Role of GRKs and Arrestins. *Front. Pharmacol.* **2019**, *10*, 125. [[CrossRef](#)] [[PubMed](#)]
3. Heng, B.C.; Aubel, D.; Fussenegger, M. An overview of the diverse roles of G-protein coupled receptors (GPCRs) in the pathophysiology of various human diseases. *Biotechnol. Adv.* **2013**, *31*, 1676–1694. [[CrossRef](#)] [[PubMed](#)]

4. Rajagopal, S.; Rajagopal, K.; Lefkowitz, R.J. Teaching old receptors new tricks: Biasing seven-transmembrane receptors. *Nat. Rev. Drug Discov.* **2010**, *9*, 373–386. [[CrossRef](#)] [[PubMed](#)]
5. Santos, R.; Ursu, O.; Gaulton, A.; Bento, A.P.; Donadi, R.S.; Bologa, C.G.; Karlsson, A.; Al-Lazikani, B.; Hersey, A.; Oprea, T.I.; et al. A comprehensive map of molecular drug targets. *Nat. Rev. Drug Discov.* **2017**, *16*, 19–34. [[CrossRef](#)]
6. Flöser, A.; Becker, K.; Kostenis, E.; König, G.; Krasel, C.; Kolb, P.; Bünemann, M. Disentangling bias between Gq, GRK2, and arrestin3 recruitment to the M3 muscarinic acetylcholine receptor. *eLife* **2021**, *10*, e58442. [[CrossRef](#)]
7. Kwon, Y.; Mehta, S.; Clark, M.; Walters, G.; Zhong, Y.; Lee, H.N.; Sunahara, R.K.; Zhang, J. Non-canonical β -adrenergic activation of ERK at endosomes. *Nature* **2022**, *611*, 173–179. [[CrossRef](#)]
8. Smith, J.S.; Lefkowitz, R.J.; Rajagopal, S. Biased signalling: From simple switches to allosteric microprocessors. *Nat. Rev. Drug Discov.* **2018**, *17*, 243–260. [[CrossRef](#)]
9. Seyedabadi, M.; Ghahremani, M.H.; Albert, P.R. Biased signaling of G protein coupled receptors (GPCRs): Molecular determinants of GPCR/transducer selectivity and therapeutic potential. *Pharmacol. Ther.* **2019**, *200*, 148–178. [[CrossRef](#)]
10. Kolb, P.; Kenakin, T.; Alexander, S.P.H.; Bermudez, M.; Bohn, L.M.; Breinholt, C.S.; Bouvier, M.; Hill, S.J.; Kostenis, E.; Martemyanov, K.A.; et al. Community guidelines for GPCR ligand bias: IUPHAR review 32. *Br. J. Pharmacol.* **2022**, *179*, 3651–3674. [[CrossRef](#)]
11. Zhang, R.; Xie, X. Tools for GPCR drug discovery. *Acta Pharmacol. Sin.* **2012**, *33*, 372–384. [[CrossRef](#)] [[PubMed](#)]
12. Cheng, Z.; Garvin, D.; Paguio, A.; Stecha, P.; Wood, K.; Fan, F. Luciferase Reporter Assay System for Deciphering GPCR Pathways. *Curr. Chem. Genom.* **2010**, *4*, 84–91. [[CrossRef](#)] [[PubMed](#)]
13. Kroeze, W.K.; Sassano, M.F.; Huang, X.-P.; Lansu, K.; McCorvy, J.D.; Giguère, P.M.; Sciaky, N.; Roth, B.L. PRESTO-Tango as an open-source resource for interrogation of the druggable human GPCRs. *Nat. Struct. Mol. Biol.* **2015**, *22*, 362–369. [[CrossRef](#)] [[PubMed](#)]
14. Bertrand, L.; Parent, S.; Caron, M.; Legault, M.; Joly, E.; Angers, S.; Bouvier, M.; Brown, M.; Houle, B.; Ménard, L. The BRET2/Arrestin Assay in Stable Recombinant Cells: A Platform to Screen for Compounds That Interact with G Protein-Coupled Receptors (GPCRs). *J. Recept. Signal Transduct. Res.* **2002**, *22*, 533–541. [[CrossRef](#)] [[PubMed](#)]
15. Djannatian, M.S.; Galinski, S.; Fischer, T.M.; Rossner, M.J. Studying G protein-coupled receptor activation using split-tobacco etch virus assays. *Anal. Biochem.* **2011**, *412*, 141–152. [[CrossRef](#)] [[PubMed](#)]
16. Galinski, S.; Wichert, S.P.; Rossner, M.J.; Wehr, M.C. Multiplexed profiling of GPCR activities by combining split TEV assays and EXT-based barcoded readouts. *Sci. Rep.* **2018**, *8*, 8137. [[CrossRef](#)]
17. Barnea, G.; Strapps, W.; Herrada, G.; Berman, Y.; Ong, J.; Kloss, B.; Axel, R.; Lee, K.J. The genetic design of signaling cascades to record receptor activation. *Proc. Natl. Acad. Sci. USA* **2008**, *105*, 64–69. [[CrossRef](#)]
18. Guan, X.M.; Kobilka, T.S.; Kobilka, B.K. Enhancement of membrane insertion and function in a type IIIb membrane protein following introduction of a cleavable signal peptide. *J. Biol. Chem.* **1992**, *267*, 21995–21998. [[CrossRef](#)]
19. Zhang, J.; Chung, T.; Oldenburg, K. A Simple Statistical Parameter for Use in Evaluation and Validation of High Throughput Screening Experiments. *J. Biomol. Screen.* **1999**, *4*, 67–73. [[CrossRef](#)]
20. Ritz, C.; Baty, F.; Streibig, J.C.; Gerhard, D. Dose-Response Analysis Using R. *PLoS ONE* **2015**, *10*, e0146021. [[CrossRef](#)]
21. de Graaf, C.; Donnelly, D.; Wooten, D.; Lau, J.; Sexton, P.M.; Miller, L.J.; Ahn, J.-M.; Liao, J.; Fletcher, M.M.; Yang, D.; et al. Glucagon-Like Peptide-1 and Its Class B G Protein-Coupled Receptors: A Long March to Therapeutic Successes. *Pharmacol. Rev.* **2016**, *68*, 954–1013. [[CrossRef](#)] [[PubMed](#)]
22. Graham, G.V.; Conlon, J.M.; Abdel-Wahab, Y.H.; Flatt, P.R. Glucagon-related peptides from phylogenetically ancient fish reveal new approaches to the development of dual GCGR and GLP1R agonists for type 2 diabetes therapy. *Peptides* **2018**, *110*, 19–29. [[CrossRef](#)] [[PubMed](#)]
23. Drucker, D.J. Mechanisms of Action and Therapeutic Application of Glucagon-like Peptide-1. *Cell Metab.* **2018**, *27*, 740–756. [[CrossRef](#)] [[PubMed](#)]
24. Finan, B.; Yang, B.; Ottaway, N.; Smiley, D.L.; Ma, T.; Clemmensen, C.; Chabenne, J.; Zhang, L.; Habegger, K.M.; Fischer, K.; et al. A rationally designed monomeric peptide triagonist corrects obesity and diabetes in rodents. *Nat. Med.* **2015**, *21*, 27–36. [[CrossRef](#)] [[PubMed](#)]
25. Shandilya, A.; Mehan, S. Dysregulation of IGF-1/GLP-1 signaling in the progression of ALS: Potential target activators and influences on neurological dysfunctions. *Neurol. Sci. Off. J. Ital. Neurol. Soc. Ital. Soc. Clin. Neurophysiol.* **2021**, *42*, 3145–3166. [[CrossRef](#)] [[PubMed](#)]
26. Kim, D.S.; Choi, H.-I.; Wang, Y.; Luo, Y.; Hoffer, B.J.; Greig, N.H. A New Treatment Strategy for Parkinson's Disease through the Gut-Brain Axis. *Cell Transplant.* **2017**, *26*, 1560–1571. [[CrossRef](#)] [[PubMed](#)]
27. Mann, A.; Keen, A.C.; Mark, H.; Dasgupta, P.; Javitch, J.A.; Canals, M.; Schulz, S.; Lane, J.R. New phosphosite-specific antibodies to unravel the role of GRK phosphorylation in dopamine D2 receptor regulation and signaling. *Sci. Rep.* **2021**, *11*, 8288. [[CrossRef](#)] [[PubMed](#)]
28. Drucker, D.J.; Dritselis, A.; Kirkpatrick, P. Liraglutide. *Nat. Rev. Drug Discov.* **2010**, *9*, 267–268. [[CrossRef](#)]
29. Mayo, K.E.; Miller, L.J.; Bataille, D.; Dalle, S.; Göke, B.; Thorens, B.; Drucker, D.J. International Union of Pharmacology. XXXV. The Glucagon Receptor Family. *Pharmacol. Rev.* **2003**, *55*, 167–194. [[CrossRef](#)]

30. Al-Zamel, N.; Al-Sabah, S.; Luqmani, Y.; Adi, L.; Chacko, S.; Schneider, T.D.; Krasel, C. A Dual GLP-1/GIP Receptor Agonist Does Not Antagonize Glucagon at Its Receptor but May Act as a Biased Agonist at the GLP-1 Receptor. *Int. J. Mol. Sci.* **2019**, *20*, 3532. [CrossRef]
31. Alonso-Gardón, M.; Estévez, R. Split-Tobacco Etch Virus (Split-TEV) Method in G Protein-Coupled Receptor Interacting Proteins. *Methods Mol. Biol. Clifton NJ* **2021**, *2268*, 223–232. [CrossRef]
32. Teufel, F.; Armenteros, J.J.A.; Johansen, A.R.; Gislason, M.H.; Pihl, S.I.; Tsigos, K.D.; Winther, O.; Brunak, S.; von Heijne, G.; Nielsen, H. SignalP 6.0 predicts all five types of signal peptides using protein language models. *Nat. Biotechnol.* **2022**, *40*, 1023–1025. [CrossRef] [PubMed]
33. Rutz, C.; Klein, W.; Schüle, R. N-Terminal Signal Peptides of G Protein-Coupled Receptors. *Prog. Mol. Biol. Transl. Sci.* **2015**, *132*, 267–287. [CrossRef] [PubMed]
34. Ågren, R.; Sahlholm, K. G protein-coupled receptor kinase-2 confers isoform-specific calcium sensitivity to dopamine D2 receptor desensitization. *FASEB J.* **2021**, *35*, e22013. [CrossRef]
35. Montakhab-Yeganeh, H.; Shafiei, R.; Najm, M.; Masoori, L.; Aspatwar, A.; Badirzadeh, A. Immunogenic properties of empty pcDNA3 plasmid against zoonotic cutaneous leishmaniasis in mice. *PLoS ONE* **2022**, *17*, e0263993. [CrossRef]
36. Yew, N.S.; Wysokenski, D.M.; Wang, K.X.; Ziegler, R.J.; Marshall, J.; McNeilly, D.; Cherry, M.; Osburn, W.; Cheng, S.H. Optimization of Plasmid Vectors for High-Level Expression in Lung Epithelial Cells. *Hum. Gene Ther.* **1997**, *8*, 575–584. [CrossRef]
37. Dueber, J.E.; Mirsky, E.A.; Lim, W.A. Engineering synthetic signaling proteins with ultrasensitive input/output control. *Nat. Biotechnol.* **2007**, *25*, 660–662. [CrossRef]
38. Shaw, W.M.; Yamauchi, H.; Mead, J.; Gowers, G.-O.F.; Bell, D.J.; Öling, D.; Larsson, N.; Wigglesworth, M.; Ladds, G.; Ellis, T. Engineering a Model Cell for Rational Tuning of GPCR Signaling. *Cell* **2019**, *177*, 782–796.e27. [CrossRef]
39. Trubetskoy, V.; Pardiñas, A.F.; Qi, T.; Panagiotaropoulou, G.; Awasthi, S.; Bigdeli, T.B.; Bryois, J.; Chen, C.-Y.; Dennison, C.A.; Hall, L.S.; et al. Mapping genomic loci implicates genes and synaptic biology in schizophrenia. *Nature* **2022**, *604*, 502–508. [CrossRef]
40. Aneja, J. Risperidone Response in Schizophrenia: A Narrative Review of Pharmacogenetic Research. *J. Ment. Health Clin. Psychol.* **2018**, *2*, 39–47. [CrossRef]
41. Owen, M.J.; Sawa, A.; Mortensen, P.B. Schizophrenia. *Lancet* **2016**, *388*, 86–97. [CrossRef] [PubMed]
42. Wang, M.; Datta, D.; Enwright, J.; Galvin, V.; Yang, S.-T.; Paspalas, C.; Kozak, R.; Gray, D.L.; Lewis, D.A.; Arnsten, A.F. A novel dopamine D1 receptor agonist excites delay-dependent working memory-related neuronal firing in primate dorsolateral prefrontal cortex. *Neuropharmacology* **2019**, *150*, 46–58. [CrossRef] [PubMed]
43. Arnt, J.; Skarsfeldt, T. Do Novel Antipsychotics Have Similar Pharmacological Characteristics? A Review of the Evidence. *Neuropsychopharmacol. Off. Publ. Am. Coll. Neuropsychopharmacol.* **1998**, *18*, 63–101. [CrossRef] [PubMed]
44. Millan, M.J.; Maiorini, L.; Cussac, D.; Audinot, V.; Boutin, J.A.; Newman-Tancredi, A. Differential Actions of Antiparkinson Agents at Multiple Classes of Monoaminergic Receptor. I. A Multivariate Analysis of the Binding Profiles of 14 Drugs at 21 Native and Cloned Human Receptor Subtypes. *J. Pharmacol. Exp. Ther.* **2002**, *303*, 791–804. [CrossRef] [PubMed]
45. Knudsen, L.B.; Kiel, D.; Teng, M.; Behrens, C.; Bhumralkar, D.; Kodra, J.T.; Holst, J.J.; Jeppesen, C.B.; Johnson, M.D.; de Jong, J.C.; et al. Small-molecule agonists for the glucagon-like peptide 1 receptor. *Proc. Natl. Acad. Sci. USA* **2007**, *104*, 937–942. [CrossRef]
46. Knudsen, L.B.; Lau, J. The Discovery and Development of Liraglutide and Semaglutide. *Front. Endocrinol.* **2019**, *10*, 155. [CrossRef]
47. La Sala, L.; Pontiroli, A.E. New Fast Acting Glucagon for Recovery from Hypoglycemia, a Life-Threatening Situation: Nasal Powder and Injected Stable Solutions. *Int. J. Mol. Sci.* **2021**, *22*, 10643. [CrossRef]
48. Cowart, K. Oral Semaglutide: First-in-Class Oral GLP-1 Receptor Agonist for the Treatment of Type 2 Diabetes Mellitus. *Ann. Pharmacother.* **2020**, *54*, 478–485. [CrossRef]
49. O’Neil, P.M.; Birkenfeld, A.L.; McGowan, B.; Mosenzon, O.; Pedersen, S.D.; Wharton, S.; Carson, C.G.; Jepsen, C.H.; Kabisch, M.; Wilding, J.P.H. Efficacy and safety of semaglutide compared with liraglutide and placebo for weight loss in patients with obesity: A randomised, double-blind, placebo and active controlled, dose-ranging, phase 2 trial. *Lancet* **2018**, *392*, 637–649. [CrossRef]
50. Kawai, T.; Sun, B.; Yoshino, H.; Feng, D.; Suzuki, Y.; Fukazawa, M.; Nagao, S.; Wainscott, D.B.; Showalter, A.D.; Droz, B.A.; et al. Structural basis for GLP-1 receptor activation by LY3502970, an orally active nonpeptide agonist. *Proc. Natl. Acad. Sci. USA* **2020**, *117*, 29959–29967. [CrossRef]
51. Saxena, A.R.; Gorman, D.N.; Esquejo, R.M.; Bergman, A.; Chidsey, K.; Buckeridge, C.; Griffith, D.A.; Kim, A.M. Danuglipron (PF-06882961) in type 2 diabetes: A randomized, placebo-controlled, multiple ascending-dose phase 1 trial. *Nat. Med.* **2021**, *27*, 1079–1087. [CrossRef] [PubMed]
52. Choe, H.J.; Cho, Y.M. Peptidyl and Non-Peptidyl Oral Glucagon-Like Peptide-1 Receptor Agonists. *Endocrinol. Metab.* **2021**, *36*, 22–29. [CrossRef] [PubMed]
53. Li, Y.; Chigurupati, S.; Holloway, H.W.; Mughal, M.; Tweedie, D.; Bruestle, D.A.; Mattson, M.P.; Wang, Y.; Harvey, B.K.; Ray, B.; et al. Exendin-4 Ameliorates Motor Neuron Degeneration in Cellular and Animal Models of Amyotrophic Lateral Sclerosis. *PLoS ONE* **2012**, *7*, e32008. [CrossRef] [PubMed]
54. Sun, H.; Knippenberg, S.; Thau, N.; Ragancokova, D.; Körner, S.; Huang, D.; Dengler, R.; Döhler, K.; Petri, S. Therapeutic Potential of N-Acetyl-Glucagon-Like Peptide-1 in Primary Motor Neuron Cultures Derived From Non-Transgenic and SOD1-G93A ALS Mice. *Cell. Mol. Neurobiol.* **2013**, *33*, 347–357. [CrossRef] [PubMed]

55. Keerie, A.; Brown-Wright, H.; Kirkland, I.; Grierson, A.; Alix, J.J.P.; Holscher, C.; Mead, R.J. The GLP-1 receptor agonist, liraglutide, fails to slow disease progression in SOD1G93A and TDP-43Q331K transgenic mouse models of ALS. *Sci. Rep.* **2021**, *11*, 17027. [[CrossRef](#)]
56. Herholt, A.; Galinski, S.; Geyer, P.E.; Rossner, M.J.; Wehr, M.C. Multiparametric Assays for Accelerating Early Drug Discovery. *Trends Pharmacol. Sci.* **2020**, *41*, 318–335. [[CrossRef](#)] [[PubMed](#)]
57. Herholt, A.; Sahoo, V.K.; Popovic, L.; Wehr, M.C.; Rossner, M.J. Dissecting intercellular and intracellular signaling networks with barcoded genetic tools. *Curr. Opin. Chem. Biol.* **2022**, *66*, 102091. [[CrossRef](#)]
58. Yang, D.; Zhou, Q.; Labroska, V.; Qin, S.; Darbalaei, S.; Wu, Y.; Yuliantie, E.; Xie, L.; Tao, H.; Cheng, J.; et al. G protein-coupled receptors: Structure- and function-based drug discovery. *Signal Transduct. Target. Ther.* **2021**, *6*, 7. [[CrossRef](#)]

Disclaimer/Publisher's Note: The statements, opinions and data contained in all publications are solely those of the individual author(s) and contributor(s) and not of MDPI and/or the editor(s). MDPI and/or the editor(s) disclaim responsibility for any injury to people or property resulting from any ideas, methods, instructions or products referred to in the content.

6. Paper II

Comprehensive split TEV based protein-protein interaction screening reveals TAOK2 as a key modulator of Hippo signalling to limit growth¹

Authors:

Xiao Ma^{1†}, Fiona J. Mandausch^{1†}, Yuxin Wu^{1†}, Vivek K. Sahoo², Wenbo Ma¹, Giovanna Leoni², Madalina Hostiuc^{1,4}, Jan P. Wintgens¹, Jiajun Qiu^{5,6}, Nirmal Kannaiyan², Moritz J. Rossner^{2,3}, Michael C. Wehr^{1,2*}

Affiliations:

¹Research Group Cell Signalling, Department of Psychiatry and Psychotherapy, LMU University Hospital, LMU Munich, Nussbaumstr. 7, 80336 Munich, Germany

²Systasy Bioscience GmbH, Balanstr. 6, 81669 Munich, Germany

³Section of Molecular Neurobiology, Department of Psychiatry and Psychotherapy, LMU University Hospital, LMU Munich, Nussbaumstr. 7, 80336 Munich, Germany

⁴Current address: Psychiatric University Hospital Zurich, Lenggstrasse 31, 8008 Zürich, Switzerland

⁵Department of Otolaryngology Head & Neck Surgery, The Ninth People's Hospital, Shanghai Jiao Tong University School of Medicine, Shanghai, 200011, China

⁶Current address: Global Computational Biology and Digital Sciences, Boehringer Ingelheim Pharma GmbH & Co. KG, Birkendorfer Str. 65, 88400 Biberach an der Riß

†These authors contributed equally to this work.

*Corresponding author: Email: Michael.Wehr@med.uni-muenchen.de

¹ Ma X, Mandausch FJ, Wu Y, Sahoo VK, Ma W, Leoni G, Hostiuc M, Wintgens JP, Qiu J, Kannaiyan N, Rossner MJ, Wehr MC. Comprehensive split TEV based protein-protein interaction screening reveals TAOK2 as a key modulator of Hippo signalling to limit growth. Cellular Signalling. 2023;110917. <https://doi.org/https://doi.org/10.1016/j.cellsig.2023.110917>.

7. Paper III

Integrated profiling of ERBB family receptor activities and downstream pathway responses reveals selectivity and hidden phenotypes of known and novel ERBB4 antagonists¹

Authors:

Lukša Popović^{1,2}, Jan P. Wintgens^{1,2}, Yuxin Wu¹, Ben Brankatschk², Sascha Menninger³, Carsten Degenhart³, Niels Jensen⁴, Sven P. Wichert^{2,4}, Bert Klebl³, Moritz J. Rossner^{2,4}, Michael C. Wehr^{1,2*}

Affiliations:

¹ Research Group Cell Signalling, Department of Psychiatry and Psychotherapy, LMU University Hospital, LMU Munich, Nussbaumstr. 7, 80336 Munich, Germany

² Systasy Bioscience GmbH, Balanstr. 6, 81669 Munich, Germany

³ Lead Discovery Center GmbH, Otto-Hahn-Str. 15, 44227 Dortmund, Germany

⁴ Section of Molecular Neurobiology, Department of Psychiatry and Psychotherapy, LMU University Hospital, LMU Munich, Nussbaumstr. 7, 80336 Munich, Germany

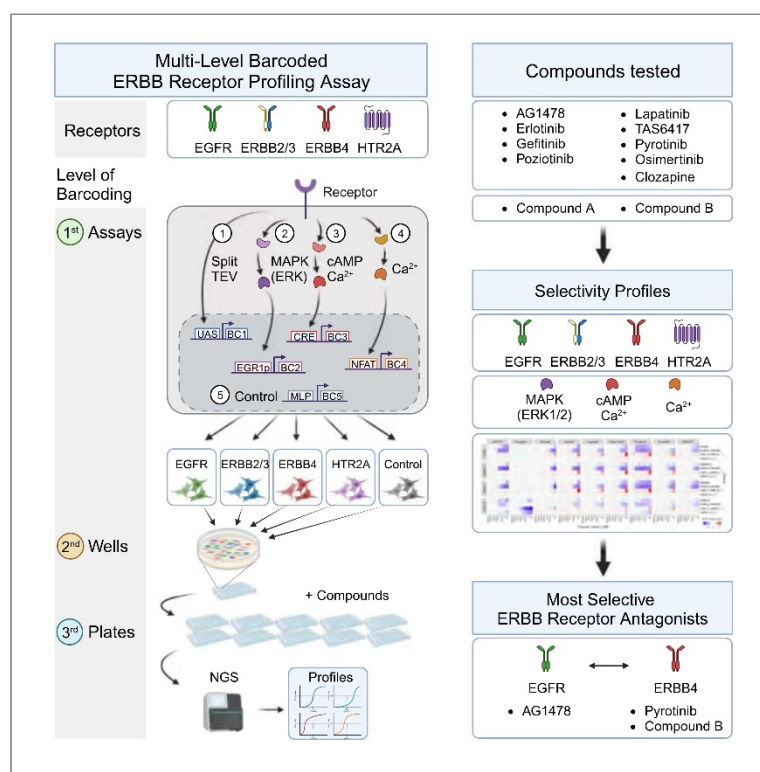
(*) Author for correspondence:

Michael C. Wehr; email: michael.wehr@med.uni-muenchen.de; phone: +49 (0) 89 4400 53275

¹ Popović L, Wintgens JP, Wu Y, Brankatschk B, Menninger S, Degenhart C, Jensen N, Wichert SP, Klebl B, Rossner MJ, Wehr MC. Profiling of ERBB receptors and downstream pathways reveals selectivity and hidden properties of ERBB4 antagonists. *iScience*. 2024:108839. <https://doi.org/https://doi.org/10.1016/j.isci.2024.108839>.

Article

Profiling of ERBB receptors and downstream pathways reveals selectivity and hidden properties of ERBB4 antagonists



Lukša Popović, Jan P. Wintgens, Yuxin Wu, ..., Bert Klebl, Moritz J. Rossner, Michael C. Wehr

michael.wehr@med.uni-muenchen.de

Highlights

Multilevel barcoded reporter assay for profiling of ERBB receptors and pathways

Discriminating on-target from off-target effects of ERBB receptor antagonists

Profiled eight known ERBB receptor antagonists and two new ERBB4 selective leads

Pyrotinib and novel compound B show a substantial preference for ERBB4 over EGFR

Popović et al., iScience 27, 108839
February 16, 2024 © 2024 The Author(s).
<https://doi.org/10.1016/j.isci.2024.108839>



Article

Profiling of ERBB receptors and downstream pathways reveals selectivity and hidden properties of ERBB4 antagonists

Lukša Popović,^{1,2} Jan P. Wintgens,^{1,2} Yuxin Wu,¹ Ben Brankatschk,² Sascha Menninger,³ Carsten Degenhart,³ Niels Jensen,⁴ Sven P. Wichert,^{2,4} Bert Klebl,³ Moritz J. Rossner,^{2,4} and Michael C. Wehr^{1,2,5,*}

SUMMARY

ERBB receptor tyrosine kinases are involved in development and diseases like cancer, cardiovascular, neurodevelopmental, and mental disorders. Although existing drugs target ERBB receptors, the next generation of drugs requires enhanced selectivity and understanding of physiological pathway responses to improve efficiency and reduce side effects. To address this, we developed a multilevel barcoded reporter profiling assay, termed 'ERBBprofiler', in living cells to monitor the activity of all ERBB targets and key physiological pathways simultaneously. This assay helps differentiate on-target therapeutic effects from off-target and off-pathway side effects of ERBB antagonists. To challenge the assay, eight established ERBB antagonists were profiled. Known effects were confirmed, and previously uncharacterized properties were discovered, such as pyrotinib's preference for ERBB4 over EGFR. Additionally, two lead compounds selectively targeting ERBB4 were profiled, showing promise for clinical trials. Taken together, this multiparametric profiling approach can guide early-stage drug development and lead to improved future therapeutic interventions.

INTRODUCTION

ERBB receptor family kinases are a sub family of receptor tyrosine kinases (RTKs) and are implicated in various human disorders, such as various types of cancer, e.g., breast cancer and non-small cell lung cancer, as well as neurological disorders and mental disorders, including schizophrenia.¹⁻⁴ The ERBB family consists of four type I transmembrane receptors, which are the epidermal growth factor receptor (EGFR, also known as ERBB1), ERBB2 receptor tyrosine kinase 2 (also known as HER2), ERBB3 (HER3), and ERBB4 (HER4).² ERBB receptors are activated by epidermal growth factor (EGF) and heregulin-like family ligands and can homo- and heterodimerize, leading to the phosphorylation on cytoplasmic tyrosine residues and the activation of cellular signaling cascades. While ERBB2 does not bind any endogenous ligand, it can still signal downstream when dimerized.⁵⁻⁷ ERBB3 favors heterodimerization with its preferred dimerization partner ERBB2 due to an impaired kinase domain to elicit cellular signaling.⁸ Canonical cellular signaling pathways initiated by activated ERBB receptors are the KRAS-RAF-mitogen-activated protein kinase (MAPK) cascade, phosphatidylinositol 3-kinase (PI3-K), and STAT signaling.^{9,10} In particular, the MAPK axis, which is initiated by the binding of the growth factor receptor-bound protein 2 (GRB2) adapter to phosphorylated tyrosine residues of ERBB receptors and ultimately results in extracellular regulated kinase 1 and 2 (ERK1/2) activation, is a bona-fide pathway that links ERBB receptor activity to cellular phenotypes, like cell cycle progression and proliferation.^{11,12}

Cancer formation is linked to an increased expression of EGFR,¹³ ERBB2,¹⁴ ERBB3,¹⁵ and ERBB4.^{16,17} Notably, ERBB receptors play overlapping roles in various cancers, with, however, distinct mechanisms.¹⁸ For example, both EGFR and ERBB4 are linked to colorectal cancer^{19,20} and non-small cell lung cancer (NSCLC),²¹ but mutations for either EGFR or ERBB4 generally occur separately. Inhibiting ERBB signaling using small molecules is an attractive approach to treat multiple types of cancer. For example, gefitinib, the first EGFR tyrosine kinase inhibitor (TKI) developed, was approved by the US Food and Drug Association (FDA) in 2003 to treat NSCLC,²² followed by the FDA approval of erlotinib for NSCLC in 2004²³ and lapatinib for the treatment of ERBB2 positive breast cancer in 2007.²⁴ However, resistance patterns to ERBB inhibitor treatment emerged due to secondary mutations at gatekeeper residues (e.g., T790M in EGFR) i.e., larger residues sterically impeded inhibitor binding.²⁵ Furthermore, triggering alternative downstream signaling routes and the activation of bypass survival tracks via other RTKs also accounts for the acquired drug resistance to ERBB receptors.^{26,27} To avoid resistance, various third generation TKI drugs were developed, such as osimertinib targeting the sensitizing mutation EGFR-T790M to treat NSCLC.^{28,29} Furthermore, overactive ERBB4 is associated with

¹Research Group Cell Signalling, Department of Psychiatry and Psychotherapy, LMU University Hospital, LMU Munich, Nussbaumstrasse 7, 80336 Munich, Germany

²Systasy Bioscience GmbH, Balanstrasse 6, 81669 Munich, Germany

³Lead Discovery Center GmbH, Otto-Hahn-Strasse 15, 44227 Dortmund, Germany

⁴Section of Molecular Neurobiology, Department of Psychiatry and Psychotherapy, LMU University Hospital, LMU Munich, Nussbaumstrasse 7, 80336 Munich, Germany

⁵Lead contact

*Correspondence: michael.wehr@med.uni-muenchen.de

<https://doi.org/10.1016/j.isci.2024.108839>



reduced interneuron activity in the prefrontal cortex leading to an imbalance of excitation and inhibition, and consecutively to symptoms of schizophrenia.^{30,31} Thus, ERBB4 is regarded as a critical target for schizophrenia, and drug development is required to identify compounds that selectively target ERBB4,³² but not EGFR, its most related receptor within the ERBB family.

As activated ERBB receptors can form homo or heterodimers restricted to their sub family,² targeting only one family member and modulating its downstream signaling is difficult. In addition to those challenges, the development of kinase inhibitors is challenging in general, as kinases are targeted by only 3% of all marketed drugs.³³ Notably, kinases and especially RTKs, together with G protein-coupled receptors (GPCRs), represent one of the two most important drug targets in human cells.³³ Biochemical binding assays and FRET-based assays are frequently used to profile compounds that interact with RTKs, including ERBB receptors, and offer valuable insights into the binding properties of various compounds. However, it is essential to recognize their limitations, particularly the lack of physiological context in test tube (*in-vitro*) settings, the inability to account for physiologically relevant interactions at the cell membrane (which is crucial for RTKs), and the potential artifacts from those *in-vitro* conditions.³⁴ Standard reporter gene assays in living cells may solve some aspects of the limitations mentioned above. However, single assays are not able to deliver functionally diverse phenotypes from the very same cell population (i.e., an agonistic and antagonistic effect monitored on different pathways from one well). Therefore, the development of a holistic cell-based assay system that enables the monitoring of ERBB activities and downstream pathways may substantially contribute to the advancement of better therapeutic agents targeting ERBB receptors.

Here, we describe a barcoded profiling assay, termed 'ERBBprofiler', to simultaneously assess the activity of ERBB receptors in their native environment at the cell membrane and their downstream responses to key cellular pathways in living cells. Selective activities of individual ERBB receptors and pathway responses associated with receptor activation or inhibition can be monitored in the same well upon drug treatment. While ERBB receptor activities at the membrane were monitored by split TEV recruitment assays, pathway responses were measured by optimized nuclear pathway sensors. By profiling target selectivity and physiological responses of established drugs and compounds that are either approved, currently tested in clinical phases, or failed, we have demonstrated the capabilities of the cell-based assay platform to identify relevant features of ERBB antagonists. Lastly, we used the assay platform to profile novel ERBB4 selective antagonists, supporting the notion that the profiling assay can be used to accelerate early drug discovery campaigns.

RESULTS

Design of a barcoded ERBB family receptor and pathway profiling assay

Profiling of both ERBB targets and downstream pathway activities was performed by genetically encoded split TEV and pathway reporter gene assays, respectively, and requires a readout that is amenable to parallelization (Figure 1A). Therefore, the firefly luciferase reporter of each reporter plasmid was replaced by a unique DNA barcode that is transcribed into an RNA barcode, which can be isolated from cells and quantified by next-generation sequencing (NGS).^{35,36} For establishing the multiparametric ERBB receptor profiling assay, we first cloned small ($n \leq 20$) libraries of the reporter plasmids encoding (1) a barcoded Gal4-VP16 reporter for split TEV assays consisting of clustered upstream activating sequences (10xUAS), (2) a barcoded pathway sensor for MAP kinase signaling based on the early growth response 1 promoter (EGR1p sensor), (3) a barcoded pathway sensor for cAMP/calcium signaling based on cAMP response element (CRE sensor), (4) a barcoded pathway sensor for calcium signaling based on the response element of the nuclear factor of activated T-cells (NFAT sensor), and (5) a barcoded sensor for assessing baseline activities based on the major late promoter (MLP) from adenovirus. For the simultaneous monitoring of target and pathway activities, a subset of these barcode reporters (3 unique barcodes for UAS, 2 unique barcodes each for CRE, EGR1p, NFAT, and 1 for MLP) was transfected with plasmids encoding split TEV compatible ERBB receptors (i.e., EGFR, ERBB2 in combination with ERBB3, or ERBB4) and the split TEV RTK adapter 3xSH2-GRB2³⁷ into PC12 cells for ERBB receptor assays. In addition, we wished to add an unrelated target as a control assay. Thus, another subset of the reporter plasmids was transfected with the split TEV compatible serotonin receptor 2A (HTR2A), a G α_q -coupled GPCR, and the split TEV GPCR adapter ARBB2-CTEV³⁸ for an HTR2A assay (Figures S1A–S1F; Table S1). Therefore, each batch of cells contained the plasmids encoding a receptor, its cognate adapter, and the split TEV and pathway reporters with a set of unique barcodes enabling to assess the activities of one target, i.e., an ERBB receptor, or HTR2A, and its downstream signals. Multiplexing of target and pathway assays was then further conducted by mixing cell batches into one well and continued at the plate level. Thus, barcoding occurred at the levels of single assays, wells, and plates, and enabled the generation of thousands of data points from one ERBBprofiler experiment (Figure 1B). In a typical profiling experiment, batches of transfected PC12 cells were mixed, plated onto 24-well plates, cultured for 20 h, starved for 16 h in medium with reduced serum conditions, and treated with increasing doses of epidermal growth factor (EGF, ligand for EGFR), EGF-like domain (EGF_{ld}, ligand for ERBB3 and ERBB4), and serotonin (ligand for HTR2A) for 6 h before lysis (Figure S1G). To proceed to the sequencing of barcodes using next-generation sequencing and to reduce handling, a unique DNA barcode oligo, termed well barcode, was added to each lysate originating from one well, enabling the tracking of individual lysates in a pool. Next, all lysates from one 24-well plate were pooled for combined processing, a process called 'Tag&Pool' (read 'Tag-and-Pool', see STAR Methods) (Figures S1H and S1I).

Selectivity of ERBB receptor activation, HTR2A activation, and their downstream signaling by single ligands correlate in barcoded assays

In the initial ERBBprofiler assay experiment, we examined the impact of EGF, EGF_{ld}, and serotonin on the activation on ERBB receptors, HTR2A, and their key downstream pathways. While EGF treatment selectively stimulated the activity of EGFR, addition of EGF_{ld} led to

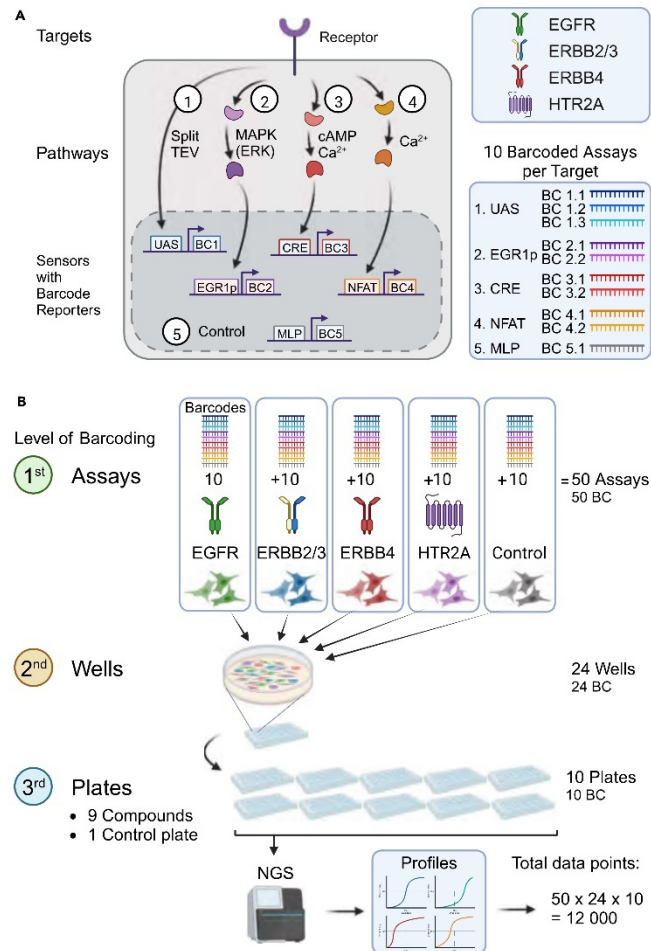


Figure 1. Design of a fully integrated, multiplexed assay to profile activities of ERBB receptor family and physiological signaling in parallel

(A) Summary schematic showing target and pathway assays of the barcoded ERBBprofiler assay. Activities of receptors were monitored using split TEV assays, while activities of pathways were measured using pathway sensors. BC, barcode. Upper inset: targets used in this study. Lower inset: Barcode reporters for targets (UAS), pathways (EGR1p for MAPK/ERK signaling, CRE for cAMP/Ca²⁺ signaling, and NFAT for Ca²⁺ signaling), and a control (MLP).

(B) Workflow for molecular barcoding of assays, wells, and plates. On the first level of barcoding, 50 assays, each with a unique barcode, are monitored in one well. On the second level, the lysates of the wells are barcoded, and on the third level, the plates are barcoded. Barcodes are sequenced using next generation sequencing (NGS), and data are analyzed. In a typical experiment comprising ten 24-well plates, 12,000 data points are generated from ten Tag&Pool (a method to process 24 lysates combined, see STAR Methods section) samples. See also Figure S1 and Table S1.

the activation of ERBB2/3 and ERBB4 (Figure 2A). The responsiveness to the ligands was clearly observed in dose-response graphs for EGFR (Figure 2B) and ERBB4 (Figure 2C). PC12 endogenously express EGFR, and EGFR stimulation leads to the activation of the ERK1/2 branch of MAPK signaling.³⁹ In our cellular profiling assay, this branch of MAPK signaling was captured by the EGR1p sensor. As expected, PC12 cells that were transfected with the EGR1p sensor only responded to increasing EGF concentrations (Figures 2A and 2D). Conversely, EGFld treatment did not lead to any response. When ERBB4 was co-transfected with the EGR1p sensor, EGFld indeed induced an EGR1p response, as

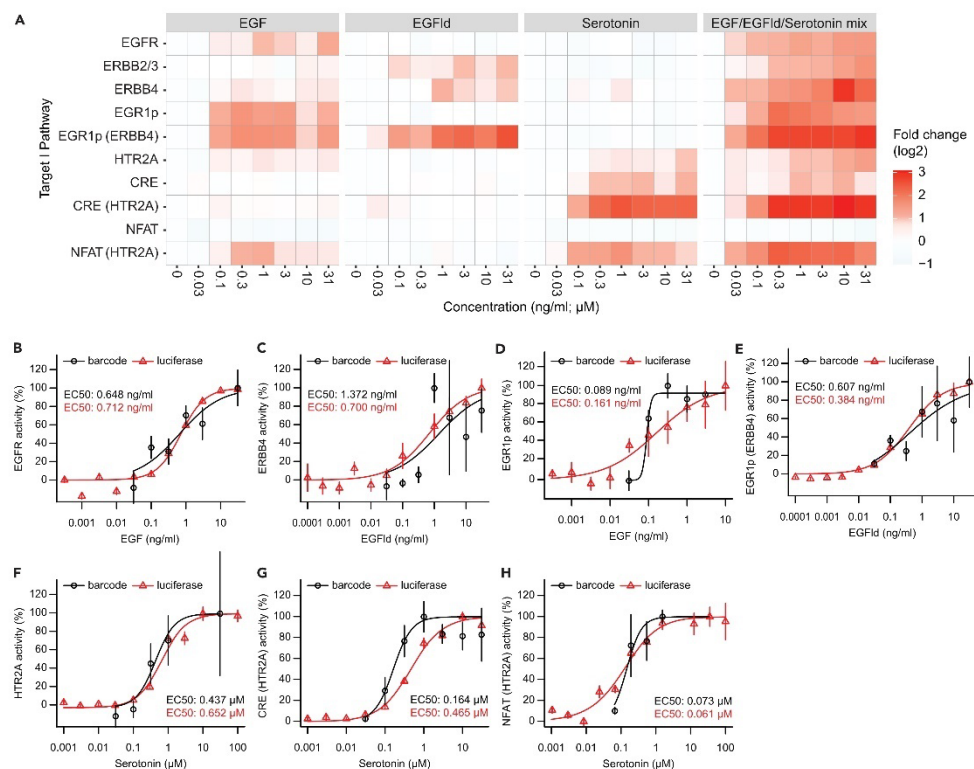


Figure 2. Selectivity of receptor activation and downstream signaling by single ligands correlate in barcoded assays

(A) Heatmap showing stimulation profiles on ERBB receptors, HTR2A, and downstream signaling pathways. Assays for receptors were performed using barcoded split TEV, assays for signaling pathways with pathway sensors coupled to barcodes. Compound effects are shown as log₂-transformed fold change.

(B–H) Barcoded assays align with luciferase readouts. Visualization of selected data from (A), comparing barcoded assays (black) with luciferase assay readouts (red). Assays for receptors were performed using split TEV, assays for signaling pathways with pathway sensors. Dose response graphs for EGFR (B), ERBB4 (C), EGR1p only (D), and EGR1p and ERBB4 transfected (E), HTR2A (F), CRE and HTR2A transfected (G), and NFAT and HTR2A transfected (H) with single stimuli applied at increasing concentrations. EGFld, EGF-like domain. Error bars represent SEM, n = 3 for barcoded assays, and n = 6 for luciferase assays. See also Figure S2 and Table S2.

evident from an increase in EGR1p sensor activity (Figures 2A and 2E). Serotonin treatment selectively activated HTR2A, and physiologically linked calcium signaling was induced when HTR2A was activated, as indicated by increased CRE and NFAT reporter activities (Figures 2A and 2F–2H). EGF treatment led to a low activation of the NFAT sensor in the presence of co-transfected HTR2A, a finding that can be explained by crosstalk between EGFR and HTR2A.⁴⁰ Notably, neither EGF nor EGFld activated CRE and NFAT sensors in the absence of HTR2A, nor did serotonin lead to the activation of the EGR1p sensor, supporting the notion that the stimuli were selective for both targets and physiological pathways. To benchmark the performance of barcoded assays, target and pathway assays for EGFR, ERBB4, and HTR2A were replicated with a luciferase-based readout at dose response (Figures 2B–2H). Barcoded and luciferase assays showed comparable dose-response curves and EC₅₀ values for each assay tested. Responses to target activation (measured by split TEV) and cellular signaling (measured by pathway sensors) correlated for both barcoded assays and luciferase assays (see Figure S2). In addition, cells were treated with a mix of all three ligands to assess any potential synergistic effects among ligands, as this mix of ligands was planned to be applied in antagonist profiling assays to reduce sample numbers. Notably, the effects observed by the individual stimuli and the mix matched for both targets and pathway assays (Figures 2A and S2), enabling a simultaneous assessment in compound profiling assays. All EC₅₀ values for barcoded assays are summarized in Table S2.

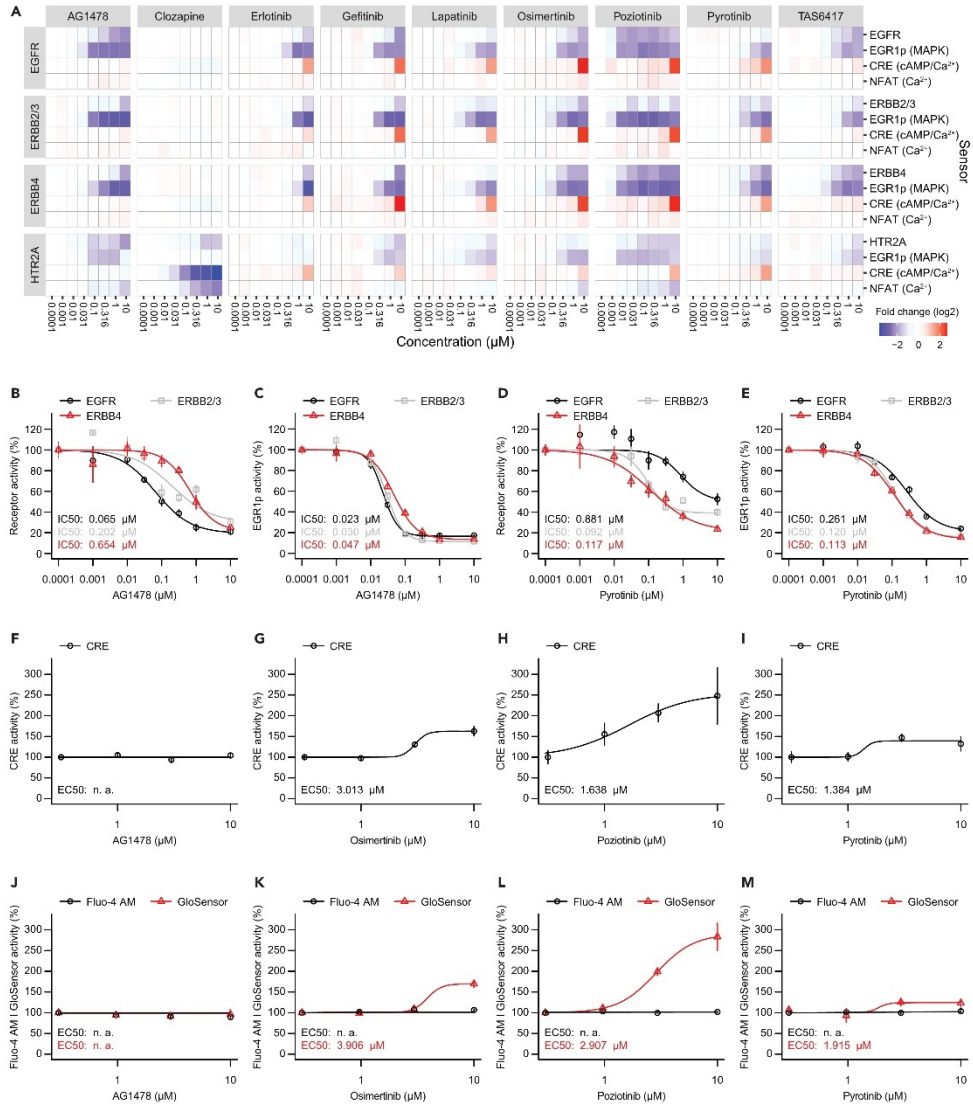


Figure 3. The barcoded ERBBprofiler reveals known and previously uncharacterized selectivity properties of ERBB receptor antagonists

(A) Heatmap showing antagonistic effects of compounds on ERBB receptors, HTR2A, and downstream signaling pathways in PC12 cells. Assays for receptors were performed using barcoded split TEV assays, assays for signaling pathways with barcoded pathway sensors. In addition to the increasing concentrations of the compounds shown, all assays contained constant concentrations of EGF (30 ng/mL), EGF-like domain (10 ng/mL), and serotonin (1 μM). Compound effects are shown as log₂-transformed fold change.

(B–E) Dose response graphs comparing drug selectivity for receptors EGFR and ERBB4 (B, D) and downstream MAPK signaling (C, E) of compounds AG1478 (B, C), and pyrotinib (D, E). Data was extracted from the heatmap shown in (A). n = 3.

Figure 3. Continued

(F–I) Dose response graphs for CRE sensor responses in PC12 cells using luciferase as readout for AG1478 (F), osimertinib (G), poziotinib (H), and pyrotinib (I). In addition to the increasing concentrations of the compounds shown, all assays contained the constant stimulation mix as in (A). (J–M) Dose response graphs for calcium and cAMP assays using Fluo-4 a.m. and GloSensor, respectively, as readouts in PC12 cells treated with increasing concentrations of AG1478 (J), osimertinib (K), poziotinib (L), and pyrotinib (M). As in luciferase assays, the constant stimulation mix was constantly present, next to the mentioned compounds. Error bars represent SEM, n = 3 for barcode assays (B–E), n = 6 for luciferase, Fluo-4 a.m., and GloSensor assays (F–M). See also Figure S3, Tables S3 and S4.

The ERBBprofiler assay reveals known and previously uncharacterized selectivity properties of ERBB receptor antagonists

Next, we sought to challenge the barcoded ERBBprofiler assay and selected various ERBB receptor antagonists, which included approved drugs (erlotinib, gefitinib, lapatinib, osimertinib),^{22,24,41,42} but also a failed compound (AG1478),⁴³ and drug candidates that are in a clinical trial stage (poziotinib, pyrotinib, TAS6417).^{44–46} Clozapine was selected as an approved drug for targeting HTR2A.⁴⁷ As antagonist assays require activated receptors and pathways, we selected the mix of ligands to stimulate ERBB receptors and HTR2A, as well as signaling pathways. As receptors and pathway sensors were sufficiently activated at a concentration of 30 ng/mL EGF, 10 ng/mL EGFd, and 1 μM serotonin (Figure 2A), dose response treatments for all selected drugs were performed in PC12 cells using those agonist concentrations and the same experimental setup as outlined before. Agonists were applied as a mix to reduce sample number. To further simplify handling, antagonist and agonist treatments were conducted simultaneously (Figure S1G). From a total of 240 samples, batches of 24 samples were pooled at the lysis stage using the Tag-and-Pool process to produce ten samples that were processed for barcode sequencing, yielding 12000 data points in total (Figure 1B). For each compound, we obtained a dose-response dataset for each receptor (EGFR, ERBB2/3, ERBB4, and HTR2A) measured by split TEV assays and pathway sensors (EGR1p for the ERK branch of MAPK signaling, CRE for cAMP/calcium signaling, NFAT for calcium signaling) linked to each receptor (Figures 1A and 3A).

All ERBB antagonists inhibited activities of stimulated EGFR, ERBB2/3, and ERBB4, indicating a pan-ERBB-selective profile, albeit with different selectivity (see Table S3 for all IC₅₀ values). Erlotinib and poziotinib had similar affinities for all ERBB receptors, and rather displayed an evenly distributed pan-ERBB selectivity profile (Figures 3A and S3). Gefitinib showed a mild preference for EGFR (EGFR IC₅₀, 0.51 μM; ERBB2/3 IC₅₀, 0.752 μM; ERBB4 IC₅₀, 1.23 μM) (Figure S3). Conversely, lapatinib had a preference for ERBB2/3 over EGFR and ERBB4 (EGFR IC₅₀, 0.942 μM; ERBB2/3 IC₅₀, 0.093 μM; ERBB4 IC₅₀, 0.825 μM), which is consistent with previous observations we made in standard split TEV luciferase assays.³⁷ Similarly, osimertinib favorably antagonized ERBB2/3 and ERBB4 over EGFR (EGFR IC₅₀, 0.201 μM; ERBB2/3 IC₅₀, 0.032 μM; ERBB4 IC₅₀, 0.082 μM). TAS6417 preferentially inhibited both EGFR and ERBB4 over ERBB2/3, although these differences were minor (EGFR IC₅₀, 0.092 μM; ERBB2/3 IC₅₀, 0.206 μM; ERBB4 IC₅₀, 0.091 μM). In agreement with published data from *in-vitro* assays,⁴⁸ our data confirmed antagonistic effects of TAS6417 on ERBB2/3 and ERBB4 activity for the first time *in cellulo*, as well as on ERK signaling downstream of ERBB2/3 and ERBB4. Clozapine, chosen as non-ERBB receptor inhibitor control, selectively antagonized HTR2A and downstream pathways as measured by CRE and NFAT sensors, but did not inhibit any ERBB receptor, nor ERBB mediated signaling (Figures 3A and S3). However, the most striking differences in antagonizing EGFR or ERBB4 for the selected compounds were identified for AG1478 and pyrotinib. AG1478 showed a clear preference for antagonizing EGFR over ERBB2/3 and ERBB4 activities in barcoded split TEV assays (EGFR IC₅₀, 0.065 μM; ERBB2/3 IC₅₀, 0.202 μM; ERBB4 IC₅₀, 0.654 μM) (Figure 3B). Conversely, pyrotinib preferentially antagonized ERBB4 activity over EGFR activity in our assay (EGFR IC₅₀, 0.881 μM; ERBB4 IC₅₀, 0.117 μM) (Figure 3C). Notably, pyrotinib is reported to efficiently bind to EGFR in biochemical assays,⁴⁹ but activity on ERBB4 has not been reported so far.⁵⁰ In the pathway based EGR1p readout, the preferential antagonistic effects of AG1478 and pyrotinib were still measurable, but less pronounced (Figures 3D and 3E). All measured effects for the eight ERBB antagonists and clozapine are summarized in Table S3 and compared to known effects from literature in Table S4.

When comparing our results to IC₅₀ values of phospho-blot and cell proliferation studies, we either had comparable potency values (e.g., for AG1478 on EGFR,⁵¹ erlotinib on phospho-ERK,⁵² osimertinib on ERBB4,²⁸ poziotinib on EGFR and ERBB2/3,⁵³ and TAS6417 on EGFR⁴⁸) or an order of magnitude higher IC₅₀ values, possibly due to the use of different cell lines and assay readouts (e.g., for erlotinib on EGFR, gefitinib on EGFR and ERBB4,^{54,55} osimertinib on EGFR,⁵⁶ and pyrotinib on EGFR.⁴⁹ Furthermore, our data were comparable to results for clozapine effects with three other assays, namely the commercial DiscoverX PathHunter assay for the HTR2A receptor, a cAMP accumulation assay, and a Fluo-4 assay to measure Ca²⁺.^{57–59}

Of note, many ERBB antagonists, including osimertinib, poziotinib, and pyrotinib, caused an upregulation of the CRE sensor at high compound concentration of 10 μM. An increased CRE sensor activity may pinpoint to both increased cAMP and calcium concentrations that may arise from cellular stress.⁶⁰ To validate the results from the barcoded profiling assay, we conducted single luciferase assays using the CRE sensor as readout for these three compounds and AG1478, as the latter did not cause any increased CRE sensor activities in the barcoded assay. In PC12 cells that were transfected with the CRE sensor only, we found similar patterns of CRE sensor activation at high compound concentrations of osimertinib, poziotinib, and pyrotinib, but not for AG1478 (Figures 3F–3I), suggesting a cell intrinsic response caused by a subset of inhibitors. To identify whether the CRE sensor responded to increased cAMP or calcium concentrations, we conducted orthogonal assays in PC12 cells to measure cAMP using a GloSensor assay, while calcium was assessed using Fluo-4 a.m., a cell permeable calcium indicator. AG1478 treatment did not cause any increase in neither cAMP nor calcium (Figure 3J), while higher concentrations (≥ 3 μM) of osimertinib (Figure 3K), poziotinib (Figure 3L), and pyrotinib (Figure 3M) resulted in elevated cAMP, but not calcium levels.

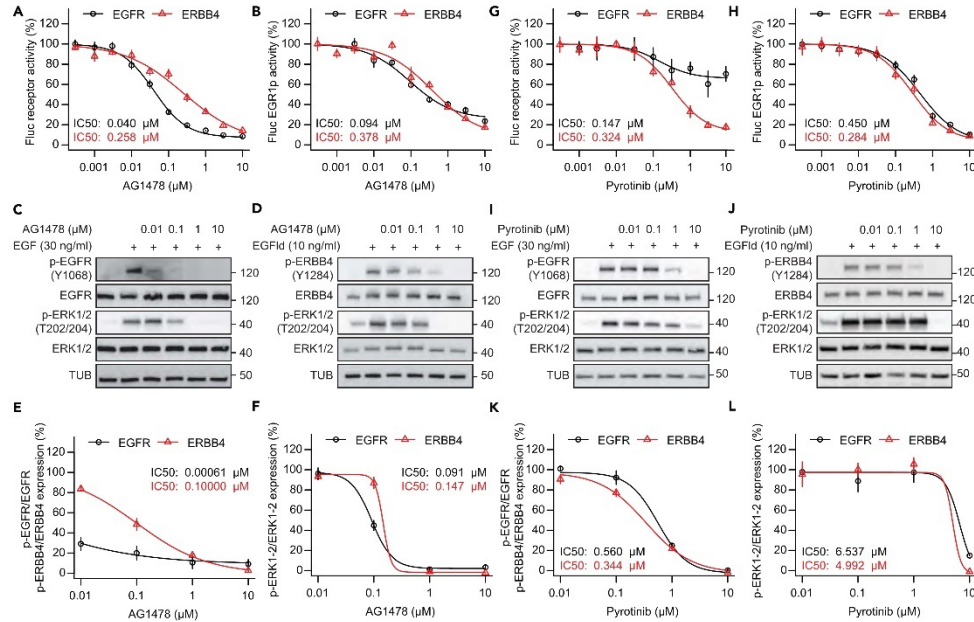


Figure 4. Pyrotinib reveals selectivity for ERBB4 over EGFR

(A and B) Dose response assays comparing AG1478 selectivity for receptors EGFR and ERBB4 (A) and downstream MAPK signaling (B) using firefly luciferase assays in PC12 cells. Assays for receptors were performed using split TEV, assays for MAPK signaling were conducted with an EGR1p pathway sensor. In addition to the increasing concentrations of AG1478, EGFR and ERBB4 assays contained a constant concentration of EGF (30 ng/mL) or EGF-like domain (10 ng/mL), respectively.

(C and D) Western blot analyses of p-EGFR (in A549 cells) (C) and p-ERBB4 (in T-47 cells) (D) using increasing concentrations of AG1478.

(E and F) Quantification of (C) and (D).

(G and H) Dose response assays comparing pyrotinib selectivity for receptors EGFR and ERBB4 (G) and downstream MAPK signaling (H) using firefly luciferase assays in PC12 cells. Assays were conducted as in (A, B).

(I and J) Western blot analyses of p-EGFR (in A549 cells) (I) and p-ERBB4 (in T-47 cells) (J) using increasing concentrations of pyrotinib.

(K and L) Quantification of (I) and (J). Error bars represent SEM, n = 6 for luciferase assays (A, B, G, H), n = 3 for Western blot assays (E, F, K, L).

Pyrotinib reveals selectivity for ERBB4 over EGFR

A key feature of the established ERBB profiling assay should be that it can discriminate between EGFR and ERBB4 selective compounds. Next, we aimed to validate the barcode assay results for AG1478 and pyrotinib using single luciferase assays and Western blotting as orthogonal assays. AG1478 inhibited EGFR over ERBB4 in split TEV luciferase assays (Figure 4A). However, this preference for EGFR was not present anymore when the EGR1p pathway sensor was used as readout (Figure 4B), indicating that a direct coupling of the reporter to the target, as in split TEV assays, is required to detect subtle differences. To confirm AG1478's activity on EGFR over ERBB4, A549 cells, which endogenously express EGFR,⁶¹ and T-47D cells, which endogenously express ERBB4,^{37,62} were treated with constant concentrations of agonists (i.e., EGF for A549 cells, and EGFld for T-47D cells) and increasing concentrations of AG1478. Indeed, AG1478 preferentially antagonized phospho-EGFR over phospho-ERBB4 in Western blot analyses (Figures 4C–4F). In addition, AG1478 inhibited EGFR mediated downstream ERK signaling, a finding that was quantified *in cellulo* for the first time by our barcoded assay (Figures 3A–3C). These results were validated by the luciferase assay using the EGR1p sensor as well as biochemically by assessing phospho-ERK1/2 in a Western blot analysis (Figures 4B and 4F). In sum, the preference for AG1478-mediated EGFR over ERBB4 inhibition was present at receptor level but was lost at pathway level in both the barcoded assays and Western blot assays.

Conversely, pyrotinib preferentially inhibited ERBB4 activity over EGFR activity in split TEV receptor assays (Figure 4G). However, pyrotinib's preference for ERBB4 was compromised in pathway assays using the EGR1p sensor as downstream readout (Figure 4H). To confirm pyrotinib's activity on ERBB4 over EGFR, we treated A549 cells and T-47D cells with constant concentrations of agonists (i.e., EGF for A549 cells, and EGFld for T-47D cells) and increasing concentrations of pyrotinib. Indeed, pyrotinib treatment led to a more potent inhibition of ERBB4

activity as measured by phospho-ERBB4 and phospho-EGFR (Figures 4I–4L). Similar to the barcoded and luciferase EGR1p pathway assays, EGFR and ERBB4-dependent phospho-ERK1/2 signals did not substantially differ in pyrotinib treated cells (Figures 4H and 4L). Taken together, the barcoded ERBB profiling assay can assess antagonistic actions on ERBB receptors and key physiological pathways, assess a compound's selectivity, and identify potential side effects in one experiment.

Discovery of novel ERBB4 selective antagonists

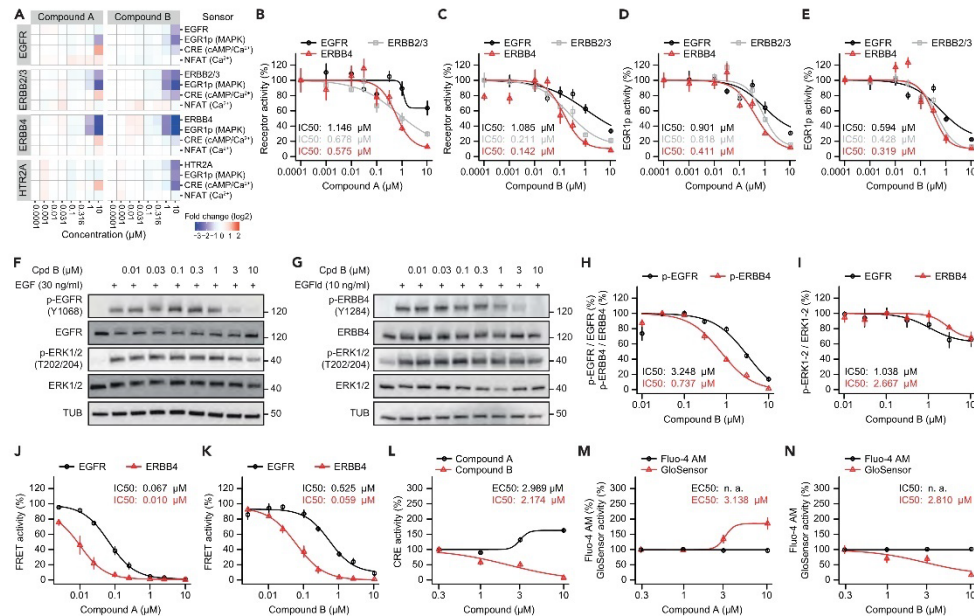
Previously, we identified spironolactone as ERBB4 antagonist in a drug repurposing screen, while spironolactone's metabolite canrenone did not inhibit ERBB4 activity.³² To test the capabilities of the barcoded ERBB profiler assay, we treated PC12 assay cells with increasing concentrations of both spironolactone and canrenone and agonists. Results confirmed the antagonistic effect of spironolactone on ERBB4 with similar activity (IC₅₀: 4.327 μM) (Figure S4). Conversely, canrenone did not inhibit any ERBB receptor nor pathway monitored. Furthermore, we found that spironolactone inhibited HTR2A at 10 μM, but not at lower concentrations (Figure S4).

Next, we sought to profile potentially selective ERBB4 antagonists, termed compounds A and B, that were designed and synthesized in a proprietary kinase inhibitor program to challenge our barcoded ERBB family profiling assay. The main goal was to identify compounds that show a selectivity for ERBB4 over EGFR for the potential use in follow-up drug discovery campaigns. Both compounds A and B more efficiently inhibited ERBB4 than EGFR (Figure 5A). When extracting the data from this heatmap and computing dose-response curves, we found that both compounds showed a higher activity for ERBB4 than for EGFR and to some extent for ERBB2/3 (Table S3). Importantly, compound B had both better efficacy and preference for ERBB4 over EGFR (ERBB4 IC₅₀: 0.142 μM, EGFR IC₅₀: 1.085 μM, about 8-fold) than compound A (ERBB4 IC₅₀: 0.575 μM, EGFR IC₅₀: 1.146 μM, about 2-fold) (Figures 5B and 5C), defining compound B as frontrunner compound. Similarly, ERK signaling was inhibited by these two compounds in an EGFR, ERBB2/3, and ERBB4 mediated manner, reflecting the inhibition at receptor level (Figures 5D and 5E). Biochemical validation by Western blotting of phospho-EGFR (in A549 cells) (Figure 5F) and phospho-ERBB4 (in T-47D cells) (Figure 5G) confirmed that compound B preferentially antagonized ERBB4, as revealed by quantification of phosphorylation levels (Figure 5H). An analysis of downstream phospho-ERK1/2 showed that compound B reduced the ERK pathway activity to about 70% of activated EGFR and ERBB4 (Figure 5I). To confirm that compounds A and B inhibited EGFR and ERBB4 at different potencies, we conducted LANCE kinase activity assays. In this *in vitro* executed enzymatic assay, synthetic substrates are incubated with EGFR and ERBB4 purified protein, and the amount of phosphorylated substrate is detected by a specific anti-phosphopeptide antibody, resulting in a time resolved fluorescence resonance energy transfer (TR-FRET) signal. Notably, both compounds A and B inhibited ERBB4 more effectively than EGFR (Figures 5J and 5K). In addition, compound B displayed a better preference profile for ERBB4 than EGFR, as evident from IC₅₀ values for compound B (ERBB4: 0.059, EGFR: 0.525) and compound A (ERBB4: 0.01, EGFR: 0.067). Thus, compound B showed an about 9-fold preference for ERBB4, while compound A only displayed an about 7-fold preference, validating the findings of our cellular profiling assay that compound B had better selectivity for ERBB4.

An analysis of downstream pathway activities further showed that compound A treatment at 10 μM led to the activation of the CRE sensor for all targets tested (Figure 5A). A separate validation assay in PC12 cells by transfecting only a CRE sensor linked to luciferase readout confirmed this opposite behavior of these two novel ERBB4 antagonists. In this assay, PC12 cells were treated with increasing concentrations of either compound A or B and the stimulation mix containing EGF, EGFid, and serotonin to mimic the conditions from the barcoded assays. While compound A treatment led to increased CRE activity at concentrations of ≥ 3 μM, compound B treatment inhibited CRE activity in a dose-dependent manner (Figure 5L). To assess whether the CRE sensor is modulated by altered levels of cAMP or calcium in response to ERBB4 antagonist treatment, the GloSensor assay was used to measure cAMP and Fluo-4 a.m. to assess calcium. As in luciferase validation assays, PC12 cells were treated with increasing concentrations of either compound A or B and the stimulation mix. Calcium levels were neither affected by compound A nor by compound B. However, compound A concentrations of ≥ 3 μM caused an increase in cAMP levels, while compound B treatment, starting with 1 μM and higher, caused a steady decrease in cAMP, mirroring the effects from the CRE sensor barcode and luciferase assays (Figures 5M and 5N). Furthermore, treatment with compound B, but not compound A, resulted in an inhibition of HTR2A at target (split TEV assay) and pathway levels (CRE assay) in PC12 cells (Figures 5A, 5SA, and 5SB), a finding that was validated by independent luciferase assays for compound B (Figure 5SC). Taken together, we identified two novel ERBB4 selective antagonists, with compound B being more selective and, at least in cell culture, more potent than compound A.

DISCUSSION

We describe the establishment of a barcoded ERBB receptor profiling assay that enables the simultaneous profiling of compound actions on ERBB targets and key downstream pathways in living cells. Specifically, split TEV assays for monitoring the activities of full-length EGFR, ERBB2/3, ERBB4, and HTR2A (a GPCR as non-ERBB receptor control) are parallelized with pathway assays for cAMP/Ca²⁺ signaling (CRE sensor), pure Ca²⁺ signaling (NFAT sensor), and the ERK branch of MAPK signaling (EGR1p sensor) in this multiparametric assay platform. Notably, downstream pathway responses were uniquely assigned to each receptor, allowing the identification of functionally distinct activities when treated with a compound from one well. For example, while the MAPK sensor EGR1p was inhibited by pyrotinib, the CRE sensor was activated at high concentrations for all ERBB receptors. Furthermore, varying intensities of inhibition or activation for one pathway were clearly assigned to a specific ERBB receptor activity. Barcoded assays are as responsive and robust as single luciferase assays, as evidenced by similar EC₅₀ values obtained from these two assay types for targets and pathways tested. Through applying a multilevel barcoding strategy for analyzing cellular activities (i.e., sensors with unique barcodes for targets and pathways), wells (sample barcoding through pooling of cell lysates using Tag&Pool and PCR-based barcoding), and cell culture plates (PCR-based barcoding) in parallel, we reduced sample numbers



and hands-on time for sample processing and NGS analyses, while processing thousands of data points. In addition, we reduced sample numbers in drug profiling assays even further by stimulating ERBB receptor and HTR2A targets with a ligand mix. The principle of the bar-coded profiling assay can be extended in the future to any other RTK, GPCR, or other targets for which split TEV assays are available or can be developed. Pathway sensors used here can be applied to any RTK or GPCR assay, and additional sensors can be developed to capture activities of other cellular pathways. However, the number of pathway sensors possibly used per target is limited by the well size (i.e., number of cells that fit into a well), the number of targets used per well, and the depth of the sequencing, thus affecting the overall assay's complexity.

Commonly used kinase profiling assays for ERBB receptors are based on biochemical kinase platforms, which can be divided into two classes, activity assays and binding assays. Activity assays directly or indirectly measure the catalytic product and include radiometric platforms (e.g., HotSpot),⁶³ luminescence-based (e.g., Kinase-Glo), and fluorescence-based platforms (e.g., Lance TR-FRET assay or LanthaScreen TR-FRET assay).⁶⁴ (Note that compounds A and B were validated using the Lance TR-FRET kinase activity assay.) In contrast, binding assays measure the binding of compounds to the kinase active site, but not the catalytic product (e.g., KinomeScan).⁶⁴ All of these are single assays and

biochemical in nature. A more focused platform for the analysis of RTK activities uses a membrane-based sandwich immunoassay with phosphotyrosine antibodies and some degree of multiplexing as one cellular lysate can be used to profile 49 different RTKs.⁶⁵ RTKs and cellular downstream effectors can also be profiled using an image-based approach, as described for EGFR.⁶⁶ This method was reported to be robust but rather labor intensive, making multiplexing inefficient. Although most of these assays use smaller well formats than we did in this study, multiplexing at the assay level (including both targets and pathways), well level, and plate level as introduced for our multilevel barcoded reporter profiling assay is not feasible. In contrast, using NGS as a readout for our barcoded assay, we simultaneously monitored the effects of compounds on ERBB receptors and their downstream pathways, using 50 assays per well and obtaining 12,000 data points from a standard assay setup.

We challenged the ERBB receptor profiling assay with eight different ERBB receptor antagonists (AG1478, erlotinib, gefitinib, lapatinib, osimertinib, poziotinib, pyrotinib, and TAS6417) that were developed to target different types of cancers. All these drugs inhibited the activity of EGFR, ERBB2/3, ERBB4 at different levels, and likewise, canonical downstream ERK signaling. When systematically comparing our IC₅₀ data with published data obtained from cellular assays, we noticed that we had comparable potencies for some of the eight ERBB antagonists on selected targets and pathways,^{28,48,51–53} while for other combinations our potency values were an order of magnitude higher (cf. Table S4).^{49,52,54–56} The latter case may be due to different cell types and/or assay systems applied. Nevertheless, a substantial number of studies used phospho-blot to demonstrate the drug effect on ERBB receptors. Although this is a very reliable technique, due to its technical demands, most of these findings were only qualitative in nature, especially when studying pathway activities. Conversely, our ERBB profiling assay allows the monitoring of multiple compounds on ERBB receptors and linked pathways in parallel, saving both hands-on time and money. We validated our previous findings for lapatinib that showed a preference for ERBB2/3 and ERBB4 over EGFR,³¹ while spironolactone was an ERBB4 selective antagonist.³² Most strikingly, AG1478 displayed a preference for EGFR, while pyrotinib showed a preference for ERBB4. As this was expected for AG1478,⁶⁷ pyrotinib's effect on ERBB4 is novel. Together, these features verify that the barcoded ERBB receptor profiling assay can detect both preferred activities of compounds for EGFR versus ERBB4 and represents an optimal route to assess ERBB antagonists in living cells. The ERBB profiler assay enables the simultaneous monitoring of target and pathway effects in living cells. In this respect, we identified pathway characteristics for AG1478, as we quantified its effect on ERBB4 and MAPK signaling downstream of EGFR for the first time *in cellulo*. Likewise, we monitored effects of TAS6417 on ERBB2/3 and ERBB4 for the first time *in cellulo*.^{57,68,69} Poziotinib was the only covalent inhibitor we tested, and it is known to inhibit ERBB receptor activities at nanomolar range.^{53,70} Indeed, we observed a very strong activity of this drug, both at target and pathway level, arguing that our platform reliably detects compound effects across several magnitudes of molar range.

Frequently, we observed enhanced potency of drugs on pathway assays (i.e., lower IC₅₀ values) when compared to target assays, suggesting that compound effects are amplified within the process of cellular signaling.⁷¹ Conversely, target assays were more useful in identifying a drug's selectivity for a given ERBB receptor. Importantly, activity trends for targets aligned well with pathway activities in our profiling assay, supporting the notion that both assay types can be used to assess compound actions. Nevertheless, for some conditions, drug effects on targets may be very subtle or even hidden,^{72,73} and pathway assays may be used to unveil these effects through cellular signal amplification.

At high drug concentrations of 10 μM, we observed an upregulated CRE sensor response for many of the tested drugs (i.e., erlotinib, gefitinib, lapatinib, osimertinib, poziotinib, pyrotinib, TAS6417, canrenone, and compound A). Using orthogonal assays specific for cAMP and calcium we found that high concentrations of poziotinib treatment led to an increase of cAMP. Increased cAMP concentrations are linked to cellular stress pathways, cellular energy status, as well as oxidative and proteotoxic stress,^{14,74–76} suggesting that high concentrations of selected ERBB antagonist are the cause for this abnormal cellular signature. Remarkably, clozapine, spironolactone, and compound B did not activate the CRE sensor at 10 μM, suggesting that these compounds are also better tolerated at higher, albeit non-physiological, concentrations. In fact, PC12 cells treated with compound B, and without transfecting any other plasmids than the GloSensor, resulted in a concentration-dependent decrease of cAMP, which might be mediated by antagonizing activities conferred by HTR6A, a Gα_s protein coupled GPCR expressed in PC12 cells,⁷⁷ or by inhibiting components of the protein kinase A/cAMP pathway.

Increased ERBB4 activity leads to an excitation/inhibition imbalance in schizophrenic patients,^{30,31} and antagonizing ERBB4 activity using spironolactone improved schizophrenia relevant phenotypes including cognition in a *Nrg1* transgenic mouse model,³² prompting also a clinical trial with spironolactone as adjuvant to antipsychotic medication, i.e., co-administering spironolactone with an established antipsychotic, e.g., risperidone or aripiprazole.⁷⁸ Notably, a separately conducted clinical trial using spironolactone as add-on therapeutic to risperidone reported improvements for positive and negative symptoms, but not cognitive deficits.⁷⁹ In addition, spironolactone as mineralocorticoid receptor antagonist was shown to improve cognition in mouse models of type II diabetes⁸⁰ and Alzheimer's disease.⁸¹ In our profiling assay, we found that spironolactone also inhibits HTR2A, and antagonists to HTR2A are frequently used for the treatment of schizophrenia,⁸² suggesting that such a polypharmacological profile may be beneficial for alleviating symptoms in schizophrenic patients.

When targeting ERBB4, at least in the CNS, a drug's selectivity over EGFR is most crucial, as EGFR activity is key for the propagation of neural precursors and the differentiation of these into neurons, while ERBB4 is linked to schizophrenic phenotypes.^{83,84} In addition, ERBB4 is most closely related to EGFR.^{85,86} A recent study reported two investigational compounds that are ERBB4-selective over EGFR, with a 2.5-fold pref.⁸⁷ However, compounds with a higher selectivity are required to bypass any non-desired effects that may be mediated through EGFR inhibition. Here, we identify two novel compounds that were synthesized in a proprietary kinase inhibitor program and that have an increased selectivity for ERBB4 over EGFR, with compound B displaying an about 8-fold preference. Importantly, this strong preference for ERBB4 for compound B we observed in the cellular profiling assay was confirmed by *in-vitro* kinase assays, albeit to a lesser degree. Furthermore, compound B, but not compound A also inhibited HTR2A. Therefore, compound B with its pharmacological profile may represent a lead structure



for a therapeutic application targeting schizophrenia in stratified patients with an ERBB4 dependent cognitive deficit, requiring further work on pharmacokinetics, pharmacodynamics, elucidating the mechanism of action, and the compound's effect on behavior in mice. Given a sufficient compound availability in the brain, this novel ERBB4 antagonist should be tested in an add-on study paradigm to assess any improvement in behavioral tests in a relevant mouse model.^{88,89} Moreover, ERBB4 overexpression is associated with numerous cancer types (e.g., gastric cancer, non-small cell lung cancer, inflammatory breast cancer, pancreatic cancer, prostate cancer).^{17,90-92} Thus, the newly developed compounds A and B may also be lead structures for targeting ERBB4 positive cancers.

In summary, we have developed a multiplexed cell-based profiling assay, termed ERBBprofiler assay that assesses drug effects on ERBB family receptors and key cellular signaling pathways, opening an efficient route for early-stage drug discovery of ERBB antagonists. Using this assay, we described previously unknown compound properties for selected ERBB receptor inhibitors. Furthermore, we identified newly designed ERBB4 selective antagonists that have an increased selectivity and could be used as lead compounds in drug discovery programs. Due to the multilevel barcoding approach, multiple assays and treatment parameters can be run in parallel, enabling the acquisition of thousands of data points from one experiment. Stable integration of assay components into cells, expansion to additional targets, and automation through liquid handling robotics is expected to further enhance the assay robustness and throughput to enable profiling of larger compound collections.

Limitations of the study

For the ERBBprofiler assay, we focused on monitoring the activities of EGFR, ERBB2/3, and ERBB4. We did not measure the effects of ERBB2 and ERBB3 homodimers, although they could be added to an extended version of the ERBBprofiler assay. We included pathway sensors for three key downstream pathways of ERBB receptors, namely cAMP signaling, Ca²⁺ signaling, and the ERK branch of MAPK signaling. However, we excluded other ERBB receptor-regulated pathways, such as AKT signaling. In the future, sensors for AKT signaling and other relevant signaling pathways may also be added. The complexity of the ERBBprofiler assay is determined by the number of barcoded assays in each well. Here, the ERBBprofiler assay consisted of 50 individual assays per well and was performed in 24-well formats. We did not test whether the ERBBprofiler assay with a complexity of 50 assays also performs robustly in smaller well formats, like 48-well and 96-well formats, to enable a high-throughput compatible screening of compounds. Therefore, the current form of the ERBBprofiler assay is constrained to a medium throughput format that uses 24-well plates. Furthermore, it is feasible to introduce additional assays for both the receptors and pathways that would increase the complexity per well. However, this could have an adverse effect on the performance of the assay when conducted in a 24-well format, as utilized in this study. If more sensors will be added per well, more cells per well may be required for the efficient sequencing of barcoded reporters. We conducted all experiments using transient transfections. Assays with a transient transfection may, however, have a reduced robustness and reproducibility compared to stably integrated assay components. Therefore, our future investigations will primarily focus on making cell lines with receptors that have been stably integrated.

STAR★METHODS

Detailed methods are provided in the online version of this paper and include the following:

- KEY RESOURCES TABLE
- RESOURCE AVAILABILITY
 - Lead contact
 - Materials availability
 - Data and code availability
- EXPERIMENTAL MODEL AND STUDY PARTICIPANT DETAILS
 - Cell lines
 - Plasmids
 - Bacterial strains
 - Chemical reagents
- METHOD DETAILS
 - Vector construction
 - Luciferase reporter assays
 - GloSensor cAMP assay
 - Fluo-4 a.m. calcium assays
 - Barcode reporter assays
 - Biochemistry
 - *In vitro* kinase assays
- QUANTIFICATION AND STATISTICAL ANALYSIS
 - Data analysis of barcode and luciferase reporter assays
 - Data analysis of *in vitro* kinase assays
 - Statistical analysis

SUPPLEMENTAL INFORMATION

Supplemental information can be found online at <https://doi.org/10.1016/j.isci.2024.108839>.

ACKNOWLEDGMENTS

The research was supported by funding from the European Union through the PDZnet project (H2020-MSCA-ITN-2015, Marie Skłodowska-Curie Grant agreement ID 675341) and through the China Scholarship Council, grant number 201906230338. We thank Barbara Meisel, Monika Rübekel and Johanna Zach for their excellent technical support.

AUTHOR CONTRIBUTIONS

Conceptualization: L.P., M.J.R., and M.C.W. Data curation: L.P. and M.C.W. Formal analysis: L.P. Methodology: L.P., J.P.W., S.M., S.P.W., and M.C.W. Investigation: L.P., J.P.W., Y.W., B.B., S.M., C.D., N.J., S.P.W., and M.C.W. Visualization: L.P., S.M., and M.C.W. Resources: B.K., M.J.R., S.P.W., and M.C.W. Supervision: M.C.W. Writing – original draft: L.P. and M.C.W. Writing – review and editing: all authors.

DECLARATION OF INTERESTS

The authors declare competing financial interest. B.B., S.P.W., M.J.R., and M.C.W. are employees and shareholders of Systasy Bioscience GmbH.

Received: October 11, 2023

Revised: November 20, 2023

Accepted: January 3, 2024

Published: January 9, 2024

REFERENCES

- Jin, W. (2020). ErbB Family Proteins in Cholangiocarcinoma and Clinical Implications. *J. Clin. Med.* 9, 2255.
- Lemmon, M.A., and Schlessinger, J. (2010). Cell Signaling by Receptor Tyrosine Kinases. *Cell* 141, 1117–1134.
- Mei, L., and Nave, K.-A. (2014). Neuregulin-ERBB Signaling in the Nervous System and Neuropsychiatric Diseases. *Neuron* 83, 27–49.
- Tavassoly, O., Sato, T., and Tavassoly, I. (2020). Inhibition of Brain Epidermal Growth Factor Receptor Activation: A Novel Target in Neurodegenerative Diseases and Brain Injuries. *Mol. Pharmacol.* 98, 13–22.
- Klapper, L.N., Glathe, S., Vaisman, N., Hynes, N.E., Andrews, G.C., Sela, M., and Yarden, Y. (1999). The ErbB-2/HER2 oncoprotein of human carcinomas may function solely as a shared coreceptor for multiple stroma-derived growth factors. *Proc. Natl. Acad. Sci.* 96, 4995–5000.
- Olayioye, M.A., Beuving, I., Horsch, K., Daly, J.M., and Hynes, N.E. (1999). ErbB receptor-induced activation of stat transcription factors is mediated by Src tyrosine kinases. *J. Biol. Chem.* 274, 17209–17218.
- Sidhanth, C., Manasa, P., Krishnapriya, S., Sneha, S., Bindhya, S., Nagare, R.P., Garg, M., and Ganesan, T.S. (2018). A systematic understanding of signaling by ErbB2 in cancer using phosphoproteomics. *Biochem. Cell. Biol.* 96, 295–305.
- Steinkamp, M.P., Low-Nam, S.T., Yang, S., Lidke, K.A., Lidke, D.S., and Wilson, B.S. (2014). erbB3 Is an Active Tyrosine Kinase Capable of Homo- and Heterointeractions. *Mol. Cell Biol.* 34, 965–977.
- Abourehab, M.A.S., Alqahtani, A.M., Youssif, B.G.M., and Gouda, A.M. (2021). Globally Approved EGFR Inhibitors: Insights into Their Syntheses, Target Kinases, Biological Activities, Receptor Interactions, and Metabolism. *Molecules* 26, 6677.
- Quasnelle, K.M., Boehm, A.L., and Grandis, J.R. (2007). STAT-mediated EGFR signaling in cancer. *J. Cell. Biochem.* 102, 311–319.
- Kao, S., Jaiswal, R.K., Kolch, W., and Landreth, G.E. (2001). Identification of the mechanisms regulating the differential activation of the mapk cascade by epidermal growth factor and nerve growth factor in PC12 cells. *J. Biol. Chem.* 276, 18169–18177.
- Santos, S.D.M., Verwee, P.J., and Bastiaens, P.I.H. (2007). Growth factor-induced MAPK network topology shapes Erk response determining PC-12 cell fate. *Nat. Cell Biol.* 9, 324–330.
- Sigismund, S., Avanzato, D., and Lanzetti, L. (2018). Emerging functions of the EGFR in cancer. *Mol. Oncol.* 12, 3–20.
- Yu, D., and Hung, M.-C. (2000). Overexpression of ErbB2 in cancer and ErbB2-targeting strategies. *Oncogene* 19, 6115–6121.
- Sithanandam, G., and Anderson, L.M. (2008). The ERBB3 receptor in cancer and cancer gene therapy. *Cancer Gene Ther.* 15, 413–448.
- Lucas, L.M., Dwivedi, V., Senfeld, J.I., Cullum, R.L., Mill, C.P., Piazza, J.T., Bryant, I.N., Cook, L.J., Miller, S.T., Lott, J.H., et al. (2022). The Yin and Yang of ERBB4: Tumor Suppressor and Oncoprotein. *Pharmacol. Rev.* 74, 18–47.
- Segers, V.F.M., Dugaucquier, L., Feyen, E., Shakeri, H., and De Keulenaer, G.W. (2020). The role of ErbB4 in cancer. *Cell. Oncol.* 43, 335–352.
- Wang, Z. (2017). ErbB Receptors and Cancer. In *ErbB Receptor Signaling Methods in Molecular Biology*, Z. Wang, ed. (Springer New York), pp. 3–35.
- Frey, M.R., Edelblum, K.L., Mullane, M.T., Liang, D., and Polk, D.B. (2009). The ErbB4 growth factor receptor is required for colon epithelial cell survival in the presence of TNF. *Gastroenterology* 136, 217–226.
- Williams, C.S., Bernard, J.K., Demory-Beckler, M., Almohazey, D., Washington, M.K., Smith, J.J., and Frey, M.R. (2015). ERBB4 is over-expressed in human colon cancer and enhances cellular transformation. *Carcinogenesis* 36, 710–718.
- Ding, L., Getz, G., Wheeler, D.A., Mardis, E.R., McLellan, M.D., Cibulskis, K., Sougnez, C., Greulich, H., Muzny, D.M., Morgan, M.B., et al. (2008). Somatic mutations affect key pathways in lung adenocarcinoma. *Nature* 455, 1069–1075.
- Cohen, M.H., Williams, G.A., Sridhara, R., Chen, G., and Pazdur, R. (2003). FDA drug approval summary: gefitinib (ZD1839) (Iressa) tablets. *Oncol.* 8, 303–306.
- Cohen, M.H., Johnson, J.R., Chen, Y.-F., Sridhara, R., and Pazdur, R. (2005). FDA drug approval summary: erlotinib (Tarceva) tablets. *Oncol.* 10, 461–466.
- Ryan, Q., Ibrahim, A., Cohen, M.H., Johnson, J., Ko, C.w., Sridhara, R., Justice, R., and Pazdur, R. (2008). FDA drug approval summary: lapatinib in combination with capecitabine for previously treated metastatic breast cancer that overexpresses HER-2. *Oncol.* 13, 1114–1119.
- Bhullar, K.S., Lagarón, N.O., McGowan, E.M., Parmar, I., Jha, A., Hubbard, B.P., and Rupasinghe, H.P.V. (2018). Kinase-targeted cancer therapies: progress, challenges and future directions. *Mol. Cancer* 17, 48.
- Liu, Q., Yu, S., Zhao, W., Qin, S., Chu, Q., and Wu, K. (2018). EGFR-TKIs resistance via EGFR-independent signaling pathways. *Mol. Cancer* 17, 53–59.
- Niaderst, M.J., and Engelmann, J.A. (2013). Bypass mechanisms of resistance to receptor tyrosine kinase inhibition in lung cancer. *Sci. Signal.* 6, reb6.

28. Cross, D.A.E., Ashton, S.E., Ghiorghiu, S., Eberlein, C., Nebhan, C.A., Spitzler, P.J., Orme, J.P., Finlay, M.R.V., Ward, R.A., Mellor, M.J., et al. (2014). AZD9291, an irreversible EGFR TKI, overcomes T790M-mediated resistance to EGFR inhibitors in lung cancer. *Cancer Discov.* 4, 1046–1061.
29. Tan, C.-S., Kumarakulasinghe, N.B., Huang, Y.-O., Ang, Y.L.F., Choo, J.R.-E., Goh, B.-C., and Soo, R.A. (2018). Third generation EGFR TKIs: current data and future directions. *Mol. Cancer* 17, 29.
30. Chong, V.Z., Thompson, M., Beltaifa, S., Webster, M.J., Law, A.J., and Weickert, C.S. (2008). Elevated Neuregulin-1 and ErbB4 Protein in the Prefrontal Cortex of Schizophrenic Patients. *Schizophr. Res.* 100, 270–280.
31. Li, B., Woo, R.-S., Mei, L., and Malinow, R. (2007). The Neuregulin-1 Receptor ErbB4 Controls Glutamatergic Synapse Maturation and Plasticity. *Neuron* 54, 583–597.
32. Wehr, M.C., Hinrichs, W., Brzózka, M.M., Unterbarnscheidt, T., Herholt, A., Wintgens, J.P., Papiol, S., Soto-Bernardini, M.C., Kravchenko, M., Zhang, M., et al. (2017). Spironolactone is an antagonist of NRG1-ERBB4 signaling and schizophrenia-relevant endophenotypes in mice. *EMBO Mol. Med.* 9, 1448–1462.
33. Santos, R., Ursu, O., Gaulton, A., Bento, A.P., Donadi, R.S., Bologa, C.G., Karlsson, A., Al-Lazikani, B., Hersey, A., Oprea, T.I., and Overington, J.P. (2017). A comprehensive map of molecular drug targets. *Nat. Rev. Drug Discov.* 16, 19–34.
34. Hoare, S.R.J. (2021). The Problems of Applying Classical Pharmacology Analysis to Modern In Vitro Drug Discovery Assays: Slow Binding Kinetics and High Target Concentration. *SLAS Discov.* 26, 835–850.
35. Galinski, S., Wichert, S.P., Rossner, M.J., and Wehr, M.C. (2018). Multiplexed profiling of GPCR activities by combining split TEV assays and EXT-based barcoded readouts. *Sci. Rep.* 8, 8137.
36. Herholt, A., Sahoo, V.K., Popovic, L., Wehr, M.C., and Rossner, M.J. (2022). Dissecting intercellular and intracellular signaling networks with barcoded genetic tools. *Curr. Opin. Chem. Biol.* 66, 102091.
37. Wintgens, J.P., Wichert, S.P., Popovic, L., Rossner, M.J., and Wehr, M.C. (2019). Monitoring activities of receptor tyrosine kinases using a universal adapter in genetically encoded split TEV assays. *Cell. Mol. Life Sci.* 76, 1185–1199.
38. Djannatian, M.S., Galinski, S., Fischer, T.M., and Rossner, M.J. (2011). Studying G protein-coupled receptor activation using split-tobacco etch virus assays. *Anal. Biochem.* 412, 141–152.
39. Hulf, K., End, D., and Guroff, G. (1981). Nerve growth factor-induced alteration in the response of PC12 pheochromocytoma cells to epidermal growth factor. *J. Cell Biol.* 88, 189–198.
40. Gööz, M., Gööz, P., Luttrell, L.M., and Raymond, J.R. (2006). 5-HT_{2A} receptor induces ERK phosphorylation and proliferation through ADAM-17 tumor necrosis factor- α -converting enzyme (TACE) activation and heparin-bound epidermal growth factor-like growth factor (HB-EGF) shedding in mesangial cells. *J. Biol. Chem.* 281, 21004–21012.
41. Johnson, J.R., Cohen, M., Sridhara, R., Chen, Y.-F., Williams, G.M., Duan, J., Gobburu, J., Booth, B., Benson, K., Leighton, J., et al. (2005). Approval Summary for Erlotinib for Treatment of Patients with Locally Advanced or Metastatic Non-Small Cell Lung Cancer after Failure of at Least One Prior Chemotherapy Regimen. *Clin. Cancer Res.* 11, 6414–6421.
42. Koch, A.L., Vellanki, P.J., Drezner, N., Li, X., Mishra-Kalyani, P.S., Shen, Y.L., Xia, H., Li, Y., Liu, J., Zirkelbach, J.F., et al. (2021). FDA Approval Summary: Osimertinib for Adjuvant Treatment of Surgically Resected Non-Small Cell Lung Cancer, a Collaborative Project Orbis Review. *Clin. Cancer Res.* 27, 6638–6643.
43. Weglicki, W.B., Kramer, J.H., Spurney, C.F., Chmielinska, J.J., and Mak, I.T. (2012). The EGFR tyrosine kinase inhibitor typhostin AG-1478 causes hypomagnesemia and cardiac dysfunction. *Can. J. Physiol. Pharmacol.* 90, 1145–1149.
44. Piotrowska, Z., Yu, H.A., Yang, J.C.-H., Koczywas, M., Smit, E.F., Tan, D.S.-W., Lee, V.H.-F., Soo, R.A., Wrangle, J.M., Spira, A.I., et al. (2021). Safety and activity of CLN-081 (TAS6417) in NSCLC with EGFR Exon 20 insertion mutations (Ins20). *J. Clin. Oncol.* 39, 9077.
45. Uy, N.F., Merkhofer, C.M., and Baik, C.S. (2022). HER2 in Non-Small Cell Lung Cancer: A Review of Emerging Therapies. *Cancers* 14, 4155.
46. Xu, B., Yan, M., Ma, F., Hu, X., Feng, J., Ouyang, Q., Tong, Z., Li, H., Zhang, Q., Sun, T., et al. (2021). Fyrotinib plus capecitabine versus lapatinib plus capecitabine for the treatment of HER2-positive metastatic breast cancer (PHOEBE): a multicentre, open-label, randomised, controlled, phase 3 trial. *Lancet Oncol.* 22, 351–360.
47. Dragoi, A.M., Radulescu, I., Năsu, B.A., Pop, A.L., Varlas, V.N., and Trifu, S. (2020). Clozapine: An Updated Overview of Pharmacogenetic Biomarkers, Risks, and Safety—Particularities in the Context of COVID-19. *Brain Sci.* 10, 840.
48. Hasako, S., Terasaka, M., Abe, N., Uno, T., Ohsawa, H., Hashimoto, A., Fujita, R., Tanaka, K., Okayama, T., Wadhwa, R., et al. (2018). TAS6417, A Novel EGFR Inhibitor Targeting Exon 20 Insertion Mutations. *Mol. Cancer Ther.* 17, 1648–1658.
49. Li, X., Yang, C., Wan, H., Zhang, G., Feng, J., Zhang, L., Chen, X., Zhong, D., Lou, L., Tao, W., and Zhang, L. (2017). Discovery and development of pyrotinib: A novel irreversible EGFR/HER2 dual tyrosine kinase inhibitor with favorable safety profiles for the treatment of breast cancer. *Eur. J. Pharm. Sci.* 110, 51–61.
50. El-Gamal, M.I., Mewafi, N.H., Abdelmottaleb, N.E., Emara, M.A., Tarazi, H., Sbenati, R.M., Maokour, M.M., Zarei, S.-O., Shahin, A.I., and Anbar, H.S. (2021). A Review of HER4 (ErbB4) Kinase, Its Impact on Cancer, and Its Inhibitors. *Molecules* 26, 7376.
51. Fry, D.W., Kraker, A.J., McMichael, A., Ambrosio, L.A., Nelson, J.M., Leopold, W.R., Connors, R.W., and Bridges, A.J. (1994). A Specific Inhibitor of the Epidermal Growth Factor Receptor Tyrosine Kinase. *Science* 265, 1093–1095.
52. Schaefer, G., Shao, L., Totpal, K., and Akita, R.W. (2007). Erlotinib Directly Inhibits HER2 Kinase Activation and Downstream Signaling Events in Intact Cells Lacking Epidermal Growth Factor Receptor Expression. *Cancer Res.* 67, 1228–1238.
53. Dong, Q., Yu, P., Ye, L., Zhang, J., Wang, H., Zou, F., Tian, J., and Kurihara, H. (2019). PCC0208027, a novel tyrosine kinase inhibitor, inhibits tumor growth of NSCLC by targeting EGFR and HER2 aberrations. *Sci. Rep.* 9, 5692.
54. Hickinson, D.M., Klinowska, T., Speake, G., Vincent, J., Trigwell, C., Anderton, J., Beck, S., Marshall, G., Davenport, S., Callis, R., et al. (2010). AZD8931, an Equipotent, Reversible Inhibitor of Signaling by Epidermal Growth Factor Receptor, ERBB2 (HER2), and ERBB3: A Unique Agent for Simultaneous ERBB Receptor Blockade in Cancer. *Clin. Cancer Res.* 16, 1159–1169.
55. Cullum, R.L., Lucas, L.M., Senfield, J.I., Piazza, J.T., Neel, L.T., Whig, K., Zhai, L., Harris, M.H., Rael, C.C., Taylor, D.C., et al. (2020). Development and application of high-throughput screens for the discovery of compounds that disrupt ErbB4 signaling: Candidate cancer therapeutics. *PLoS One* 15, e0243901.
56. Floc'h, N., Lim, S., Bickerton, S., Ahmed, A., Orme, J., Urošević, J., Martin, M.J., Cross, D.A.E., Cho, B.C., and Smith, P.D. (2020). Osimertinib, an Irreversible Next-Generation EGFR Tyrosine Kinase Inhibitor, Exerts Antitumor Activity in Various Preclinical NSCLC Models Harboring the Uncommon EGFR Mutations G719X or L861Q or S768I. *Mol. Cancer Ther.* 19, 2298–2307.
57. Schmid, C.L., Streicher, J.M., Meltzer, H.Y., and Bohn, L.M. (2014). Clozapine Acts as an Agonist at Serotonin 2A Receptors to Counter MK-801-Induced Behaviors through a β Arrestin2-Independent Activation of Akt. *Neuropsychopharmacology* 39, 1902–1913.
58. Kozell, L.B., and Neve, K.A. (1997). Constitutive Activity of a Chimeric D₂/D₁ Dopamine Receptor. *Mol. Pharmacol.* 52, 1137–1149.
59. Röser, C., Jordan, N., Balfanz, S., Baumann, A., Walz, B., Baumann, O., and Blenau, W. (2012). Molecular and Pharmacological Characterization of Serotonin 5-HT_{2x} and 5-HT₇ Receptors in the Salivary Glands of the Blowfly *Calliphora vicina*. *PLoS One* 7, e49459.
60. Tanzarella, P., Ferretta, A., Barile, S.N., Ancona, M., De Rasmio, D., Signorile, A., Papa, S., Capitanio, N., Pacelli, C., and Cocco, T. (2019). Increased Levels of cAMP by the Calcium-Dependent Activation of Soluble Adenylyl Cyclase in Parkin-Mutant Fibroblasts. *Cells* 8, 250.
61. Zhou, P., Hu, J., Wang, X., Wang, J., Zhang, Y., and Wang, C. (2018). Epidermal growth factor receptor expression affects proliferation and apoptosis in non-small cell lung cancer cells via the extracellular signal-regulated kinase/microRNA 200a signaling pathway. *Oncol. Lett.* 15, 5201–5207.
62. Thul, P.J., and Lindskog, C. (2018). The human protein atlas: A spatial map of the human proteome. *Protein Sci.* 27, 233–244.
63. Anastasiadis, T., Deacon, S.W., Devarajan, K., Ma, H., and Peterson, S.R. (2011). Comprehensive assay of kinase catalytic activity reveals features of kinase inhibitor selectivity. *Nat. Biotechnol.* 29, 1039–1045.
64. Wang, Y., and Ma, H. (2015). Protein kinase profiling assays: a technology review. *Drug Discov. Today Technol.* 18, 1–8.
65. Neradil, J., Kyr, M., Polaskova, K., Kren, L., Macigova, P., Skoda, J., Sterba, J., and Veselska, R. (2019). Phospho-Protein Arrays



- as Effective Tools for Screening Possible Targets for Kinase Inhibitors and Their Use in Precision Pediatric Oncology. *Front. Oncol.* 9, 930.
66. Tanabe, K., Inagaki, A., Henmi, Y., and Satake, M. (2018). Image-Based Profiling Can Discriminate the Effects of Inhibitors on Signaling Pathways under Differential Ligand Stimulation. *SLAS Discov.* 23, 330–340.
 67. Fukazawa, R., Miller, T.A., Kuramochi, Y., Frantz, S., Kim, Y.D., Marchionni, M.A., Kelly, R.A., and Sawyer, D.B. (2003). Neuregulin-1 protects ventricular myocytes from anthracycline-induced apoptosis via erbB4-dependent activation of PI3-kinase/Akt. *J. Mol. Cell. Cardiol.* 35, 1473–1479.
 68. Kanda, Y., Okada, M., Ikarashi, R., Morioka, E., Kondo, T., and Ikeda, M. (2016). Bimodal modulation of store-operated Ca²⁺ channels by clozapine in astrocytes. *Neurosci. Lett.* 635, 56–60.
 69. Marazziti, D., Baroni, S., Palego, L., Betti, L., Giannacchini, G., Castagna, M., Naccarato, A.G., Luccachini, A., Catena-Dell'Osso, M., and Dell'Osso, L. (2014). Clozapine effects on adenylyl cyclase activity and serotonin type 1A receptors in human brain post-mortem. *J. Psychopharmacol.* 28, 320–328.
 70. Nam, H.-J., Kim, H.-P., Yoon, Y.-K., Hur, H.-S., Song, S.-H., Kim, M.-S., Lee, G.-S., Han, S.-W., Im, S.-A., Kim, T.-Y., et al. (2011). Antitumor activity of HM781-36B, an irreversible Pan-HER inhibitor, alone or in combination with cytotoxic chemotherapeutic agents in gastric cancer. *Cancer Lett.* 302, 155–165.
 71. Buchwald, P. (2019). A Receptor Model With Binding Affinity, Activation Efficacy, and Signal Amplification Parameters for Complex Fractional Response Versus Occupancy Data. *Front. Pharmacol.* 10, 605.
 72. Fuglestad, B., Kerstetter, N.E., and Wand, A.J. (2019). Site-Resolved and Quantitative Characterization of Very Weak Protein–Ligand Interactions. *ACS Chem. Biol.* 14, 1398–1402.
 73. Wang, J., Guo, Z., Fu, Y., Wu, Z., Huang, C., Zheng, C., Shar, P.A., Wang, Z., Xiao, W., and Wang, Y. (2017). Weak-binding molecules are not drugs?—toward a systematic strategy for finding effective weak-binding drugs. *Brief. Bioinform.* 18, 321–332.
 74. Aslam, M., and Ladilov, Y. (2022). Emerging Role of cAMP/AMPK Signaling. *Cells* 11, 308.
 75. Omar, B., Zmuda-Trzebiatowska, E., Manganiello, V., Göransson, O., and Degerman, E. (2009). Regulation of AMP-activated protein kinase by cAMP in adipocytes: roles for phosphodiesterases, protein kinase B, protein kinase A, Epac and lipolysis. *Cell. Signal.* 21, 760–766.
 76. Yin, Y., Ma, P., Wang, S., Zhang, Y., Han, R., Huo, C., Wu, M., and Deng, H. (2022). The CRTCCREB axis functions as a transcriptional sensor to protect against proteotoxic stress in *Drosophila*. *Cell Death Dis.* 13, 688.
 77. Koizumi, K., and Nakajima, H. (2014). Serotonin induces the migration of PC12 cells via the serotonin receptor 6/cAMP/ERK pathway. *Biomed. Rep.* 2, 29–33.
 78. Hasan, A., Roeh, A., Leucht, S., Langguth, B., Hansbauer, M., Oviedo-Salcedo, T., Kirchner, S.K., Papazova, I., Lohrs, L., Wagner, E., et al. (2020). Add-on spironolactone as antagonist of the NRG1-ERBB4 signaling pathway for the treatment of schizophrenia: Study design and methodology of a multicenter randomized, placebo-controlled trial. *Contemp. Clin. Trials Commun.* 17, 100537.
 79. Zandifar, A., Badrfam, R., Sanjari Moghaddam, H., and Akhondzadeh, S. (2022). Efficacy of Spironolactone as an Adjunctive Therapy to Risperidone to Improve Symptoms of Schizophrenia: A Double-Blind, Randomized, Placebo-Controlled, Clinical Trial. *Iran. J. Psychiatry* 17, 14–23.
 80. Sakata, A., Mogi, M., Iwanami, J., Tsukuda, K., Min, L.-J., Jing, F., Ohshima, K., Ito, M., and Horiuchi, M. (2012). Improvement of cognitive impairment in female type 2 diabetes mellitus mice by spironolactone. *J. Renin. Angiotensin. Aldosterone. Syst.* 13, 84–90.
 81. Chen, L., Shi, R., She, X., Gu, C., Chong, L., Zhang, L., and Li, R. (2020). Mineralocorticoid receptor antagonist-mediated cognitive improvement in a mouse model of Alzheimer's type: possible involvement of BDNF-H2 S-Nrf2 signaling. *Fundam. Clin. Pharmacol.* 34, 697–707.
 82. Ebdrup, B.H., Rasmussen, H., Arnt, J., and Glenthøj, B. (2011). Serotonin 2A receptor antagonists for treatment of schizophrenia. *Expert Opin. Investig. Drugs* 20, 1211–1223.
 83. Hahn, C.-G., Wang, H.-Y., Cho, D.-S., Talbot, K., Gur, R.E., Berrettini, W.H., Bakshi, K., Kamins, J., Borgmann-Winter, K.E., Siegel, S.J., et al. (2006). Altered neuregulin 1-erbB4 signaling contributes to NMDA> receptor hypofunction in schizophrenia. *Nat. Med.* 12, 824–828.
 84. Romano, R., and Buccì, C. (2020). Role of EGFR in the Nervous System. *Cells* 9, 1887.
 85. Okada, T., Miyagi, H., Sako, Y., Hiroshima, M., and Mochizuki, A. (2022). Origin of diverse phosphorylation patterns in the ERBB system. *Biophys. J.* 121, 470–480.
 86. Wieduwilt, M.J., and Moasser, M.M. (2008). The epidermal growth factor receptor family: Biology driving targeted therapeutics. *Cell. Mol. Life Sci.* 65, 1566–1584.
 87. Zaraei, S.-O., Sbenati, R.M., Alach, N.N., Anbar, H.S., El-Gamal, R., Tarazi, H., Shehata, M.K., Abdel-Maksoud, M.S., Oh, C.-H., and El-Gamal, M.I. (2021). Discovery of first-in-class imidazothiazole-based potent and selective ErbB4 (HER4) kinase inhibitors. *Eur. J. Med. Chem.* 224, 113674.
 88. Stephan, M., Schoeller, J., Raabe, F.J., Schmitt, A., Hasan, A., Falkai, P., Jensen, N., and Rossner, M.J. (2022). Spironolactone alleviates schizophrenia-related reversal learning in Tcf4 transgenic mice subjected to social defeat. *Schizophrenia (Heidelb).* 8, 77.
 89. Volkmann, P., Stephan, M., Krackow, S., Jensen, N., and Rossner, M.J. (2020). PsyCoP - A Platform for Systematic Semi-Automated Behavioral and Cognitive Profiling Reveals Gene and Environment Dependent Impairments of Tcf4 Transgenic Mice Subjected to Social Defeat. *Front. Behav. Neurosci.* 14, 618180.
 90. Gong, N., Wu, R., Ding, B., and Wu, W. (2020). ERBB4 promotes the progression of inflammatory breast cancer through regulating PDGFRA. *Transl. Cancer Res.* 9, 3266–3273.
 91. Kurppa, K.J., Denessiouk, K., Johnson, M.S., and Elenius, K. (2016). Activating ERBB4 mutations in non-small cell lung cancer. *Oncogene* 35, 1283–1291.
 92. Xu, J., Gong, L., Qian, Z., Song, G., and Liu, J. (2018). ERBB4 promotes the proliferation of gastric cancer cells via the PI3K/Akt signaling pathway. *Oncol. Rep.* 39, 2892–2898.
 93. Schneider, C.A., Rasband, W.S., and Eliceiri, K.W. (2012). NIH Image to ImageJ: 25 years of image analysis. *Nat. Methods* 9, 671–675.
 94. Wickham, H. (2016). ggplot2: Elegant Graphics for Data Analysis, 2nd ed (Springer International Publishing).
 95. Wickham, H. (2007). Reshaping Data with the reshape Package. *J. Stat. Softw.* 21.
 96. Wickham, H., Vaughan, D., and Gilrlich, M. (2023). Tidy: Tidy Messy Data. *Version 2023*.
 97. Wickham, H., Averick, M., Bryan, J., Chang, W., McGowan, L., François, R., Grolemund, G., Hayes, A., Henry, L., Hester, J., et al. (2019). Welcome to the Tidyverse. *J. Open Source Softw.* 4, 1686.
 98. Ritzi, C., Baty, F., Streibig, J.C., and Gerhard, D. (2015). Dose-Response Analysis Using R. *PLoS One* 10, e0146021.
 99. Herholt, A., Brankatschk, B., Kannaiyan, N., Papiol, S., Wichert, S.F., Wehr, M.C., and Rossner, M.J. (2018). Pathway sensor-based functional genomics screening identifies modulators of neuronal activity. *Sci. Rep.* 8, 17597.
 100. Wintgens, J.P., Rossner, M.J., and Wehr, M.C. (2017). Characterizing Dynamic Protein-Protein Interactions Using the Genetically Encoded Split Biosensor Assay Technique Split TEV. *Methods Mol. Biol.* 1596, 219–238.
 101. Zhang, J., Chung, T., and Oldenburg, K. (1999). A Simple Statistical Parameter for Use in Evaluation and Validation of High Throughput Screening Assays. *J. Biomol. Screen* 4, 67–73.

STAR★METHODS

KEY RESOURCES TABLE

REAGENT or RESOURCE	SOURCE	IDENTIFIER
Antibodies		
Rat monoclonal anti-HA High Affinity (clone 3F10)	Roche	Cat# 11867423001; RRID: AB_390918
Rabbit monoclonal anti-phospho-EGF Receptor (Tyr1068) (clone D7A5)	Cell Signaling Technology	Cat# 3777; RRID: AB_2096270
Rabbit monoclonal anti-phospho-HER4/ErbB4 (Tyr1284) (clone 21A9)	Cell Signaling Technology	Cat# 4757; RRID: AB_2099987
Mouse monoclonal anti-EGFR (clone A-10)	Santa Cruz Biotechnology	Cat# sc-373746; RRID: AB_10920395
Rabbit monoclonal anti-HER4/ErbB4 (clone E200)	Abcam	Cat# ab32375; RRID: AB_731579
Rabbit monoclonal anti-phospho-p44/42 MAPK (Erk1/2) (Thr202/Tyr204) (clone D13.14.4E)	Cell Signaling Technology	Cat# 4370; RRID: AB_2315112
Rabbit monoclonal anti-p44/42 MAPK (Erk1/2) (clone 137F5)	Cell Signaling Technology	Cat# 4695; RRID: AB_390779
Mouse monoclonal anti- α -tubulin (clone B-5-1-2)	Sigma-Aldrich	Cat# T5168; RRID: AB_477579
Eu-Anti-Phosphotyrosine (PT66) Antibody (AB)	PerkinElmer	Cat# AD0068
Bacterial and virus strains		
One Shot Mach1 T1 Phage-Resistant Chemically Competent <i>E. coli</i>	Thermo Fisher Scientific	Cat# C862003
Chemicals, peptides, and recombinant proteins		
AG-1478 (Tyrophostin AG-1478)	Selleckchem	Cat# 2728; CAS: 153436-53-4
Canrenone	Santa Cruz Biotechnology	Cat# sc-205616; CAS: 976-71-6
Clozapine	Sigma-Aldrich	Cat# C6305; CAS: 5786-21-0
EGFR	Thermo Fisher Scientific	Cat# PV4190
ErbB4	Thermo Fisher Scientific	Cat# PV4104
Erlotinib hydrochloride	Sigma-Aldrich	Cat# SML2156; CAS: 183319-69-9
Gefitinib	Sigma-Aldrich	Cat# SML1657; CAS: 184475-35-2
Lapatinib (GW-572016) Ditosylate	Selleckchem	Cat# S1028; CAS: 388082-77-7
Osimertinib (AZD9291)	Selleckchem	Cat# S7297; CAS:1421373-65-0
Pozotinib (HM781-36B)	Selleckchem	Cat# S7358; CAS: 1092364-38-9
Pyrotinib	MedChemExpress	Cat# HY-104065; CAS: 1269662-73-8
Spironolactone	Selleckchem	Cat# S4054; CAS: 52-01-7
TAS6417 (Zipalertinib)	Selleckchem	Cat# S8814; CAS: 1661854-97-2
hEGF	Sigma-Aldrich	Cat# E9644; CAS: 62253-63-8
Heregulin- β 1 (EGF Domain) human (EGF-like domain)	Sigma-Aldrich	Cat# H7660
Serotonin hydrochloride	Tocris Bioscience	Cat# 3547; CAS: 153-98-0
Compound A	This paper; Lead Discovery Center	N/A
Compound B	This paper; Lead Discovery Center	N/A
ATP	Sigma	Cat# A7699
LR Clonase™ II Plus enzyme	Thermo Fisher Scientific	Cat# 11538120
Critical commercial assays		
GloSensor Technology	Promega	Cat# E2301
Fluo-4, AM, cell permeant	Thermo Fisher Scientific	Cat# F14201
LANCE Ultra ULIGHT™-poly GT	PerkinElmer	Cat# TRF0100

(Continued on next page)



Continued

REAGENT or RESOURCE	SOURCE	IDENTIFIER
LANCE Ultra ULIGHT™-JAK-1 (Tyr1023) Peptide	PerkinElmer	Cat# TRF0121
NovaSeq 6000 SP Reagent Kit v1.5 (100 cycles)	Illumina	Cat# 20028401
NovaSeq 6000 SP Reagent Kit v1.5 (200 cycles)	Illumina	Cat# 20040719
Deposited data		
Analyzed data	This paper	Mendeley Data: https://doi.org/10.17632/vxyy62m2c7.1
Data of barcoded ERBBprofiler assays	This paper	Mendeley Data: https://doi.org/10.17632/vxyy62m2c7.1
Data of orthogonal validation assays (standard split TEV and reporter gene assays, Flu-4 AM calcium assays, cAMP GloSensor assays, quantification of WB assays)	This paper	Mendeley Data: https://doi.org/10.17632/vxyy62m2c7.1
DRC R script	This paper	Mendeley Data: https://doi.org/10.17632/vxyy62m2c7.1
Heatmap R script	This paper	Mendeley Data: https://doi.org/10.17632/vxyy62m2c7.1
Experimental models: Cell lines		
<i>Rattus norvegicus</i> : PC12 Tet-Off cells	Clontech	Cat# 631134; RRID: CVCL_V361
Human: A-549 cells	ATCC	Cat# CCL-185; RRID: CVCL_0023
Human: T-47D cells	ATCC	Cat# HTB133; RRID: CVCL_0553
Oligonucleotides		
See Table S7	This paper	N/A
Recombinant DNA		
See Table S4	This paper	N/A
Software and algorithms		
ImageJ	Schneider et al., 2012 ⁹³	https://imagej.nih.gov/ij/
R version 4.2.3 or higher	R Core Team (2023)	https://www.R-project.org/
RStudio2023.03.0 + 386	RStudio Team (2023)	http://www.rstudio.com/
ggplot2	Wickham, 2016 ⁹⁴	https://ggplot2.tidyverse.org
reshape	Wickham, 2007 ⁹⁵	http://www.jstatsoft.org/v21/i12/paper
tidyr	Wickham et al., 2023 ⁹⁶	https://CRAN.R-project.org/package=tidyr
tidyverse	Wickham et al., 2019 ⁹⁷	https://doi.org/10.21105/joss.01686
drc	Ritz et al., 2015 ⁹⁸	http://journals.plos.org/plosone/article?id=10.1371/journal.pone.0146021
BioRender	BioRender.com (2023)	https://app.biorender.com/biorender-templates
Adobe Illustrator CS6	Adobe Inc.	https://adobe.com/products/illustrator
MikroWin 2000 Version 4.41	Mikrotek Laborsysteme (1992–2007)	https://mikrowin-2000.software.informer.com/download/
OPTIMA Version 2.20R2	BMG Labtech	https://www.bmglabtech.com/en/microplate-reader-software/
ChemoStar Imager	Intas Pharmaceuticals	https://www.intas.de/chemilumineszenz-westernblotting/73-chemocam-imager
Echo Dose Response Software	Beckman Coulter	https://www.beckman.de/liquid-handlers/software/echo/dose-response

RESOURCE AVAILABILITY

Lead contact

Further information and requests for resources and reagents should be directed to and will be fulfilled by the Lead Contact, Michael Wehr (michael.wehr@med.uni-muenchen.de).



Materials availability

Plasmids used for standard split TEV assays and standard reporter gene assays are available from Systasy Bioscience GmbH (www.systasy.de). There are restrictions to the availability of the reporter plasmids used for the ERBBprofiler assay due to a material transfer agreement (MTA). There are restrictions to the availability of the two compounds A and B due to intellectual property considerations.

Data and code availability

- Data of barcoded ERBBprofiler assays and orthogonal validation assays have been deposited at Mendeley Data and is publicly available as of the date of publication. DOIs are listed in the [key resources table](#).
- Original code has been deposited at Mendeley Data and is publicly available as of the date of publication. DOIs are listed in the [key resources table](#).
- Any additional information required to reanalyze the data reported in this paper is available from the [lead contact](#) upon request.

EXPERIMENTAL MODEL AND STUDY PARTICIPANT DETAILS

Cell lines

PC12 Tet-Off cells (RRID:CVCL_V361) (Clontech, 631134, termed PC12 cells for simplicity) were maintained in DMEM medium (1 g/L glucose, Lonza) supplemented with 10% FBS, 5% horse serum (HS, Thermo Fisher Scientific Inc.), and 100 U/ml each of penicillin and streptomycin (Thermo Fisher Scientific Inc., Cat. No. 15140-122) and 2 mM GlutaMAX (Thermo Fisher Scientific Inc., Cat. No. 35050038). Starvation of PC12 cells was induced by 1% FCS, 100 U/ml each of penicillin and streptomycin and 2 mM GlutaMAX, but no HS. Cell-based assays for PC12 cells were performed in starvation conditions. A549 cells (RRID:CVCL_0023) (ATCC, CCL-185) were cultured in DMEM medium (4.5 g/L glucose) supplemented with 10% FCS and 100 U/ml each of penicillin and streptomycin and 2 mM GlutaMAX. T-47D cells (RRID:CVCL_0553) (ATCC, HTB-133) were cultured in RPMI 1640 medium supplemented with human insulin (f.c. 125 µg/L) (Sigma-Aldrich), 10% FCS and 100 U/ml each of penicillin and streptomycin and 2 mM GlutaMAX.

Plasmids

Plasmids for EGFR, ERBB3, and ERBB4 fused to NTEV-tcs-GV moieties and ERBB2 fused to a V5-tag were previously described,³² as well as for HTR2A and ARBB2,³⁵ and the clustered SH2 domains of GRB2.³⁷ For the cloning of pathway reporters for CRE, EGR1p, and NFAT elements, the Gateway Destination vector pGL4.16_attR1_Insert_attR2_luc2/Hygro_DEST (described in³⁵ and based on the pGL4.16_luc2/Hygro vector from Promega) was used. Entry vectors for CRE (pENTR/221_attL1-CRE-attL4, contains 6 CRE repeats), EGR1p (pENTR/221_attL4r_EGR1p_attL3r, contains a 1.0 kb promoter region of the human EGR1 promoter), NFAT (pENTR/221_attL1_NFAT-RE_attL4, contains 6 NFAT repeats), a dummy Entry vector for attL1-attL4 sites (pENTR/221_attL1_dummy_attL4) and an Entry vector carrying a unique 49-mer barcode sequence (pENTR/221_attL3_BarcodeLibrary_attL2) were obtained from a previous study.³⁹ pcDNA3.1(+) was obtained from Thermo Fisher Scientific. All plasmids used in this study are listed in [Table S1](#).

Bacterial strains

The Mach1 competent cells were purchased from Thermo Fisher Scientific and used as competent cells to construct the vectors.

Chemical reagents

The following commercial compounds were used in this study: AG1478 (Selleckchem, S2728), canrenone (Santa Cruz, sc-205616), clozapine (Sigma-Aldrich, C6305), erlotinib (Sigma-Aldrich, SML2156), gefitinib (Sigma-Aldrich, SML1657), lapatinib (Selleckchem, S1028), osimertinib (Selleckchem, S7297), poziotinib (Selleckchem, S7358), pyrotinib (MedChemExpress, HY-104065), spironolactone (Selleckchem, S4054), TAS6417 (Selleckchem, S8814), EGF (Sigma-Aldrich, E9644, EGF-like domain (Sigma-Aldrich, H7660), serotonin (Tocris, 3547). Compounds A and B were synthesized by the Department of Medicinal Chemistry of the Lead Discovery Center, Dortmund, Germany, as part of a proprietary kinase inhibitor program.

METHOD DETAILS

Vector construction

Pathway reporters for CRE, EGR1p, and NFAT elements were cloned using a Multisite Gateway recombination (Thermo Fisher Scientific) strategy as described in³⁹ and linked to a firefly luciferase gene and unique barcodes for multiparametric assays. Entry vectors harboring CRE and NFAT sensors were combined with an Entry vector harboring an adenovirus major late promoter (MLP) (pENTR/221_attL4r_MLP_attL3r) and an Entry vector carrying a unique 49-mer barcode (pENTR/221_attL3_Barcode_attL2). The EGR1p Entry vector (pENTR/221_attL4r_EGR1p_attL3r) was combined with the dummy Entry vector (pENTR/221_attL1_dummy_attL4) and a unique 49-mer barcode Entry vector (pENTR/221_attL3_BarcodeLibrary_attL2). Each of the sets containing three Entry vectors were recombined using LR Clonase II Plus enzyme (Thermo Fisher Scientific) into pGL4.16_attR1_Insert_attR2_luc2/Hygro_DEST to yield expression vectors, which are listed in [Table S1](#). The sequences of the expression plasmids were verified using Sanger sequencing.

Luciferase reporter assays

50,000 PC12 cells were seeded per 96-well onto poly-L-lysine (PLL)-coated plates and transfected the following day (day *in vitro* 1, DIV1) with assay plasmids using Lipofectamine 3000 (Thermo Fisher Scientific). For split TEV assays, plasmids (pcDNA3 or pTag4C backbone) encoding receptor-NTEV-tcs-GV, GRB2-SH2-CTEV (for ERBB receptors) or ARBB2-1-383-CTEV (for HTR2A) (all 10 ng/well), and the p10xUAS-luc2 reporter plasmid (10 ng/well) were used. For pathway assays, the receptor plasmids (15 ng/well) and pathway reporter plasmids (15 ng/well) pEGFP-luc2 for monitoring MAPK signaling, pCRE-CMVmin-luc2 for monitoring cAMP/Ca²⁺ signaling, or p6xNFAT-CMVmin-luc2 for Ca²⁺ signaling were used. Combinations of assays conducted are summarized in Table S5. Transient transfections were conducted according to the manufacturer's instructions. On DIV2, cells were starved in medium containing 1% FCS for 16 h. On DIV3, a stimulus was added at increasing doses or, for antagonist assays, at single concentrations (30 ng/mL EGF for activating EGFR; 10 ng/mL EGFld for activating ERBB2/3 and ERBB4; and 1 μ M serotonin for activating HTR2A) for 6 h. In the case of antagonist assays, compounds were added at increasing doses together with the stimulus. Cells were lysed in 1x passive lysis buffer (Promega) and subjected to a firefly luciferase assay using a self-made substrate for firefly luciferase.¹⁰⁰ Luciferase activity was analyzed in a Mithras LB 940 Multimode Microplate Reader (Berthold Technologies). All assays were run in 96-well plates using six replicates per condition.

GloSensor cAMP assay

The GloSensor cAMP assay was conducted with the same parameters (50,000 PC12 cells per 96-well) as described above for the firefly luciferase assay, with however, three differences. Specifically, (1) 30 ng/well of the pGloSensor-22F plasmid (Promega, E2301) was used for transfection, and (2) on DIV3, cells were equilibrated in assay medium containing a 2% v/v dilution of D-luciferin (Synchem, bc219) for 2 h at 37°C before (3) the treatment of compounds for 15 min and lysis in 1x passive lysis buffer (Promega) and luciferase activity measurement.

Fluo-4 a.m. calcium assays

50,000 PC12 cells were seeded per 96-well onto poly-L-lysine (PLL)-coated clear bottom plates (PerkinElmer, 6055302) and starved on DIV1 for 24 h. On DIV2, cells were pre-equilibrated in 10 μ M Fluo-4 a.m. (Thermo Fisher Scientific, F14201) away from light for 1 h at 37°C. Next, cells were incubated in the indicator-free starvation medium to allow de-esterification for 20 min away from light at 37°C. Background fluorescence was then measured using the BMG POLARstar Optima Microplate Reader prior to adding the treatments and continuously measuring the fluorescence for the next 30 min. Fluorescence was measured using the bottom optics.

Barcode reporter assays

Transfection of reporter plasmids and stimulation conditions

Multiplexed barcoded reporter assays were conducted in PC12 cells using 24-well plates, with 3 replicates per condition. Per well, 250,000 PC12 cells were transfected *in solution* with assay plasmids using Lipofectamine 3000. Per well, 5 batches of transfected cells were used. Per well, amounts of assay plasmids were 33 ng of target and adapter plasmids, and 27 ng of each reporter plasmid (note that 10 reporters were used per batch), totaling to 336 ng/well. Combinations of barcoded assays conducted are summarized in Table S6, barcode sequences used as RNA reporters are listed in Table S1. Transfected cells were incubated for 2 h at 37°C and 5% CO₂. Tubes (15 mL or 50 mL Falcon tubes) containing transfected cells were loosely closed to allow the CO₂ flow and put tilted at 45° angle to enhance transfection efficiency and viability. Cells were then centrifuged for 5 min at 1000 rpm, the whole supernatant was carefully aspirated, and cells were plated in maintenance medium into PLL-coated 24-well plates for 24 h. Cells were then starved for 16 h as described above and treated for 6 h with compounds. Agonists and antagonists were applied simultaneously. Cells were lysed in 400 μ L/well in a wash and lysis buffer (100 mM Tris/HCl pH 7.5, 500 mM LiCl, 10 mM EDTA, 5 mM DTT, 1% LiDS). Plates were shaken for 10 min at 200 rpm for thorough lysis.

Isolation of barcodes, library preparation, and next-generation-sequencing

For Tag&Pool, a procedure to combine multiple cell lysates for single purification and processing of barcode reporter RNAs, second level barcodes (to track wells, see Figures 1 and S11) were added to the lysates to a final concentration of 0.125 μ M for annealing at 65°C for 15 min. Once cooled to room temperature, all 24 lysates from one 24-well plate and 20 μ L of M-PVA Odt2 beads (Chemagen, Cat. No. CMG-231) were pooled. Next, beads were subjected to a series of wash steps, including one wash with 100 μ L of 1x High-Capacity reaction buffer (High-Capacity cDNA Reverse Transcription Kit, Thermo Fisher Scientific, Cat. No. 4368814). Finally, cDNA synthesis from beads was performed in 20 μ L of cDNA High-Capacity cDNA Reverse Transcription mix at 25°C for 25 min. For barcoded ('tagged') cDNA amplification, a forward primer containing the Read1 Illumina adapter sequence and an UMI sequence was used, in combination with a Read2 reverse primer (30 PCR cycles). Illumina indices and sequencing adapters were attached (10 PCR cycles), the final barcode libraries were pooled in equimolar ratio (2 p.m.) and subjected to paired end, dual index sequencing with the NovaSeq 6000 SP Reagent Kit v1.5 (Illumina GmbH, Cat. No. 20028401 or 20040719). Oligos used are listed in Table S7.

Biochemistry

Phosphorylation levels of EGFR were assessed³⁷ in A549 cells, while phosphorylation levels of ERBB4 were assessed in T-47D cells. Before stimulation experiments were performed, both cell types were starved overnight in 1% FCS and compounds were incubated for 1 h. A549 were stimulated with 30 ng/mL EGF for 5 min, while T-47D cells were stimulated with 10 ng/mL EGFld for 5 min. For lysis, cells were washed

1x with PBS and lysed in a Triton X- lysis buffer (1% Triton X-100, 50 mM Tris pH7.5, 150 mM NaCl, 1 mM EGTA) containing the Complete protease inhibitor cocktail (Roche) and PhosSTOP phosphatase inhibitor (Roche). Briefly, cells were lysed and kept on ice for 10 min, sonicated 3x for 10 s at 4°C, and denatured for 10 min at 70°C. The Mini-PROTEAN Tetra Electrophoresis System and Trans-Blot Turbo Botting System (both Bio-Rad) were used for running and blotting protein gels. Chemiluminescence detection of proteins by Western blot analysis was performed using the Western LightningPlus-ECL kit (PerkinElmer). HA-tagged proteins were visualised using an HA antibody (RRID: AB_390918) (clone 3F10, dilution 1:1000, No. 11 867 423 001, Roche). Phosphorylation levels of EGFR and ERBB4 were assayed using p-EGFR-Y1068 (RRID: AB_2096270) (clone D7A5, dilution 1:500, No. 3777, Cell Signaling Technology) and p-ERBB4-Y1284 antibodies (RRID: AB_2099987) (clone 21A9, dilution 1:500, No. 4757, Cell Signaling Technology). Total EGFR and ERBB4 protein levels were determined using an anti-EGFR antibody (RRID: AB_10920395) (clone A-10, dilution 1:1000, sc-373746, Santa Cruz Biotechnology) and an anti-ERBB4 antibody (RRID: AB_731579) (clone E200, dilution 1:1000, ab32375, Abcam). Phosphorylation levels of ERK1/2 were assayed using p-p44/42 MAPK (Erk1/2) (RRID: AB_2315112) (clone D13.14.4E, dilution 1:5000, No. 4370, Cell Signaling Technology), total ERK1/2 protein levels were assayed using p44/42 MAPK (Erk1/2) (RRID: AB_390779) (clone 137F5, dilution 1:5000, No. 4695, Cell Signaling Technology). Tubulin levels were determined using an anti-Tubulin antibody (RRID: AB_477579) (dilution 1:2000, No. T 5168, Sigma-Aldrich). For quantification, phosphorylation levels of p-EGFR relative to EGFR as well as p-ERBB4 relative to ERBB4 were calculated using the Lukemiller protocol (<http://lukemiller.org/index.php/2010/11/analyzing-gels-and-western-blot-with-image-j/>). Assays were run in triplicates.

In vitro kinase assays

In vitro kinase assays for compounds A and B were conducted using the LANCE Ultra TR-FRET kinase activity assays for EGFR and ERBB4. The principle of this enzymatic assay is based on the phosphorylation of the *ULight*-peptide substrate, labeled with an acceptor fluorophore, by a purified protein kinase. Phosphorylation is detected by a specific Europium-labelled anti-phospho-peptide antibody, labeled with a donor fluorophore. The binding of the Europium-labelled anti-phospho-peptide antibody to the phosphorylated *ULight*-labeled peptide produces an FRET signal. Binding of an inhibitor to the kinase prevents phosphorylation of the *ULight*-substrate, resulting in a loss of FRET. For every sample, 2 μ L of assay buffer (50 mM HEPES pH 7.5, 10 mM MgCl₂, 1 mM EGTA 0.01% Tween 20, 1% DMSO, 2 mM DTT) were transferred into a 384-well plate (Corning #4513). Compounds were added in a concentration range from 10 μ M to 0.0025 μ M using an acoustic dispenser (Echo520 from Labcyte, San Jose, USA) equipped with Echo Dose Response software. Next, 6 μ L of either (1) EGFR (0.5 nM, Thermo Fisher) and *ULight*-JAK-1 (Tyr1023) Peptide substrate (50 nM, PerkinElmer, TRF0121) mix or (2) ERBB4 (0.1 nM, Thermo Fisher) and *ULight*-poly GT peptide substrate (100 nM, PerkinElmer, TRF0100) mix was added. The reaction was started by addition of 2 μ L ATP (final concentration 29 μ M for EGFR assay; 0.59 μ M for ERBB4 assay, Sigma-Aldrich) working solution and mixed using a Bioshake 5000 microplate shaker (Q Instruments, Jena, Germany). After 1 h incubation at room temperature, the reaction was stopped with 10 μ L detection mix containing the 2 nM Europium-anti-phosphotyrosine (PT66) antibody (PerkinElmer, AD0068) and 10 mM EDTA. After a second incubation period of 1 h at room temperature, the FRET signal was measured at 340 nm excitation, 665 nm and 615 nm emission (for the *ULight*-substrate and Europium antibody, respectively) with an Envision microplate reader (PerkinElmer, Waltham, MA, USA) with 50 μ s delay and 300 μ s integration time. A kinase reaction without an inhibitor was set as positive control (using DMSO), representing the maximum readability of the system; conversely, a reaction without kinase was set as negative control using DMSO, representing the minimum readability of the system. Both positive and negative controls were run in parallel with every compound measurement as a calibration.

QUANTIFICATION AND STATISTICAL ANALYSIS

Data analysis of barcode and luciferase reporter assays

For barcode reporter assays, sequencing reads of each transfected batch from each sample were normalized to their respective MLPmin sensor controls for every biological replicate and every condition. The MLPmin sensor-based normalization controlled technical aspects (cell number and transfection effects) and retained cell intrinsic effects (e.g., expression of signaling pathways). MLPmin sensors thus enabled to control for both target and cellular pathways activities, as observed in this study for e.g., the EGFR-dependent MAPK signaling captured by the EGR1p sensor (note that PC12 cells endogenously express EGFR, which, when activated, resulted in robust activation of MAPK/ERK signaling). Internal barcode replicates (3 for receptors, 2 for pathways; Figure 1A) were averaged and considered as one biological replicate. For luciferase assays, raw firefly values were used for analysis. Biological replicates were averaged, their respective standard errors were calculated, and both averages and standard errors were normalized to enable curve fitting from 0% to 100% for agonist dose-response curves. For antagonist treatments, the activity of the lowest compound concentration was set to 100%. Dose-response curves were visualized with R using the *drc* package. The robustness of the assays was calculated using the *Z'* factor (cf. section on statistics). *Z'* factors for barcoded assays obtained with strong inhibition of selected compounds are listed in Table S8. For heatmaps, the smallest concentration of each compound was set to 0 using the logarithmic scale to base 2. Heatmaps were plotted with R using the *ggplot2* package.

Data analysis of in vitro kinase assays

The mean values of the negative control reactions were subtracted from each reading of compound treated kinase reactions, followed by the division of the mean values of positive controls, from which the negative control means were also subtracted. Assays were run in triplicates. Dose-response curves and IC₅₀ values were plotted and calculated using *drc* package in R.



Statistical analysis

Robustness of dose response assays was calculated using the Z' factor that integrates both means and standard deviations of low and high concentration values.¹⁰¹ The Z' factor was calculated by this formula: $Z' = 1 - \{3(SD_H + SD_L) / |\text{mean}_H - \text{mean}_L|\}$. SD_H and SD_L are designated the standard deviation of the high and low control values, mean_H and mean_L are designated the averages of high and low control values. A value above $Z \geq 0.5$ is considered as robust assay. Barcoded assays and *in vitro* kinase assays were run in triplicates, luciferase assays in six replicates, and Western blots in triplicates.

8. Discussion and perspective

8.1 Considerations in developing barcoded GPCR assays.

Several key criteria must be considered to avoid the problems and pitfalls associated with reporter gene assays, such as cell background, long incubation time for gene expression and high baseline due to amplification effect^[64, 91, 94].

An appropriate cell background is the first consideration when designing a reporter gene assay. Cellular signaling architecture is widely conserved, albeit some pathways may be distorted (up-/downregulated) due to the cell line identity. The selected cells must express the relevant signalling molecules following GPCR activation^[91]. Several cell lines have been reported in GPCR reporter gene assays, including HEK293 cells, PC12 Tet-Off cells, N1E cells and yeast, but HEK293 cells are intensively selected^[71-72, 95-97]. HEK293 cells are a human embryonic adrenal progenitor cell line that closely resembles adrenal cells and has many characteristics of immature neurons^[98]. For example, the neuronal markers, such as 160 kDa neurofilament medium chain (NFEM, NCBI Gene ID: 4741), 200 kDa neurofilament heavy chain (NEFH, NCBI Gene ID: 4744), tubulin beta 3 class III (TUBB3, NCBI Gene ID: 10381), RNA binding fox-1 homolog 3 (RBFOX3, NCBI Gene ID: 146713; also known as neuronal nuclei (NeuN) antigen), synaptophysin (SYP, NCBI Gene ID: 6855), microtubule associated protein 2 (MAP2, NCBI Gene ID: 4133) and postsynaptic density protein 95 (DLG4, also known as PSD95, NCBI Gene ID: 1742) are expressed in HEK293 based on the RNA sequencing data within the Human Protein Atlas, whereas other neuronal makers such as neuronal differentiation 1 (NEUROD1) (NCBI Gene ID: 4760) and doublecortin (DCX, NCBI Gene ID: 1641) are not expressed. As I have shown in the barcoded pathway assay experiment using the broad band stimulus PMA and the selective stimulus forskolin (**Figure 7**), multiple pathway sensors responded in a differential manner. This suggests that HEK293 cells have multiple functional signalling pathways making them a suitable tool for target and pathway-based screens. Furthermore, HEK293 cells are widely used in GPCR-related reporter gene assays^[85], indicating that HEK293 cells are a generally suitable cell line for the design of a GPCR reporter gene assay. However, it is important to consider that signalling pathways in cell lines, such as HEK293 cells, may be distorted to some extent and may generate non-natural signalling profiles^[99].

The extended incubation time required for reporter gene assays (hours vs minutes) raises concerns about secondary effects of ligands, such as toxicity or cell tolerance, especially when using proteins as reporters due to the time required for protein expression^[85, 100]. This is why efforts are being made to develop destabilised reporters, because destabilized reporters with shorter half-lives can improve the dynamic range and reduce the incubation time by reducing

the baseline in the steady state^[85]. Barcoded reporter gene assays can overcome this hurdle with shorter half-lives of transcribed barcodes and reduced incubation times (1-4 hours), which could ultimately minimize side effects^[101].

In general, baseline, also known as background or noise, is a key consideration in the development, optimization, and use of reporter assays, as it can greatly influence the regression equation of standard curves, e.g. the higher the baseline, the lower the slope of a linear standard curve. Baseline is also strongly related to the usable dynamic range of a given assay^[102], because when fold change is used for evaluation within a given linear dynamic range, the higher the baseline, the narrower the usable dynamic range, as the limit is more easily approached. The destabilized reporters have a shorter half-life to present less accumulated reporters in the unstimulated situation, reducing the signal baseline to improve the sensitivity of reporter gene assays^[85]. The half-life of barcodes is generally shorter than that of proteins, suggesting that barcodes may be a suitable destabilized reporter^[100].

8.2 Advantage and limits of the barcoded GPCR assay

Multiplex barcode assays have the potential to provide more stable readouts due to their use of artificially introduced cis-regulatory elements, which can partially decrease biological variability from cell sources, lineages, and culture conditions. From the perspective of statistics, it is important to note that random errors can arise from various factors, making them unavoidable. Higher errors can reduce the efficiency and efficacy of an assay, resulting in decreased sensitivity ($1-\beta$, also known as 1-Type II error) and specificity ($1-\alpha$, also known as 1-Type I error). Therefore, reducing biological variability in multiplex assays can lead to higher sensitivity and specificity^[103], allowing for the study of specific cis-regulatory element activities following GPCR activation.

By focusing on the cis-regulatory elements and consolidating the cis-regulatory elements of interest into the same cell, the multiplex profiling of GPCR activation can be achieved effectively with lower costs.

Generally, reporter gene assays are used to monitor the weak activities of agonists due to their high sensitivity. Our developed barcoded GPCR pathway assay has been validated to quantify the inverse induction such the negative log₂ foldchanges for the sensors in **Figure 7C**, which indicates it is useable in detecting antagonist activities.

Like all reporter gene assays, multiplex barcode assays, commonly termed multiparametric reporter gene assays (MPRA), can help researchers investigate gene regulation. However,

they often test cis-regulatory elements outside of their normal genomic context, which may not fully reflect their function in vivo^[91].

8.3 Further improvements of the barcoded GPCR assays

With the above results, I have provided a proof-of-concept that the barcoded GPCR pathway assay is feasible, although it needs to be further optimised. First, the barcoded GPCR receptor assay may be complemented with split TEV GPCR β -arrestin-2 recruitment assay for the GPCRs linked to Gai, such as DRD2, whose pathway sensors are difficult to identify at the stage of generating stable cell lines. Second, to avoid the crosstalk problems in **Figure 8**, it is necessary to optimise the barcoded GPCR pathway assays. This can be achieved by removing the index barcodes and retaining the firefly luciferase reporter gene only or, alternatively, by increasing the MOIs of the lentivirus-based sensor library. Due to the ease of implementation, the optimisation experiment using an increased MOI of the sensor library could be carried out first in the near future.

8.4 The perspectives of barcoded GPCR assays in drug discovery for brain disorders

Numerous GPCRs are highly expressed in the central nervous system (CNS), especially in the brain. Some GPCRs appear to have regional specificity in the brain, indicating that they play important roles in regulating CNS functions. Relevant data can be found in the Human Protein Atlas. For example, dopaminergic neurons are primarily distributed into retina and four nuclei, including substantia nigra (SA), ventral tegmental area (VTA)^[104], arcuate nucleus (AR)^[105], supramammillary nucleus (SuM)^[106], and periaqueductal gray (PAG)^[107]. In addition, most neurotransmitters use GPCRs (metabotropic receptors) as their receptors, whereas the other neurotransmitter receptors are ligand-gated ion channel receptors (ionotropic receptors)^[108]. These metabotropic receptors are heavily implicated in psychiatric disorders, neurodegenerative diseases and even brain cancer and brain injuries such as pituitary tumors, gliomas, ischemic stroke, traumatic brain injury and so on.

In the future, the brain-expressed GPCRs and RTKs can be selected and integrated into the barcoded GPCR assays for drug discovery for brain disorders. For example, psychedelics are known to have antidepressant activity that is independent of BDNF/NTRK2 signalling, but hallucinogenic effects that are dependent on HTR2A signalling, and the high-affinity NTRK2-positive drugs that lack HTR2A activity may retain the antidepressant potential without the hallucinogenic effects^[109]. To better understand and accelerate drug discovery for brain disorders,

in addition to GPCRs and RTKs, other targets such as nuclear hormone receptors, ion channels, kinases, and proteases can also be included and developed. The barcoded GPCR assays can also be used for reverse pharmacology in brain disorders, where an brain-expressed orphan GPCR, such as GPR88 which is enriched in the basal ganglia, is used as a 'bait' to identify its 'prey' or ligand^[110]. After compound library processing, the barcoded GPCR assays can simultaneously monitor massive signalling pathways and would have the potential to identify potential endogenous ligands for brain-expressed orphan GPCRs in order to de-orphan them.

References

1. Foster SR, Hauser AS, Vedel L, Strachan RT, Huang XP, Gavin AC, Shah SD, Nayak AP, Haugaard-Kedström LM, Penn RB, Roth BL, Bräuner-Osborne H, Gloriam DE. Discovery of Human Signaling Systems: Pairing Peptides to G Protein-Coupled Receptors. *Cell*. 2019;179(4):895-908.e21. <https://doi.org/10.1016/j.cell.2019.10.010>.
2. Pándy-Szekeres G, Caroli J, Mamyrbekov A, Kermani AA, Keserü György M, Kooistra Albert J, Gloriam DE. GPCRdb in 2023: state-specific structure models using AlphaFold2 and new ligand resources. *Nucleic Acids Research*. 2023;51(D1):D395-D402. <https://doi.org/10.1093/nar/gkac1013>.
3. Hauser AS, Attwood MM, Rask-Andersen M, Schiöth HB, Gloriam DE. Trends in GPCR drug discovery: new agents, targets and indications. *Nature Reviews Drug Discovery*. 2017;16(12):829-42. <https://doi.org/10.1038/nrd.2017.178>.
4. Gloriam DE, Fredriksson R, Schiöth HB. The G protein-coupled receptor subset of the rat genome. *BMC Genomics*. 2007;8:338. <https://doi.org/10.1186/1471-2164-8-338>.
5. Lagerström MC, Schiöth HB. Structural diversity of G protein-coupled receptors and significance for drug discovery. *Nature Reviews Drug Discovery*. 2008;7(4):339-57. <https://doi.org/10.1038/nrd2518>.
6. Yang D, Zhou Q, Labroska V, Qin S, Darbalaei S, Wu Y, Yuliantie E, Xie L, Tao H, Cheng J, Liu Q, Zhao S, Shui W, Jiang Y, Wang M-W. G protein-coupled receptors: structure- and function-based drug discovery. *Signal Transduction and Targeted Therapy*. 2021;6(1):7. <https://doi.org/10.1038/s41392-020-00435-w>.
7. Brown NA, Schrevens S, van Dijk P, Goldman GH. Fungal G-protein-coupled receptors: mediators of pathogenesis and targets for disease control. *Nature Microbiology*. 2018;3(4):402-14. <https://doi.org/10.1038/s41564-018-0127-5>.
8. Zhou XE, Melcher K, Xu HE. Structure and activation of rhodopsin. *Acta Pharmacol Sin*. 2012;33(3):291-9. <https://doi.org/10.1038/aps.2011.171>.
9. 7TM proteins. Accessed on 01/02/2024. Human Genome Organization Gene Nomenclature Committee, [Available from: <https://www.genenames.org/data/genegroup/#!/group/2054>].
10. Schiöth HB, Fredriksson R. The GRAFS classification system of G-protein coupled receptors in comparative perspective. *Gen Comp Endocrinol*. 2005;142(1-2):94-101. <https://doi.org/10.1016/j.ygcen.2004.12.018>.
11. Munk C, Isberg V, Mordalski S, Harpsøe K, Rataj K, Hauser AS, Kolb P, Bojarski AJ, Vriend G, Gloriam DE. GPCRdb: the G protein - coupled receptor database - an introduction. *British Journal of Pharmacology*. 2016;173(14):2195-207. <https://doi.org/10.1111/bph.13509>.
12. G protein-coupled receptors. Accessed on 01/02/2024. IUPHAR/BPS Guide to PHARMACOLOGY, [Available from: <http://www.guidetopharmacology.org/GRAC/FamilyDisplayForward?familyId=694>].
13. Bassilana F, Nash M, Ludwig M-G. Adhesion G protein-coupled receptors: opportunities for drug discovery. *Nature Reviews Drug Discovery*. 2019;18(11):869-84. <https://doi.org/10.1038/s41573-019-0039-y>.
14. Wu H, Wang C, Gregory KJ, Han GW, Cho HP, Xia Y, Niswender CM, Katritch V, Meiler J, Cherezov V, Conn PJ, Stevens RC. Structure of a class C GPCR metabotropic glutamate receptor 1 bound to an allosteric modulator. *Science*. 2014;344(6179):58-64. <https://doi.org/10.1126/science.1249489>.
15. Syrovatkina V, Alegre KO, Dey R, Huang XY. Regulation, Signaling, and Physiological Functions of G-Proteins. *J Mol Biol*. 2016;428(19):3850-68. <https://doi.org/10.1016/j.jmb.2016.08.002>.
16. Fredriksson R, Lagerström MC, Lundin LG, Schiöth HB. The G-protein-coupled receptors in the human genome form five main families. Phylogenetic analysis, paralogon groups, and fingerprints. *Mol Pharmacol*. 2003;63(6):1256-72. <https://doi.org/10.1124/mol.63.6.1256>.
17. Nagata T, Inoue K. Rhodopsins at a glance. *J Cell Sci*. 2021;134(22). <https://doi.org/10.1242/jcs.258989>.

-
18. Lefkowitz RJ. A brief history of G-protein coupled receptors (Nobel Lecture). *Angew Chem Int Ed Engl.* 2013;52(25):6366-78. <https://doi.org/10.1002/anie.201301924>.
19. Zhou Q, Yang D, Wu M, Guo Y, Guo W, Zhong L, Cai X, Dai A, Jang W, Shakhnovich EI, Liu ZJ, Stevens RC, Lambert NA, Babu MM, Wang MW, Zhao S. Common activation mechanism of class A GPCRs. *eLife.* 2019;8. <https://doi.org/10.7554/eLife.50279>.
20. **Ligand coverage of GPCR classes. Accessed on 01/02/2024.:** GPCRdb; [Available from: <https://gpcrdb.org/ligand/coverage>].
21. Wu Y, von Hauff IV, Jensen N, Rossner MJ, Wehr MC. Improved Split TEV GPCR β -arrestin-2 Recruitment Assays via Systematic Analysis of Signal Peptide and β -arrestin Binding Motif Variants. *Biosensors.* 2023;13(1). <https://doi.org/10.3390/bios13010048>.
22. Huang HC, Klein PS. The Frizzled family: receptors for multiple signal transduction pathways. *Genome Biol.* 2004;5(7):234. <https://doi.org/10.1186/gb-2004-5-7-234>.
23. Strutt DI. Asymmetric Localization of Frizzled and the Establishment of Cell Polarity in the *Drosophila* Wing. *Molecular Cell.* 2001;7(2):367-75. [https://doi.org/10.1016/S1097-2765\(01\)00184-8](https://doi.org/10.1016/S1097-2765(01)00184-8).
24. Skoda AM, Simovic D, Karin V, Kardum V, Vranic S, Serman L. The role of the Hedgehog signaling pathway in cancer: A comprehensive review. *Bosn J Basic Med Sci.* 2018;18(1):8-20. <https://doi.org/10.17305/bjbms.2018.2756>.
25. GPCR list: ClassB. Accessed on 01/02/2024.:
- IUPHAR/BPS Guide to PHARMACOLOGY; [Available from: <https://www.guidetopharmacology.org/GRAC/GPCRListForward?class=B>].
26. Ishihara T, Nakamura S, Kaziro Y, Takahashi T, Takahashi K, Nagata S. Molecular cloning and expression of a cDNA encoding the secretin receptor. *Embo j.* 1991;10(7):1635-41. <https://doi.org/10.1002/j.1460-2075.1991.tb07686.x>.
27. Drug target classification tree. Accessed on 01/02/2024.:
- GPCRdb; [Available from: <https://gpcrdb.org/drugs/drugmapping>].
28. Kolb P, Kenakin T, Alexander SPH, Bermudez M, Bohn LM, Breinholt CS, Bouvier M, Hill SJ, Kostenis E, Martemyanov KA, Neubig RR, Onaran HO, Rajagopal S, Roth BL, Selent J, Shukla AK, Sommer ME, Gloriam DE. Community guidelines for GPCR ligand bias: IUPHAR review 32. *British Journal of Pharmacology.* 2022;179(14):3651-74. <https://doi.org/10.1111/bph.15811>.
29. Gurevich VV, Gurevich EV. GPCR Signaling Regulation: The Role of GRKs and Arrestins. *Frontiers in Pharmacology.* 2019;10. <https://doi.org/10.3389/fphar.2019.00125>.
30. Smrcka AV. G protein $\beta\gamma$ subunits: Central mediators of G protein-coupled receptor signaling. *Cellular and Molecular Life Sciences.* 2008;65(14):2191-214. <https://doi.org/10.1007/s00018-008-8006-5>.
31. Inoue A, Raimondi F, Kadji FMN, Singh G, Kishi T, Uwamizu A, Ono Y, Shinjo Y, Ishida S, Arang N, Kawakami K, Gutkind JS, Aoki J, Russell RB. Illuminating G-Protein-Coupling Selectivity of GPCRs. *Cell.* 2019;177(7):1933-47.e25. <https://doi.org/10.1016/j.cell.2019.04.044>.
32. Flock T, Hauser AS, Lund N, Gloriam DE, Balaji S, Babu MM. Selectivity determinants of GPCR–G-protein binding. *Nature.* 2017;545(7654):317-22. <https://doi.org/10.1038/nature22070>.
33. Okashah N, Wan Q, Ghosh S, Sandhu M, Inoue A, Vaidehi N, Lambert NA. Variable G protein determinants of GPCR coupling selectivity. *Proceedings of the National Academy of Sciences.* 2019;116(24):12054-9. <https://doi.org/doi:10.1073/pnas.1905993116>.
34. Kamada S, Miwa T. A protein binding to CArG box motifs and to single-stranded DNA functions as a transcriptional repressor. *Gene.* 1992;119(2):229-36. [https://doi.org/10.1016/0378-1119\(92\)90276-u](https://doi.org/10.1016/0378-1119(92)90276-u).
35. Masuho I, Skamangas NK, Muntean BS, Martemyanov KA. Diversity of the G $\beta\gamma$ complexes defines spatial and temporal bias of GPCR signaling. *Cell Syst.* 2021;12(4):324-37.e5. <https://doi.org/10.1016/j.cels.2021.02.001>.
36. Clapham DE, Neer EJ. G protein beta gamma subunits. *Annu Rev Pharmacol Toxicol.* 1997;37:167-203. <https://doi.org/10.1146/annurev.pharmtox.37.1.167>.

-
37. Kwon Y, Mehta S, Clark M, Walters G, Zhong Y, Lee HN, Sunahara RK, Zhang J. Non-canonical β -adrenergic activation of ERK at endosomes. *Nature*. 2022;611(7934):173-9. <https://doi.org/10.1038/s41586-022-05343-3>.
38. The Human Protein Atlas. Accessed on 30/07/2024. scRNA-seq data. [Available from: https://www.proteinatlas.org/about/assays+annotation#singlecell_rna].
39. The Human Protein Atlas. Accessed on 30/07/2024. Knowledge-based annotation. [Available from: https://www.proteinatlas.org/about/assays+annotation#ih_ape].
40. Sulon SM, Benovic JL. Targeting G protein-coupled receptor kinases (GRKs) to G protein-coupled receptors. *Curr Opin Endocr Metab Res*. 2021;16:56-65. <https://doi.org/10.1016/j.coemr.2020.09.002>.
41. Rumpf M, Pautz S, Drebes B, Herberg FW, Müller H-AJ. Microtubule-Associated Serine/Threonine (MAST) Kinases in Development and Disease. *International Journal of Molecular Sciences*. 2023;24(15):11913
42. Ahn S, Shenoy SK, Luttrell LM, Lefkowitz RJ. SnapShot: β -Arrestin Functions. *Cell*. 2020;182(5):1362-e1. <https://doi.org/10.1016/j.cell.2020.07.034>.
43. Li H, Eishingdrelo A, Kongsamut S, Eishingdrelo H. G-protein-coupled receptors mediate 14-3-3 signal transduction. *Signal Transduction and Targeted Therapy*. 2016;1(1):16018. <https://doi.org/10.1038/sigtrans.2016.18>.
44. Labus J, Röhrs K-F, Ackmann J, Varbanov H, Müller FE, Jia S, Jahreis K, Vollbrecht A-L, Butzlaff M, Schill Y, Guseva D, Böhm K, Kaushik R, Bijata M, Marin P, Chaumont-Dubel S, Zeug A, Dityatev A, Ponimaskin E. Amelioration of Tau pathology and memory deficits by targeting 5-HT7 receptor. *Progress in Neurobiology*. 2021;197:101900. <https://doi.org/https://doi.org/10.1016/j.pneurobio.2020.101900>.
45. Couvineau A, Gomariz RP, Tan YV. Editorial: GPCR in Inflammatory and Cancer Diseases. *Front Endocrinol (Lausanne)*. 2020;11:588157. <https://doi.org/10.3389/fendo.2020.588157>.
46. Pickering C, Hägglund M, Szmydynger-Chodobska J, Marques F, Palha JA, Waller L, Chodobski A, Fredriksson R, Lagerström MC, Schiöth HB. The Adhesion GPCR GPR125 is specifically expressed in the choroid plexus and is upregulated following brain injury. *BMC Neurosci*. 2008;9:97. <https://doi.org/10.1186/1471-2202-9-97>.
47. National Institute of Mental Health. Prevalence of Schizophrenia: NIMH; Access Data: 2024-02-01; [Available from: <https://www.nimh.nih.gov/health/statistics/schizophrenia>].
48. Brisch R, Saniotis A, Wolf R, Bielau H, Bernstein HG, Steiner J, Bogerts B, Braun K, Jankowski Z, Kumaratilake J, Henneberg M, Gos T. The role of dopamine in schizophrenia from a neurobiological and evolutionary perspective: old fashioned, but still in vogue. *Front Psychiatry*. 2014;5:47. <https://doi.org/10.3389/fpsy.2014.00047>.
49. Stahl SM. Beyond the dopamine hypothesis of schizophrenia to three neural networks of psychosis: dopamine, serotonin, and glutamate. *CNS Spectr*. 2018;23(3):187-91. <https://doi.org/10.1017/s1092852918001013>.
50. Abbasian S, Yoosefee S, Shahsavand-Ananloo E. Association between brain-derived neurotrophic factor gene variant (rs6265; C > T) and schizophrenia, its psychopathology and intelligence. *The European Journal of Psychiatry*. 2021;35(4):207-15. <https://doi.org/https://doi.org/10.1016/j.ejpsy.2021.04.004>.
51. Lin Z, Su Y, Zhang C, Xing M, Ding W, Liao L, Guan Y, Li Z, Cui D. The Interaction of BDNF and NTRK2 Gene Increases the Susceptibility of Paranoid Schizophrenia. *PLoS One*. 2013;8(9):e74264. <https://doi.org/10.1371/journal.pone.0074264>.
52. McCutcheon RA, Abi-Dargham A, Howes OD. Schizophrenia, Dopamine and the Striatum: From Biology to Symptoms. *Trends Neurosci*. 2019;42(3):205-20. <https://doi.org/10.1016/j.tins.2018.12.004>.
53. Dopamine System. *Encyclopedic Reference of Molecular Pharmacology*. Berlin, Heidelberg: Springer Berlin Heidelberg; 2004. p. 310-5.

-
54. Verharen JPH, Adan RAH, Vanderschuren LJMJ. Differential contributions of striatal dopamine D1 and D2 receptors to component processes of value-based decision making. *Neuropsychopharmacology*. 2019;44(13):2195-204. <https://doi.org/10.1038/s41386-019-0454-0>.
55. Regard JB, Sato IT, Coughlin SR. Anatomical profiling of G protein-coupled receptor expression. *Cell*. 2008;135(3):561-71. <https://doi.org/10.1016/j.cell.2008.08.040>.
56. Surmeier DJ, Ding J, Day M, Wang Z, Shen W. D1 and D2 dopamine-receptor modulation of striatal glutamatergic signaling in striatal medium spiny neurons. *Trends Neurosci*. 2007;30(5):228-35. <https://doi.org/10.1016/j.tins.2007.03.008>.
57. Robinson DR, Wu Y-M, Lin S-F. The protein tyrosine kinase family of the human genome. *Oncogene*. 2000;19(49):5548-57. <https://doi.org/10.1038/sj.onc.1203957>.
58. Wang Y, Chang H, Rattner A, Nathans J. Frizzled Receptors in Development and Disease. *Curr Top Dev Biol*. 2016;117:113-39. <https://doi.org/10.1016/bs.ctdb.2015.11.028>.
59. Donnelly D. The structure and function of the glucagon-like peptide-1 receptor and its ligands. *British Journal of Pharmacology*. 2012;166(1):27-41. <https://doi.org/10.1111/j.1476-5381.2011.01687.x>.
60. Nauck MA, Meier JJ. Incretin hormones: Their role in health and disease. *Diabetes Obes Metab*. 2018;20 Suppl 1:5-21. <https://doi.org/10.1111/dom.13129>.
61. Knudsen LB, Lau J. The Discovery and Development of Liraglutide and Semaglutide. *Front Endocrinol (Lausanne)*. 2019;10:155. <https://doi.org/10.3389/fendo.2019.00155>.
62. Alruwaili H, Dehestani B, le Roux CW. Clinical Impact of Liraglutide as a Treatment of Obesity. *Clin Pharmacol*. 2021;13:53-60. <https://doi.org/10.2147/cpaa.S276085>.
63. Lau J, Bloch P, Schäffer L, Pettersson I, Spetzler J, Kofoed J, Madsen K, Knudsen LB, McGuire J, Steensgaard DB, Strauss HM, Gram DX, Knudsen SM, Nielsen FS, Thygesen P, Reedtz-Runge S, Kruse T. Discovery of the Once-Weekly Glucagon-Like Peptide-1 (GLP-1) Analogue Semaglutide. *J Med Chem*. 2015;58(18):7370-80. <https://doi.org/10.1021/acs.jmedchem.5b00726>.
64. Zhang R, Xie X. Tools for GPCR drug discovery. *Acta Pharmacologica Sinica*. 2012;33(3):372-84. <https://doi.org/10.1038/aps.2011.173>.
65. Zhou Y, Meng J, Xu C, Liu J. Multiple GPCR Functional Assays Based on Resonance Energy Transfer Sensors. *Frontiers in Cell and Developmental Biology*. 2021;9
66. Yasi EA, Kruyer NS, Peralta-Yahya P. Advances in G protein-coupled receptor high-throughput screening. *Current Opinion in Biotechnology*. 2020;64:210-7. <https://doi.org/https://doi.org/10.1016/j.copbio.2020.06.004>.
67. Djannatian MS, Galinski S, Fischer TM, Rossner MJ. Studying G protein-coupled receptor activation using split-tobacco etch virus assays. *Anal Biochem*. 2011;412(2):141-52. <https://doi.org/10.1016/j.ab.2011.01.042>.
68. Barnea G, Strapps W, Herrada G, Berman Y, Ong J, Kloss B, Axel R, Lee KJ. The genetic design of signaling cascades to record receptor activation. *Proceedings of the National Academy of Sciences*. 2008;105(1):64-9. <https://doi.org/10.1073/pnas.0710487105>.
69. Asher WB, Geggier P, Holsey MD, Gilmore GT, Pati AK, Meszaros J, Terry DS, Mathiasen S, Kaliszewski MJ, McCauley MD, Govindaraju A, Zhou Z, Harikumar KG, Jaqaman K, Miller LJ, Smith AW, Blanchard SC, Javitch JA. Single-molecule FRET imaging of GPCR dimers in living cells. *Nat Methods*. 2021;18(4):397-405. <https://doi.org/10.1038/s41592-021-01081-y>.
70. Avet C, Mancini A, Breton B, Le Gouill C, Hauser AS, Normand C, Kobayashi H, Gross F, Hogue M, Lukashova V, St-Onge S, Carrier M, Héroux M, Morissette S, Fauman EB, Fortin J-P, Schann S, Leroy X, Gloriam DE, Bouvier M. Effector membrane translocation biosensors reveal G protein and β arrestin coupling profiles of 100 therapeutically relevant GPCRs. *eLife*. 2022;11:e74101. <https://doi.org/10.7554/eLife.74101>.
71. Galinski S, Wichert SP, Rossner MJ, Wehr MC. Multiplexed profiling of GPCR activities by combining split TEV assays and EXT-based barcoded readouts. *Scientific Reports*. 2018;8(1):8137. <https://doi.org/10.1038/s41598-018-26401-9>.

-
72. Jones EM, Jajoo R, Cancilla D, Lubock NB, Wang J, Satyadi M, Cheung R, De March C, Bloom JS, Matsunami H, Kosuri S. A Scalable, Multiplexed Assay for Decoding GPCR-Ligand Interactions with RNA Sequencing. *Cell Systems*. 2019;8(3):254-60.e6. <https://doi.org/10.1016/j.cels.2019.02.009>.
73. Mishina YM, Wilson CJ, Bruett L, Smith JJ, Stoop-Myer C, Jong S, Amaral LP, Pedersen R, Lyman SK, Myer VE, Kreider BL, Thompson CM. Multiplex GPCR Assay in Reverse Transfection Cell Microarrays. *SLAS Discovery*. 2004;9(3):196-207. <https://doi.org/10.1177/1087057103261880>.
74. Fang Y, Frutos AG, Lahiri J. G-protein-coupled receptor microarrays. *Chembiochem*. 2002;3(10):987-91. [https://doi.org/10.1002/1439-7633\(20021004\)3:10<987::Aid-cbic987>3.0.Co;2-m](https://doi.org/10.1002/1439-7633(20021004)3:10<987::Aid-cbic987>3.0.Co;2-m).
75. Tewson PH, Quinn AM, Hughes TE. A multiplexed fluorescent assay for independent second-messenger systems: decoding GPCR activation in living cells. *J Biomol Screen*. 2013;18(7):797-806. <https://doi.org/10.1177/1087057113485427>.
76. Sarrion-Perdigones A, Chang L, Gonzalez Y, Gallego-Flores T, Young DW, Venken KJT. Examining multiple cellular pathways at once using multiplex hextuple luciferase assaying. *Nature Communications*. 2019;10(1). <https://doi.org/10.1038/s41467-019-13651-y>.
77. Wehr MC, Laage R, Bolz U, Fischer TM, Grünwald S, Scheek S, Bach A, Nave KA, Rossner MJ. Monitoring regulated protein-protein interactions using split TEV. *Nat Methods*. 2006;3(12):985-93. <https://doi.org/10.1038/nmeth967>.
78. Herho A. Dissecting intercellular and intracellular signaling networks with barcoded genetic to. 2022. <https://doi.org/10.1016/j.cbpa.2021.09.002>.
79. Muzzey D, Evans EA, Lieber C. Understanding the Basics of NGS: From Mechanism to Variant Calling. *Curr Genet Med Rep*. 2015;3(4):158-65. <https://doi.org/10.1007/s40142-015-0076-8>.
80. Chen H, Rosen CE, González-Hernández JA, Song D, Potempa J, Ring AM, Palm NW. Highly multiplexed bioactivity screening reveals human and microbiota metabolome-GPCR interactions. *Cell*. 2023;186(14):3095-110.e19. <https://doi.org/10.1016/j.cell.2023.05.024>.
81. Chong ZX, Yeap SK, Ho WY. Transfection types, methods and strategies: a technical review. *PeerJ*. 2021;9:e11165. <https://doi.org/10.7717/peerj.11165>.
82. Yu JN, Ma SF, Miao DQ, Tan XW, Liu XY, Lu JH, Tan JH. Effects of cell cycle status on the efficiency of liposome-mediated gene transfection in mouse fetal fibroblasts. *J Reprod Dev*. 2006;52(3):373-82. <https://doi.org/10.1262/jrd.17097>.
83. Xiong F, Mi Z, Gu N. Cationic liposomes as gene delivery system: transfection efficiency and new application. *Pharmazie*. 2011;66(3):158-64
84. Hamann A, Thomas AK, Kozisek T, Farris E, Lück S, Zhang Y, Pannier AK. Screening a chemically defined extracellular matrix mimetic substrate library to identify substrates that enhance substrate-mediated transfection. *Experimental Biology and Medicine*. 2020;245(7):606-19. <https://doi.org/10.1177/1535370220913501>.
85. Cheng Z, Garvin D, Paguio A, Stecha P, Wood K, Fan F. Luciferase Reporter Assay System for Deciphering GPCR Pathways. *Curr Chem Genomics*. 2010;4:84-91. <https://doi.org/10.2174/1875397301004010084>.
86. Azimzadeh P, Olson JA, Jr., Balenga N. Reporter gene assays for investigating GPCR signaling. *Methods Cell Biol*. 2017;142:89-99. <https://doi.org/10.1016/bs.mcb.2017.07.006>.
87. Moore JE, Purcaro MJ, Pratt HE, Epstein CB, Shores N, Adrian J, Kawli T, Davis CA, Dobin A, Kaul R, Halow J, Van Nostrand EL, Freese P, Gorkin DU, Shen Y, He Y, Mackiewicz M, Pauli-Behn F, Williams BA, Mortazavi A, Keller CA, Zhang XO, Elhajjajy SI, Huey J, Dickel DE, Snetkova V, Wei X, Wang X, Rivera-Mulia JC, Rozowsky J, Zhang J, Chhetri SB, Zhang J, Victorsen A, White KP, Visel A, Yeo GW, Burge CB, Lécuyer E, Gilbert DM, Dekker J, Rinn J, Mendenhall EM, Ecker JR, Kellis M, Klein RJ, Noble WS, Kundaje A, Guigó R, Farnham PJ, Cherry JM, Myers RM, Ren B, Graveley BR, Gerstein MB, Pennacchio LA, Snyder MP, Bernstein BE, Wold B, Hardison RC, Gingeras TR, Stamatoyannopoulos JA, Weng Z. Expanded encyclopaedias of DNA elements in the human and mouse genomes. *Nature*. 2020;583(7818):699-710. <https://doi.org/10.1038/s41586-020-2493-4>.
88. Field A, Adelman K. Evaluating Enhancer Function and Transcription. *Annu Rev Biochem*. 2020;89:213-34. <https://doi.org/10.1146/annurev-biochem-011420-095916>.

-
89. Fry DJ. Teaching experimental design. *Ilar j.* 2014;55(3):457-71. <https://doi.org/10.1093/ilar/ilu031>.
90. Carr GJ, Gorelick NJ. Statistical tests of significance in transgenic mutation assays: considerations on the experimental unit. *Environ Mol Mutagen.* 1994;24(4):276-82. <https://doi.org/10.1002/em.2850240404>.
91. Grailer J, Moravec RA, Cheng ZJ, Grassi M, Ott V, Fan F, Cong M. Considerations in Developing Reporter Gene Bioassays for Biologics. Springer US; 2020. p. 131-56.
92. Tamma G, Di Mise A, Ranieri M, Geller A, Tamma R, Zallone A, Valenti G. The V2 receptor antagonist tolvaptan raises cytosolic calcium and prevents AQP2 trafficking and function: an in vitro and in vivo assessment. *Journal of Cellular and Molecular Medicine.* 2017;21(9):1767-80. <https://doi.org/10.1111/jcmm.13098>.
93. Shifera AS, Hardin JA. PMA induces expression from the herpes simplex virus thymidine kinase promoter via the activation of JNK and ERK in the presence of adenoviral E1A proteins. *Archives of Biochemistry and Biophysics.* 2009;490(2):145-57. <https://doi.org/10.1016/j.abb.2009.08.013>.
94. Wu Y, Jensen N, Rossner MJ, Wehr MC. Exploiting Cell-Based Assays to Accelerate Drug Development for G Protein-Coupled Receptors. *International Journal of Molecular Sciences.* 2024;25(10):5474
95. Inoue A, Ishiguro J, Kitamura H, Arima N, Okutani M, Shuto A, Higashiyama S, Ohwada T, Arai H, Makide K, Aoki J. TGF α shedding assay: an accurate and versatile method for detecting GPCR activation. *Nature Methods.* 2012;9(10):1021-9. <https://doi.org/10.1038/nmeth.2172>.
96. Zeghal M, Laroche G, Freitas JD, Wang R, Giguère PM. Profiling of basal and ligand-dependent GPCR activities by means of a polyvalent cell-based high-throughput platform. *Nature Communications.* 2023;14(1):3684. <https://doi.org/10.1038/s41467-023-39132-x>.
97. Shaw WM, Yamauchi H, Mead J, Gowers G-OF, Bell DJ, Öling D, Larsson N, Wigglesworth M, Ladds G, Ellis T. Engineering a Model Cell for Rational Tuning of GPCR Signaling. *Cell.* 2019;177(3):782-96.e27. <https://doi.org/10.1016/j.cell.2019.02.023>.
98. Shaw G, Morse S, Ararat M, Graham FL. Preferential transformation of human neuronal cells by human adenoviruses and the origin of HEK 293 cells. *The FASEB Journal.* 2002;16(8):869-71. <https://doi.org/https://doi.org/10.1096/fj.01-0995fje>.
99. Vincent F, Loria P, Pregel M, Stanton R, Kitching L, Nocka K, Doyonnas R, Steppan C, Gilbert A, Schroeter T, Peakman MC. Developing predictive assays: the phenotypic screening "rule of 3". *Sci Transl Med.* 2015;7(293):293ps15. <https://doi.org/10.1126/scitranslmed.aab1201>.
100. Naruse M, Saito T. Immediate protein expression from exogenous mRNAs in embryonic brain. *Scientific Reports.* 2022;12(1):17145. <https://doi.org/10.1038/s41598-022-21668-5>.
101. Buccitelli C, Selbach M. mRNAs, proteins and the emerging principles of gene expression control. *Nature Reviews Genetics.* 2020;21(10):630-44. <https://doi.org/10.1038/s41576-020-0258-4>.
102. Yamada M, Nagasaki SC, Suzuki Y, Hirano Y, Imayoshi I. Optimization of Light-Inducible Gal4/UAS Gene Expression System in Mammalian Cells. *iScience.* 2020;23(9):101506. <https://doi.org/10.1016/j.isci.2020.101506>.
103. Mendenhall W, Beaver RJ, Beaver BM. Introduction to Probability and Statistics: Cengage Learning; 2012.
104. Cai J, Tong Q. Anatomy and Function of Ventral Tegmental Area Glutamate Neurons. *Front Neural Circuits.* 2022;16:867053. <https://doi.org/10.3389/fncir.2022.867053>.
105. Korf HW, Møller M. Arcuate nucleus, median eminence, and hypophysial pars tuberalis. *Handb Clin Neurol.* 2021;180:227-51. <https://doi.org/10.1016/b978-0-12-820107-7.00015-x>.
106. Kesner AJ, Shin R, Calva CB, Don RF, Junn S, Potter CT, Ramsey LA, Abou-Elnaga AF, Cover CG, Wang DV, Lu H, Yang Y, Ikemoto S. Supramammillary neurons projecting to the septum regulate dopamine and motivation for environmental interaction in mice. *Nat Commun.* 2021;12(1):2811. <https://doi.org/10.1038/s41467-021-23040-z>.

-
107. Taylor NE, Pei J, Zhang J, Vlasov KY, Davis T, Taylor E, Weng FJ, Van Dort CJ, Solt K, Brown EN. The Role of Glutamatergic and Dopaminergic Neurons in the Periaqueductal Gray/Dorsal Raphe: Separating Analgesia and Anxiety. *eNeuro*. 2019;6(1). <https://doi.org/10.1523/eneuro.0018-18.2019>.
108. Knapp R, Rubenzik M, Malatynska E, Varga E, Roeske WR, Yamamura HI. Neurotransmitter Receptors. In: Aminoff MJ, Daroff RB, editors. *Encyclopedia of the Neurological Sciences*. New York: Academic Press; 2003. p. 602-14.
109. Moliner R, Girysh M, Brunello CA, Kovaleva V, Biojone C, Enkavi G, Antenucci L, Kot EF, Goncharuk SA, Kaurinkoski K, Kuutti M, Fred SM, Elsilä LV, Sakson S, Cannarozzo C, Diniz C, Seiffert N, Rubiolo A, Haapaniemi H, Meshi E, Nagaeva E, Öhman T, Róg T, Kankuri E, Vilar M, Varjosalo M, Korpi ER, Permi P, Mineev KS, Saarma M, Vattulainen I, Casarotto PC, Castrén E. Psychedelics promote plasticity by directly binding to BDNF receptor TrkB. *Nat Neurosci*. 2023;26(6):1032-41. <https://doi.org/10.1038/s41593-023-01316-5>.
110. Wise A, Gearing K, Rees S. Target validation of G-protein coupled receptors. *Drug Discovery Today*. 2002;7(4):235-46. [https://doi.org/https://doi.org/10.1016/S1359-6446\(01\)02131-6](https://doi.org/https://doi.org/10.1016/S1359-6446(01)02131-6).

Acknowledgements

First of all, I would like to express my sincere gratitude to my fantastic supervisor, PD Dr. Michael Wehr and thank him for providing me with the opportunities to learn and practice the massive either novel wet lab or novel dry lab assays, and for supervising my PhD project in bi-weekly jour fixe meetings with his continuous support and patience. He helped me to establish an intimate relationship with him where I felt comfortable and could think independently to carry out my project with his immediate valuable feedback.

I would also like to acknowledge the supervision of Dr. Niels Jensen. He imparted a lot of valuable knowledge and showed me how to perform many assays, which helped me to quickly familiarise myself with the lab and provided me with a solid foundation to carry out my PhD project efficiently.

I would also like to express my immense gratitude to Prof. Dr. Moritz Rossner for his invaluable knowledge, experience, and generous support. His guidance has been nothing short of amazing! And I'm so thankful for the monthly meeting to discuss my doctoral project.

Many thanks to Dr. Ben Brankatschk for introducing me to the multiplex barcode assays and showing me the vast knowledge of their development.

I'd also like to thank Prof. Dr. Volker Scheuss for being such a great TAC member and for always being there for me with his support.

Special thanks to my colleague Thomas Zerbes for his help in efficiently establishing the stable cell lines and performing the expression and functional validation of the stable cell lines.

I would also like to thank Lukša Popović, Vivek Sahoo, Isabelle V. von Hauff, Xiao Ma, Min Chen, and Fiona J. Mandausch for their invaluable feedback and help in life and research.

I would also like to thank all the members of the laboratory who supported me in various scientific aspects and created a scientifically stimulating working environment.

I would also like to thank the China Scholarship Council (CSC) and Systasy Bioscience GmbH for funding my PhD studies.

I would like to express my heartfelt thanks to my absolutely wonderful family! I am so grateful to them for their incredible support. I dedicate this work to them!